Spring 2000

# A statistical study of the dependence of the integrated wave power of geomagnetic pulsations between 01 Hz and 10 Hz upon the solar wind dynamic pressure

Cristian C. Cocheci
*University of New Hampshire, Durham*

# INFORMATION TO USERS

This manuscript has been reproduced from the microfilm master. UMI films the text directly from the original or copy submitted. Thus, some thesis and dissertation copies are in typewriter face, while others may be from any type of computer printer.

The quality of this reproduction is dependent upon the quality of the copy submitted. Broken or indistinct print, colored or poor quality illustrations and photographs, print bleedthrough, substandard margins, and improper alignment can adversely affect reproduction.

In the unlikely event that the author did not send UMI a complete manuscript and there are missing pages, these will be noted. Also, if unauthorized copyright material had to be removed, a note will indicate the deletion.

Oversize materials (e.g., maps, drawings, charts) are reproduced by sectioning the original, beginning at the upper left-hand corner and continuing from left to right in equal sections with small overlaps.

Photographs included in the original manuscript have been reproduced xerographically in this copy. Higher quality 6" x 9" black and white photographic prints are available for any photographs or illustrations appearing in this copy for an additional charge. Contact UMI directly to order.

Bell & Howell Information and Learning
300 North Zeeb Road, Ann Arbor, MI 48106-1346 USA
800-521-0600

UMI®

# A Statistical Study of the Dependence of the Integrated Wave Power of Geomagnetic Pulsations between 0.1 Hz and 1.0 Hz upon the Solar Wind Dynamic Pressure

BY

Cristian C. Cocheci

Diploma, University of Bucharest (1993)

DISSERTATION

Submitted to the University of New Hampshire
in partial fulfillment of
the requirements for the degree of

Doctor of Philosophy

in

Physics

May 2000

This dissertation has been examined and approved.

Dissertation Director, Roger L. Arnoldy
Professor of Physics and Earth, Oceans, and Space

Eberhard Moebius
Professor of Physics and Earth, Oceans, and Space

Joseph V. Hollweg
Professor of Physics and Earth, Oceans, and Space

Kristina A. Lynch
Research Associate Professor of Physics and Earth, Oceans, and Space

Harvey Shepard
Professor of Physics

03/24/2000
Date

# Dedication

*To my dear parents*

*and friends*

# Acknowledgments

First and foremost, I thank my advisor Professor Roger Arnoldy. This dissertation would not have been possible without his knowledge and patience, without his friendship and experience. Thank you for being there for me, for being the best advisor that a graduate student could hope for. Thank you for giving me the opportunity to work with you and for believing that this research was possible. There are not enough words that could express my gratitude to you.

I am thankful to the members of my thesis committee, Kristina Lynch, Harvey Shepard, Joseph Hollweg and Eberhard Moebius. They gave me excellent advice and they encouraged me throughout my research progress.

Many thanks to all the professors at UNH that I have taken classes from. They were all very good teachers and excellent professionals. All the people from the Space Science Center were very kind to me and made every effort to help me with my questions and inquiries, so I thank them all for that. My special thanks go to Charlie Farrugia who let me work with him, taught me a lot of space physics and was a good friend.

I would like to thank the members of the Magnetosphere Research Laboratory, Hank Dolben and Mark Widholm , for their great help and advice. Very special thanks to Brett Austin who was a great friend, taught me a lot of things, and most of all taught me how to program. Thanks to David Pietrowski and David Rau for their friendship and more. Thanks to all physics graduate students who were very nice to me and made me feel welcome among them.

Being far away from my home country was quite hard, but it would have been a lot harder without the friendship of all of my fellow Romanian graduate students at UNH, and

particularly Tavi's. Thanks to all my Romanian friends on this side of the ocean: Motanu' and the rest of the Bostonians, Bogdan and Ioana Mihaila, Misu, Liviu, Radu, Victor, and all my friends from Columbus, especially Adam, Diana and Dumi.

My thoughts also go to my high school physics teacher, professor Ilina Rebedea. She showed me the first steps in physics and it was her influence that steered my focus towards physics, culminating with me becoming a physicist. Also a big influence on my career were astrophysicists Adrian Oncica and Mihai Ghizaru of the Astronomical Institute in Bucharest. Thanks to them I started to love the space part of physics and I ended up studying just that in graduate school. I express my gratitude to all my professors from the College of Physics, University of Bucharest.

In the end I would like to thank my parents. I know that their love and thoughts were here with me at all times. They believed that I could get accepted to graduate school in the US and that I could pursue a graduate career in physics. They helped me with all their energy towards achieving this goal, even though the fact that their only child was going far away was very hard to conceive.

# TABLE OF CONTENTS

# List of Tables

# List of Figures

# ABSTRACT

## A Statistical Study of the Dependence of the Integrated Wave Power of Geomagnetic Pulsations between 0.1 Hz and 1.0 Hz upon the Solar Wind Dynamic Pressure

by

Cristian C. Cocheci
University of New Hampshire, May, 2000

We present a statistical study of the influence of the solar wind dynamic pressure on the power of geomagnetic pulsations in the frequency range of 0.1 to 1.0 Hz (around the superposition of the Pc1 and Pc1-2 frequency ranges). The solar wind parameters are calculated using data from the Solar Wind Experiment and from the Magnetic Field Instrument on board the WIND spacecraft. Using ground data from the Antarctic AGO arrays and northern hemisphere stations we have compared the integrated power of pulsations between 0.1 and 1.0 Hz with the variations of the solar wind dynamic pressure, on scales of several hours. On the dayside there is a better than 80% correlation between increases/decreases of solar wind dynamic pressure and enhancements/depletions of wave power. Many wave events occur during periods of constant solar wind dynamic pressure.

These results suggest that the wave production mechanism driven by the magnetospheric compression due to solar wind dynamic pressure represents a trigger of the ULF waves produced in the outer magnetosphere and recorded on the ground. The presence of the waves during periods of low constant solar wind pressure is not in contradiction with our proposed mechanism, it just means that the dynamic pressure is not the only compression mechanism.

# Chapter 1

# Introduction

The Sun represents the source of energy for all solar-terrestrial phenomena. The streaming ionized plasma flowing through the interplanetary space radially away from the Sun is called the solar wind. In its complicated interaction with the magnetized Earth, the solar wind creates a comet-like shaped magnetosphere and establishes different distinct plasma regimes within it. Magnetospheric physics is the part of space physics that studies the phenomena occurring inside the magnetosphere and at the boundary between the magnetosphere and the solar wind, called the magnetopause. Some magnetospheric research is carried out remotely from the ground with instruments such as magnetometers, riometers, and antennas. *In situ* observations are made possible by flying different instruments on rockets and satellites. These *in situ* data have resulted in a huge growth of our knowledge and understanding of magnetospheric phenomena, and they complement the ground observations rather than making them obsolete.

Ground observations are made possible by plasma waves. These plasma waves carry information about the plasma that produces them, and about the plasma that they go through. Plasma waves can energize or take energy away from the plasma. The ground signatures of ultra-low frequency (ULF) plasma waves which originate in space are known as geomagnetic pulsations or simply micropulsations, and they can be measured with the aid of simple instruments called magnetometers. Depending on the frequency of the ULF waves to be measured, there are two types of magnetometers used. Induction magnetometers, also

Table 1.1: Micropulsation classification scheme.

| Type | Pc1 | Pc2 | Pc3 | Pc4 | Pc5 | Pi1 | Pi2 |
|---|---|---|---|---|---|---|---|
| Period (s) | 0.2-5 | 5-10 | 10-45 | 45-150 | 150-600 | 1-40 | 40-150 |

called search coils, are used to measure the variation of the magnetic field ($\partial B/\partial t$), and they sample the high end of the ULF regime, from 0.1 Hz up to several hundred Hz. Fluxgate magnetometers are used to measure the magnitude of the magnetic field and are used for looking at ULF waves with periods ranging between 2 and 600 seconds (the maximum sampling frequency of the fluxgate magnetometers is 1 Hz). Micropulsation magnetometers can be conveniently placed at different locations on the Earth, such that different types of studies can be done. They can be placed in chains (latitudinal or longitudinal), thus making possible studies of latitudinal or longitudinal motions or propagation of various phenomena (aurora, waves etc.). The magnetometers used in this study are placed at high latitudes, at the footpoint of magnetic field lines that belong to the outer magnetosphere, making possible the sensing of phenomena that occur at those locations. The sampling frequencies of the search coils used in this study are 10 Hz for the Iqaluit and South Pole coils and 2 Hz for the BAS-A81 coils.

Micropulsations have been classified according to their period and spectral signature [Saito, 1969]; the accepted classification scheme is presented in Table 1.1. 'P' stands for pulsations, 'c' stands for continuous and 'i' stands for irregular. The continuous pulsations are band limited within the respective frequency intervals, whereas the irregular pulsations are broadband pulsations. Another type of continuous pulsations called Pc1-2 was defined

later [Fukunishi et al., 1981]. These have a frequency range intermediary to the Pc1 and Pc2 ranges (0.1 and 0.4 Hz) and a somewhat different spectral signature (very narrow banded, occurring only in the afternoon and night sectors); we mention them here because they are part of our study.

Micropulsations have many different causes and originate in many different locations in space. The flow shear between the magnetosheath and the magnetopause gives rise to the Kelvin-Helmholtz instability and creates ripples on the magnetopause, which propagate along the Earth's magnetic field and are recorded on the ground as Pc5 pulsations [Farrugia et al., 1989]. Solar wind pressure pulses hit the dayside magnetosphere making it ring at its resonant frequencies. Standing waves are generated and they are recorded on the ground as Pc3-4 pulsations. Another known source of Pc3 pulsations is located in the upstream solar wind [Paschmann et al., 1979]. They are the result of the interaction between low cone angle interplanetary magnetic field and the bowshock (M. J. Engebretson, private communication, 1999), and they are transported along by the solar wind to the magnetosphere. The broadband Pi waves are associated with particle precipitation in the ionosphere and therefore are an indication of aurora.

Pulsations in the Pc1 and Pc1-2 frequency ranges, which are the topic of this thesis, are commonly observed on the ground at middle to high geomagnetic latitudes [Arnoldy et al., 1996a, Hayashi et al., 1981, Kato and Tonegawa, 1995] and they have also been measured by satellites in the outer magnetosphere [Perraut et al., 1978, Young et al., 1981, Roux et al., 1982, Anderson et al., 1990]. In spectrograms Pc1 and Pc1-2 display many signatures indicating that they have different source regions [Fraser, 1975, Fukunishi et al., 1981]. Ground observations of these pulsations can serve as diagnos-

tics of remote processes and particle populations [Menk et al., 1992] if their source regions can be determined. Several studies have attempted to classify them by magnetospheric source region [Bolshakova et al., 1980, Morris and Cole, 1991, Menk et al., 1992, Popecki et al., 1993, Dyrud et al., 1997]. The current understanding is that there are two main regions inside the magnetosphere where Pc1 originate. One of them is in the dayside equatorial outer magnetosphere earthward of the low latitude boundary layer (LLBL), and it extends 1 to 2 Re radially [Anderson et al., 1996a]. This Pc1 wave population is the focus of this thesis. The other source of Pc1 waves is at the plasmapause [Kozyra et al., 1984], where the interaction between the energetic ring current ions and the cold plasmaspheric heavy ion population dramatically lowers the cyclotron instability threshold, which is responsible for Pc1 wave generation.

Pc1 micropulsations are electromagnetic proton cyclotron waves (hereinafter referred to as proton cyclotron waves) produced by wave-particle interactions with the magnetospheric hot proton populations with $T_{\perp p} \cong 10$ to 50 keV and a positive temperature anisotropy, $A_p \equiv T_{\perp p}/T_{\|p} - 1 > 0$, where $T_{\perp p}$ and $T_{\|p}$ are the perpendicular and parallel proton temperatures, respectively [Cornwall, 1965, Kennel and Petschek, 1966, Liemohn, 1967]. The dominant population of proton cyclotron waves studied in this thesis occurs in the outer magnetosphere, beyond geosynchronous orbits [Jacobs and Watanabe, 1967, Obayashi, 1965, Anderson et al., 1992a]. The hot magnetospheric protons responsible for cyclotron wave growth are of solar wind origin. They enter the magnetosphere through reconnection processes in the Earth's magnetotail, then $\vec{E} \times \vec{B}$ drift earthward due to the crosstail electric field, and then they reach the outer magnetosphere by drifting around the Earth driven by a combination of the magnetic field curvature and gradient drifts and the magnetospheric

$\vec{E} \times \vec{B}$ drift. The conditions in the compressed subsolar magnetosphere are such that these populations become unstable to the cyclotron instability and Pc1 waves are generated. The proton cyclotron instability threshold is conveniently parameterized in terms of $A_p$ and $\beta_{\|p}$ in the form $A_p = a\beta_{\|p}^c$ with $a \cong 0.4$ and $c \cong -0.45$, where $\beta_{\|p} \equiv 8\pi n_p T_{\|p}/B_0^2$ is the proton parallel beta [Gary et al., 1994, Gary and Lee, 1994]. Because it corresponds to a threshold of the proton cyclotron instability, this relation represents an upper bound on the proton temperature anisotropy. If the anisotropy is less than the threshold value there is no significant instability growth, no wave-particle scattering, and no change in $T_{\perp p}/T_{\|p} - 1$. On the other hand, if the plasma is driven by macroscopic forces (e.g. sustained high solar wind dynamic pressure) such that $T_{\perp p}/T_{\|p} - 1$ exceeds the threshold condition for a given $\beta_{\|p}$, the proton cyclotron instability will arise and will pitch angle scatter the protons. If the convection of wave energy away from the region of excitation is not too rapid, this scattering will return the anisotropy to the threshold value, and a steady state will be reached where the anisotropy is maintained at the threshold value and waves are produced.

Our study has begun from an observation of the influence of solar wind dynamic pressure, as measured by detectors on-board the WIND spacecraft, on the Pc1 power spectrum of the ground micropulsations recorded at one of our stations. We study this influence from a statistical point of view, addressing the necessary solar wind pressure conditions in order to create cyclotron waves inside the magnetosphere. We conclude that in $\sim 80\%$ of the cases, a solar wind dynamic pressure increase above a certain lower limit will produce similar Pc1 wave power variation on the ground.

# Chapter 2

# Fundamentals

In this chapter we are going to solve the dispersion relation for a plasma like the one in the terrestrial outer magnetosphere, a hot anisotropic plasma population superposed over a cold background isotropic plasma. The dispersion relation for such a plasma will have a cold and a hot part, so we will find general dispersion relations for both cold and hot plasmas. We will find the necessary conditions for the commencement of the proton cyclotron anisotropy instability and we will explain the current understanding on the influence of magnetospheric compressions on the production mechanism of proton cyclotron waves (Pc1).

## 2.1 The Electromagnetic Ion Cyclotron Dispersion Relation. Cold Plasma Approximation

A plasma is a collection of charged particles possessing certain electrodynamic properties. Relatively high temperatures are necessary to produce a plasma, therefore the plasma particles are in fast motion (thousands of km/s). This will generate microscopic charge separations and currents, which in turn will create fluctuations of the electric and magnetic field, called thermal fluctuations. In addition to these fluctuations, disturbances will contribute to the generation of waves that will propagate through a plasma. The measured frequencies of waves in a plasma cover a very wide range from several milihertz up to several megahertz.

A disturbance can be considered a wave only if its amplitude exceeds the level of thermal

fluctuations: if the amplitude of a disturbance is smaller than the level of fluctuations and no mechanism will act to amplify it, that disturbance will not affect the plasma and is not considered a wave. In addition to this, a disturbance has to satisfy the appropriate plasma equations in order to be a wave. This implies that the spectrum of waves that can propagate in a plasma is discrete.

### 2.1.1 General Wave Equation

A plasma with no external magnetic field can support the three simplest wave modes that can propagate in a plasma: the electrostatic Langmuir mode, the electrostatic ion-acoustic mode and the electromagnetic ordinary mode (the one that also propagates in a vacuum). The presence of the magnetic field will introduce a large variety of other possible modes. We assume that the thermal noise level is much smaller than the wave amplitudes. Hence, the plasma is assumed to be sufficiently cold. On the other hand, we assume that the wave amplitudes are small enough to allow any disturbance to be represented as a linear superposition of plane waves.

In deriving the general linear wave equation, one starts from the set of Maxwell's equations, which are obeyed by the electromagnetic fields and plasma parameters:

$$\nabla \times \vec{B} = \epsilon_0 \mu_0 \frac{\partial \vec{E}}{\partial t} + \mu_0 \vec{j} \tag{2.1.1}$$

$$\nabla \times \vec{E} = -\frac{\partial \vec{B}}{\partial t} \tag{2.1.2}$$

$$\nabla \cdot \vec{B} = 0 \tag{2.1.3}$$

$$\nabla \cdot \vec{E} = \frac{\rho}{\epsilon_0} \tag{2.1.4}$$

Taking the partial derivative of equation (2.1.1) with respect to time and eliminating $\partial\vec{B}/\partial t$ from equation (2.1.2) one gets

$$-\nabla \times (\nabla \times \vec{E}) \equiv \epsilon_0\mu_0 \frac{\partial^2 \vec{E}}{\partial t^2} + \mu_0 \frac{\partial \vec{j}}{\partial t} \tag{2.1.5}$$

and using the vector identity

$$\nabla \times (\nabla \times \vec{E}) \equiv \nabla(\nabla \cdot \vec{E}) - \nabla^2 \vec{E} \tag{2.1.6}$$

one finds an inhomogeneous wave equation for the electric field

$$\nabla^2 \vec{E} - \nabla(\nabla \cdot \vec{E}) - \epsilon_0\mu_0 \frac{\partial^2 \vec{E}}{\partial t^2} \equiv \mu_0 \frac{\partial \vec{j}}{\partial t} \tag{2.1.7}$$

The dependence of the current $\vec{j}$ on the electric field $\vec{E}$ can be expressed by the time varying Ohm's law:

$$\vec{j} \equiv \int d^3x' \int_{-\infty}^{t} dt' \bar{\sigma}(\vec{x} - \vec{x}', t - t') \cdot \vec{E} \tag{2.1.8}$$

where we assumed that the plasma responds linearly to the presence of a wave disturbance, so the conductivity tensor $\bar{\sigma}$ depends on relative position and time only. With this supposition one may linearize equation (2.1.7) by considering small perturbations of the electric field with $\vec{E}_0 = 0$ (no DC electric field) and $\vec{E}(\vec{x}, t) \equiv \delta\vec{E}(\vec{x}, t)$, by keeping only the first order terms in the small perturbations (in this case actually there are no higher order terms in the perturbations, but generally these are dropped if they are present):

$$\nabla^2 \delta\vec{E} - \nabla(\nabla \cdot \delta\vec{E}) - \epsilon_0\mu_0 \frac{\partial^2 \delta\vec{E}}{\partial t^2} \equiv \mu_0 \frac{\partial \vec{j}}{\partial t} \tag{2.1.9}$$

where Ohm's law becomes

$$\vec{j} \equiv \int d^3x' \int_{-\infty}^{t} dt' \bar{\sigma}(\vec{x} - \vec{x}', t - t') \cdot \delta\vec{E} \tag{2.1.10}$$

Equation (2.1.9) represents the general linear wave equation. The pure electromagnetic part independent of the presence of the medium is represented by the left hand side, whereas the right hand side gives the response of the medium through the conductivity tensor $\bar{\bar{\sigma}}$.

### 2.1.2 General Wave Dispersion Relation in a Magnetized Plasma

We seek plane wave solutions for equation (2.1.9) of the form

$$\delta\vec{E}(\omega,\vec{k}) \equiv \delta\vec{E}_0(\omega,\vec{k})\exp(i\vec{k}\cdot\vec{x} - i\omega t) \tag{2.1.11}$$

The right hand side can be written as

$$\mu_0\frac{\partial\vec{j}}{\partial t} \equiv \mu_0\frac{\partial}{\partial t}\left(\int d^3x'\int_{-\infty}^{t} dt'\bar{\bar{\sigma}}(\vec{x}-\vec{x}',t-t')\cdot\delta\vec{E}\right) \tag{2.1.12}$$

$$\equiv \mu_0\left(\int d^3x'\bar{\bar{\sigma}}(\vec{x}-\vec{x}',t)\exp(i\vec{k}\cdot\vec{x} - i\omega t)\right)\cdot\delta\vec{E}_0(\omega,\vec{k}) \tag{2.1.13}$$

$$\equiv \mu_0\bar{\bar{\sigma}}(\omega,\vec{k})\cdot\delta\vec{E}_0(\omega,\vec{k}) \tag{2.1.14}$$

Note that seeking a plane wave solution of the form (2.1.11) is equivalent to replacing the operators $\nabla$ and $\partial/\partial t$ with $\vec{k}\cdot$ and $-i\omega$ respectively, so the left hand side of equation (2.1.9) becomes

$$-k^2\delta\vec{E}_0 + \vec{k}(\vec{k}\cdot\delta\vec{E}_0) + \epsilon_0\mu_0\omega^2\delta\vec{E}_0 \equiv -\left[\left(k^2 - \frac{\omega^2}{c^2}\right)\delta\vec{E}_0 - \vec{k}(\vec{k}\cdot\delta\vec{E}_0)\right] \tag{2.1.15}$$

where we used $c^2 \equiv (\epsilon_0\mu_0)^{-1}$. We want to write the term $\vec{k}(\vec{k}\cdot\delta\vec{E}_0)$ as a tensor operating on $\delta\vec{E}_0$. In order to see this more easily we can use the matrix definitions for the dot product and for the outer product of two vectors $\vec{a}$ and $\vec{b}$. If we define the dot product as

$$\vec{a}\cdot\vec{b} \equiv \begin{pmatrix} a_x & a_y & a_z \end{pmatrix}\begin{pmatrix} b_x \\ b_y \\ b_z \end{pmatrix} \equiv a_xb_x + a_yb_y + a_zb_z \tag{2.1.16}$$

and the outer product as

$$\vec{a}\vec{b} \equiv \begin{pmatrix} a_x \\ a_y \\ a_z \end{pmatrix} \begin{pmatrix} b_x & b_y & b_z \end{pmatrix} \equiv \begin{pmatrix} a_x b_x & a_x b_y & a_x b_z \\ a_y b_x & a_y b_y & a_y b_z \\ a_z b_x & a_z b_y & a_z b_z \end{pmatrix} \tag{2.1.17}$$

then $\vec{k}(\vec{k}\cdot\delta\vec{\tilde{E}}_0)$ becomes

$$\begin{aligned} \vec{k}(\vec{k}\cdot\delta\vec{\tilde{E}}_0) &\equiv \begin{pmatrix} k_x \\ k_y \\ k_z \end{pmatrix} \begin{pmatrix} k_x & k_y & k_z \end{pmatrix} \begin{pmatrix} \delta\tilde{E}_{0x} \\ \delta\tilde{E}_{0y} \\ \delta\tilde{E}_{0z} \end{pmatrix} \\ &\equiv \begin{pmatrix} k_x k_x & k_x k_y & k_x k_z \\ k_y k_x & k_y k_y & k_y k_z \\ k_z k_x & k_z k_y & k_z k_z \end{pmatrix} \begin{pmatrix} \delta\tilde{E}_{0x} \\ \delta\tilde{E}_{0y} \\ \delta\tilde{E}_{0z} \end{pmatrix} \\ &\equiv \vec{k}\vec{k}\cdot\delta\vec{\tilde{E}}_0 \end{aligned} \tag{2.1.18}$$

Finally equation (2.1.9) can be written as

$$\left[\left(k^2 - \frac{\omega^2}{c^2}\right)\bar{\bar{I}} - \vec{k}\vec{k} - i\omega\mu_0\bar{\tilde{\sigma}}(\omega,\vec{k})\right]\cdot\delta\vec{\tilde{E}}_0(\omega,\vec{k}) \equiv 0 \tag{2.1.19}$$

This equation is a tensor equation, and is equivalent with a system of three equations for every component of $\delta\vec{\tilde{E}}_0(\omega,\vec{k})$ . In order to have nontrivial solutions its determinant has to vanish

$$D(\omega,\vec{k}) \equiv Det\left[\left(k^2 - \frac{\omega^2}{c^2}\right)\bar{\bar{I}} - \vec{k}\vec{k} - i\omega\mu_0\bar{\tilde{\sigma}}(\omega,\vec{k})\right] \equiv 0 \tag{2.1.20}$$

It is customary for one to write this equation using the dielectric tensor $\bar{\tilde{\epsilon}}$ instead of the conductivity tensor $\bar{\tilde{\sigma}}$. If one defines the electric induction as

$$\delta\vec{\tilde{D}} \equiv \bar{\tilde{\epsilon}}\cdot\delta\vec{\tilde{E}} \tag{2.1.21}$$

then Ampère's law (equation 2.1.1) can be written as

$$\vec{\nabla} \times \vec{B} \equiv \epsilon_0 \mu_0 \frac{\partial \vec{D}}{\partial t} \tag{2.1.22}$$

and comparing the two equations (2.1.1 and 2.1.22) we get for the dielectric tensor

$$\bar{\epsilon}(\omega, \vec{k}) \equiv \bar{I} + \frac{i}{\omega \epsilon_0} \bar{\sigma}(\omega, \vec{k}) \tag{2.1.23}$$

With this definition equation (2.1.20) becomes

$$Det \left[ \frac{k^2 c^2}{\omega^2} \left( \frac{\vec{k}\vec{k}}{k^2} - \bar{I} \right) + \bar{\epsilon}(\omega, \vec{k}) \right] \equiv 0 \tag{2.1.24}$$

Equation (2.1.24) represents the general dispersion relation of any active medium. The solutions of this equation describe propagating linear waves of frequency $\omega \equiv \omega(\vec{k})$. To solve this equation one must solve the linear dynamic plasma equations and find the dielectric tensor.

### 2.1.3 Cold Plasma Dispersion Relation

In order to illustrate how one can find the dielectric tensor of a plasma we will use an example where the linear dynamic plasma equations are quite simple. Let us consider a cold magnetized electron plasma where the ions are infinitely massive and constitute merely a neutralizing background. In this case the electron dynamics are governed by single-particle motion in a strong magnetic field. If the electrons are cold then we can have $\vec{v}_{0e} \equiv 0$, therefore in the Lorentz force we retain only the linear term $\delta\vec{v} \times \vec{B}_0$. If we use the notation $\vec{\Omega}_e \equiv e\vec{B}_0/m_e$ for the electron gyrofrequency, the parallel and perpendicular (to

$\vec{B}_0$) equations of motion become

$$\frac{d\delta v_{\parallel}}{dt} = -\frac{e}{m_e}\delta E_{\parallel} \tag{2.1.25}$$

$$\frac{d\delta\vec{v}_{\perp}}{dt} = -\frac{e}{m_e}\delta\vec{E}_{\perp} + \vec{\Omega}_e \times \delta\vec{v}_{\perp}. \tag{2.1.26}$$

The relation between the current and the wave velocity in a cold electron plasma is given by:

$$\delta\vec{j} = -en_0\delta\vec{v} = \bar{\sigma}\cdot\delta\vec{E}, \tag{2.1.27}$$

or

$$\delta\vec{v} = -\frac{1}{en_0}\bar{\sigma}\cdot\delta\vec{E} \tag{2.1.28}$$

therefore in order to find $\bar{\sigma}$ we have to solve the system of equations of motion (2.1.25 and 2.1.26). We get for the components of the velocity:

$$\delta v_x = \epsilon_0\omega_{pe}^2\frac{i\omega}{\omega^2-\Omega_e^2}\delta E_x + \epsilon_0\omega_{pe}^2\frac{\Omega_e}{\omega^2-\Omega_e^2}\delta E_y \tag{2.1.29}$$

$$\delta v_y = -\epsilon_0\omega_{pe}^2\frac{\Omega_e}{\omega^2-\Omega_e^2}\delta E_x + \epsilon_0\omega_{pe}^2\frac{i\omega}{\omega^2-\Omega_e^2}\delta E_y \tag{2.1.30}$$

$$\delta v_z = \epsilon_0\omega_{pe}^2\frac{i}{\omega}\delta E_z \tag{2.1.31}$$

where

$$\omega_{pe} = \sqrt{\frac{n_e e^2}{\epsilon_0 m_e}} \tag{2.1.32}$$

is the electron plasma frequency. Comparing these equations with equation (2.1.28) we find the components of the conductivity tensor:

$$\sigma_{xx} \equiv \sigma_{yy} \equiv \epsilon_0 \omega_{pe}^2 \frac{i\omega}{\omega^2 - \Omega_e^2}$$

$$\sigma_{xy} \equiv -\sigma_{yx} \equiv \epsilon_0 \omega_{pe}^2 \frac{\Omega_e}{\omega^2 - \Omega_e^2}$$

$$\sigma_{xz} \equiv \sigma_{yz} \equiv \sigma_{zx} \equiv \sigma_{zy} \equiv 0$$

$$\sigma_{zz} \equiv \epsilon_0 \omega_{pe}^2 \frac{i}{\omega}$$

or

$$\bar{\bar{\sigma}}(\omega) \equiv \epsilon_0 \omega_{pe}^2 \begin{pmatrix} \frac{i\omega}{\omega^2 - \Omega_e^2} & \frac{\Omega_e}{\omega^2 - \Omega_e^2} & 0 \\ -\frac{\Omega_e}{\omega^2 - \Omega_e^2} & \frac{i\omega}{\omega^2 - \Omega_e^2} & 0 \\ 0 & 0 & \frac{i}{\omega} \end{pmatrix} \tag{2.1.33}$$

Using the definition (2.1.23) for the dielectric tensor we can easily find for the dielectric tensor of a cold plasma

$$\bar{\bar{\epsilon}}_{cold}(\omega) \equiv \begin{pmatrix} 1 + \frac{\omega_{pe}^2}{\Omega_e^2 - \omega^2} & -\frac{i\Omega_e}{\omega} \frac{\omega_{pe}^2}{\Omega_e^2 - \omega^2} & 0 \\ \frac{\Omega_e}{\omega} \frac{\omega_{pe}^2}{\Omega_e^2 - \omega^2} & 1 + \frac{\omega_{pe}^2}{\Omega_e^2 - \omega^2} & 0 \\ 0 & 0 & 1 - \frac{\omega_{pe}^2}{\omega^2} \end{pmatrix} \tag{2.1.34}$$

Inserting this into equation (2.1.24) we get the cold electron plasma dispersion relation

$$Det\left[\frac{k^2c^2}{\omega^2}\left(\bar{\bar{I}}-\frac{\vec{k}\vec{k}}{k^2}\right)-\bar{\bar{\epsilon}}_{cold}\right]=0 \tag{2.1.35}$$

We can rewrite the cold plasma dielectric tensor (2.1.34) in a shorthand version

$$\bar{\bar{\epsilon}}_{cold}\equiv\begin{pmatrix}\epsilon_1 & -i\epsilon_2 & 0\\ i\epsilon_2 & \epsilon_1 & 0\\ 0 & 0 & \epsilon_3\end{pmatrix} \tag{2.1.36}$$

where the matrix components are defined as

$$\epsilon_1 \equiv 1-\frac{\omega_{pe}^2}{\omega^2-\Omega_e^2} \tag{2.1.37}$$

$$\epsilon_2 \equiv -\frac{i\Omega_e}{\omega}\frac{\omega_{pe}^2}{\omega^2-\Omega_e^2} \tag{2.1.38}$$

$$\epsilon_3 \equiv 1-\frac{\omega_{pe}^2}{\omega^2} \tag{2.1.39}$$

Defining the vectorial refractive index as $\vec{N}\equiv\vec{k}c/\omega$, with $N^2\equiv N_\perp^2+N_\parallel^2$, and assuming that the wave vector $\vec{k}$ is in the $(x,z)$ plane, the cold plasma dispersion relation (2.1.35)

becomes

$$Det\begin{pmatrix} N_{\|}^2-\epsilon_1 & i\epsilon_2 & -N_{\|}N_{\perp} \\ -i\epsilon_2 & N^2-\epsilon_1 & 0 \\ -N_{\|}N_{\perp} & 0 & N_{\perp}^2-\epsilon_3 \end{pmatrix}=0 \qquad (2.1.40)$$

This relation is the basic dispersion relation for a cold electron plasma and it describes the propagation of high frequency waves in such a plasma [Baumjohann and Treumann, 1996].

### 2.1.4 Two Fluid Plasma Waves

At frequencies intermediate between the magnetohydrodynamic and high-frequency electron waves (frequencies comparable to the ion-cyclotron frequency, $\omega \cong \Omega_i$) one cannot anymore neglect the ion dynamics. The ion motion will be described by a set of equations similar to the ones for the electron, equations (2.1.25 and 2.1.26). Solving for the ion velocities $\delta\vec{v}_i$ as functions of the electric field $\delta\vec{E}$ and using a modified relation between the current and the velocities to include the ion contribution

$$\delta\vec{j} = en_0(\delta\vec{v}_i - \delta\vec{v}_e) = \bar{\bar{\sigma}}\cdot\delta\vec{E}, \qquad (2.1.41)$$

we obtain an equivalent expression (equation 2.1.36) for the dielectric tensor of a cold two-fluid plasma, with the matrix elements containing the contribution of the ions in an additive

way

$$\epsilon_1 \equiv 1 - \frac{\omega_{pe}^2}{\omega^2 - \Omega_e^2} - \frac{\omega_{pi}^2}{\omega^2 - \Omega_i^2} \tag{2.1.42}$$

$$\epsilon_2 \equiv -\frac{i\Omega_e}{\omega}\frac{\omega_{pe}^2}{\omega^2 - \Omega_e^2} + \frac{i\Omega_i}{\omega}\frac{\omega_{pi}^2}{\omega^2 - \Omega_i^2} \tag{2.1.43}$$

$$\epsilon_3 \equiv 1 - \frac{\omega_{pe}^2}{\omega^2} - \frac{\omega_{pi}^2}{\omega^2} \tag{2.1.44}$$

**Parallel Wave Propagation** $N_\perp$ vanishes in the case of parallel propagation, therefore the dispersion relation becomes

$$N_{R,L}^2 \equiv 1 - \frac{\omega_{pe}^2}{\omega(\omega \mp \Omega_e)} - \frac{\omega_{pi}^2}{\omega(\omega \pm \Omega_i)} \tag{2.1.45}$$

This dispersion relation has cut-offs for $N_\parallel \Rightarrow 0$, and they can be found by setting equation (2.1.45) to zero and solving for $\omega$. The R-mode has the resonance $N_{\parallel R} \Rightarrow \infty$ at the electron-cyclotron frequency

$$\omega_{R,res} \equiv \Omega_e. \tag{2.1.46}$$

while the L-mode also has a resonance (as opposed to a pure electron plasma) at the ion-cyclotron frequency, called the left-hand ion-cyclotron resonance frequency

$$\omega_{L,res} \equiv \Omega_i. \tag{2.1.47}$$

The dispersion relation for the L-mode at low frequencies can be written as

$$\omega \equiv \frac{\Omega_e}{2}\left(1 + \frac{\omega_{pe}^2}{k^2c^2}\right)^{-1}\left[\left(1 + \frac{4\omega_{pi}^2}{k^2c^2}\right)^{1/2} - 1\right]. \tag{2.1.48}$$

The long-wavelength limit is an *Alfvén* wave.

## 2.2 Wave Kinetic Theory. Ion Cyclotron Waves in a Hot Magnetized Plasma

In kinetic plasma wave theory the microscopic electric charge separation fields and particle currents become important, therefore the dispersive properties of the plasma will look rather complicated. In contrast to the fluid theory of plasma waves, the wave kinetic theory explicitly takes care of the properties of the particle distribution function and of the correlations between particles and fields. Hence, in this theory, entirely new effects that cannot be covered by the fluid approach to a plasma will appear. Because in wave kinetic theory we are dealing with distribution functions and their evolution, the set of mass, momentum and energy conservation equations of fluid theory is replaced by the set of Vlasov equations for the different components of the plasma while the field equations remain the same. This implies that the formal structure of the general linear wave dispersion relation (2.1.24) remains unchanged and the only quantity that is replaced is the dielectric tensor, $\bar{\bar{\epsilon}}(\omega, \vec{k})$, because it contains the particle dynamics.

To derive the Vlasov equation we consider a classical system containing N identical particles of charge Ze and mass m in a volume V [Ichimaru, 1992, Kaufman, 1997]. Each particle has a time dependent position $\vec{r}(t)$ and velocity $\vec{v}(t)$, therefore each particle represents a point in the phase space $(\vec{r}, \vec{v})$. We can express the exact number density of each particle as a product of delta functions:

$$\mathcal{F}_i(\vec{r}, \vec{v}, t) \equiv \delta(\vec{r} - \vec{r}_i(t))\delta(\vec{v} - \vec{v}_i(t)). \tag{2.2.1}$$

The total exact particle density function of the plasma is the sum over all single exact

particle densities given by equation (2.2.1)

$$\mathcal{F}(\vec{r},\vec{v},t) \equiv \sum_i \delta(\vec{r}-\vec{r}_i(t))\delta(\vec{v}-\vec{v}_i(t)). \tag{2.2.2}$$

$\mathcal{F}$ is called the Klimontovich distribution function, and it satisfies the continuity equation in phase space:

$$\frac{d\mathcal{F}}{dt} \equiv \frac{\partial \mathcal{F}}{\partial t} + \dot{\vec{r}}\cdot\frac{\partial \mathcal{F}}{\partial \vec{r}} + \dot{\vec{v}}\cdot\frac{\partial \mathcal{F}}{\partial \vec{v}} \equiv 0. \tag{2.2.3}$$

Equation (2.2.3) is simply a shorthand notation of Hamilton's equations of motion for N particles. The term $\dot{\vec{v}}$ represents the acceleration arising from Lorentz forces acting on a particle due to microscopic electromagnetic fields $\vec{E}_m(\vec{r},t)$ and $\vec{B}_m(\vec{r},t)$:

$$\dot{\vec{v}} \equiv \frac{Ze}{m}\left[\vec{E}_m(\vec{r},t) + \vec{v}\times\vec{B}_m(\vec{r},t)\right]. \tag{2.2.4}$$

With this equation (2.2.3) becomes:

$$\frac{d\mathcal{F}}{dt} \equiv \frac{\partial \mathcal{F}}{\partial t} + \vec{v}\cdot\frac{\partial \mathcal{F}}{\partial \vec{r}} + \frac{Ze}{m}\left[\vec{E}_m(\vec{r},t) + \vec{v}\times\vec{B}_m(\vec{r},t)\right]\cdot\frac{\partial \mathcal{F}}{\partial \vec{v}} \equiv 0. \tag{2.2.5}$$

Equation (2.2.5) is the evolution equation of the exact particle density in phase space and it is called the Klimontovich equation. We can define an ensemble averaged phase space density $\langle\mathcal{F}(\vec{r},\vec{v},t)\rangle \equiv f(\vec{r},\vec{v},t)$ and express the exact phase space density as the sum of this average and a fluctuation $\delta\mathcal{F}$:

$$\mathcal{F}(\vec{r},\vec{v},t) \equiv f(\vec{r},\vec{v},t) + \delta\mathcal{F}(\vec{r},\vec{v},t), \tag{2.2.6}$$

where the ensemble average of the fluctuations is equal to zero, $\langle\delta\mathcal{F}\rangle \equiv 0$. In a similar way

the fields can be expressed as their averages plus their fluctuations:

$$\vec{E}_m(\vec{r},t) \equiv \vec{E}(\vec{r},t) + \delta\vec{E}(\vec{r},t) \tag{2.2.7}$$

$$\vec{B}_m(\vec{r},t) \equiv \vec{B}(\vec{r},t) + \delta\vec{B}(\vec{r},t) \tag{2.2.8}$$

with $\left\langle \delta\vec{E}(\vec{r},t) \right\rangle \equiv 0$ and $\left\langle \delta\vec{B}(\vec{r},t) \right\rangle \equiv 0$. We can now take the ensemble average of the Klimontovich equation (2.2.5) to obtain:

$$\frac{\partial f}{\partial t} + \vec{v}\cdot\frac{\partial f}{\partial \vec{r}} + \frac{Ze}{m}(\vec{E} + \vec{v}\times\vec{B})\cdot\frac{\partial f}{\partial \vec{v}} \equiv -\frac{Ze}{m}\left\langle (\delta\vec{E} + \vec{v}\times\delta\vec{B})\cdot\frac{\partial \delta F}{\partial \vec{v}} \right\rangle . \tag{2.2.9}$$

We can simplify this kinetic equation by neglecting the correlations between the fields and considering only the correlations between the particles themselves via collision:

$$\frac{\partial f}{\partial t} + \vec{v}\cdot\frac{\partial f}{\partial \vec{r}} + \frac{Ze}{m}(\vec{E} + \vec{v}\times\vec{B})\cdot\frac{\partial f}{\partial \vec{v}} \equiv \left(\frac{\partial f}{\partial t}\right)_c . \tag{2.2.10}$$

Equation (2.2.10) is the generalized Boltzmann equation from statistical mechanics. Space plasmas are collisionless in most of the cases (except for the lower ionosphere), therefore we can entirely neglect the collision term:

$$\frac{\partial f}{\partial t} + \vec{v}\cdot\frac{\partial f}{\partial \vec{r}} + \frac{Ze}{m}(\vec{E} + \vec{v}\times\vec{B})\cdot\frac{\partial f}{\partial \vec{v}} = 0 \tag{2.2.11}$$

Equation (2.2.11) is called the Vlasov equation and it represents the simplest possible form of kinetic equation for a plasma. The Vlasov equation for a particle species $\sigma$ can be written as:

$$\left\{\frac{\partial}{\partial t} + \vec{v}\cdot\frac{\partial}{\partial \vec{r}} + \frac{Z_\sigma e}{m_\sigma}\left[\vec{E}(\vec{r},t) + \vec{v}\times\vec{B}(\vec{r},t)\right]\cdot\frac{\partial}{\partial \vec{v}}\right\} f_\sigma(\vec{r},\vec{v},t) = 0 \tag{2.2.12}$$

The local number density and the current density can be written as:

$$n_\sigma(\vec{r},t) \equiv n_\sigma \int d\vec{v} f_\sigma(\vec{r},\vec{v},t) \tag{2.2.13}$$

$$\delta\vec{j} \equiv \sum_\sigma Z_\sigma e n_\sigma \int d\vec{v}\vec{v} f_\sigma(\vec{v}) \tag{2.2.14}$$

where $n_\sigma \equiv N_\sigma/V$ is the average number density of particles. Once we find the current density $\vec{j}$, we can calculate the dielectric tensor using equations (2.1.10) and (2.1.23). Consider an homogeneous plasma in a stationary state characterized by the velocity distribution functions $f_\sigma(\vec{v})$, to which we apply a constant external magnetic field, $\vec{B} \equiv B\hat{z}$. We apply an electric field disturbance of the form

$$\delta\vec{E}\exp[i(\vec{k}\cdot\vec{r}-\omega t)] \tag{2.2.15}$$

The magnetic disturbance associated with this can be found using equation (2.1.2):

$$\delta\vec{B}\exp[i(\vec{k}\cdot\vec{r}-\omega t)] \equiv \frac{\vec{k}}{\omega}\times\delta\vec{E}\exp[i(\vec{k}\cdot\vec{r}-\omega t)]. \tag{2.2.16}$$

In response to these disturbances, the distribution functions depart from their stationary values; the resultant distributions may be written as:

$$f_\sigma(\vec{v}) + \delta f_\sigma(\vec{v})\exp[i(\vec{k}\cdot\vec{r}-\omega t)] \tag{2.2.17}$$

Substituting equations (2.2.15), (2.2.16) and (2.2.17) in the Vlasov equation (2.2.12) and retaining only the linear terms in $\delta\vec{E}$ and $\delta f_\sigma(\vec{v})$, we find

$$\left[\frac{\partial}{\partial t}+\vec{v}\cdot\frac{\partial}{\partial\vec{r}}+\Omega_\sigma\vec{v}\times\hat{z}\cdot\frac{\partial}{\partial\vec{v}}\right]\delta f_\sigma(\vec{v})\exp[i(\vec{k}\cdot\vec{r}-\omega t)]$$

$$= -\frac{Z_\sigma e}{m_\sigma}\frac{\partial f_\sigma}{\partial\vec{v}}\cdot\vec{\vec{T}}(\vec{k},\omega;\vec{v})\cdot\delta\vec{E}\exp[i(\vec{k}\cdot\vec{r}-\omega t)]. \tag{2.2.18}$$

where

$$\vec{\Omega}_\sigma \equiv \frac{Z_\sigma c \vec{\vec{B}}}{m_\sigma} \tag{2.2.19}$$

is the cyclotron frequency for a particle of the $\sigma$ species, and

$$\vec{\vec{T}}(\vec{k}, \omega; \vec{v}) \equiv \left(1 - \frac{\vec{k} \cdot \vec{v}}{\omega}\right) \vec{\vec{I}} + \frac{\vec{k}\vec{v}}{\omega} \tag{2.2.20}$$

is a tensor that enables one to express the electromagnetic effects in terms of $\delta \vec{\vec{E}}$ alone.

The calculation of the increment $\delta f_\sigma(\vec{v})$ from equation (2.2.18) is difficult because of the spiral orbits of the particles in the magnetic field. Consider a differential operator defined as

$$\frac{d}{dt} \equiv \frac{\partial}{\partial t} + \frac{d\vec{r}}{dt} \cdot \frac{\partial}{\partial \vec{r}} + \frac{d\vec{v}}{dt} \cdot \frac{\partial}{\partial \vec{v}} \tag{2.2.21}$$

where $\vec{r} \equiv \vec{r}(t)$ and $\vec{v} \equiv \vec{v}(t)$ describe a given trajectory of a particle in phase space $(\vec{r}, \vec{v})$. Notice that equation (2.2.21) represents a differentiation with respect to time along the prescribed particle orbit in phase space. Vectors $d\vec{r}/dt$ and $d\vec{v}/dt$ are the velocity and the acceleration of the particle. If we choose

$$\frac{d\vec{r}}{dt} = \vec{v} \tag{2.2.22}$$

$$\frac{d\vec{v}}{dt} = \Omega_\sigma \vec{v} \times \hat{z}, \tag{2.2.23}$$

the phase space position of the particle $(\vec{r}', \vec{v}')$, at a time $t'$, can be expressed as

$$\vec{v}' = \vec{\vec{B}}_\sigma(t - t') \cdot \vec{v}, \tag{2.2.24}$$

$$\vec{r}' = \vec{r} + \frac{1}{\Omega_\sigma} \vec{\vec{H}}_\sigma(t - t') \cdot \vec{v}, \tag{2.2.25}$$

where we implied the aid of the tensors

$$\bar{\bar{H}}_\sigma(t) \equiv \begin{pmatrix} \sin\Omega_\sigma t & 1-\cos\Omega_\sigma t & 0 \\ -(1-\cos\Omega_\sigma t) & \sin\Omega_\sigma t & 0 \\ 0 & 0 & \Omega_\sigma t \end{pmatrix}, \tag{2.2.26}$$

$$\bar{\bar{B}}_\sigma(t) \equiv \frac{1}{\Omega_\sigma}\frac{d\bar{\bar{H}}_\sigma(t)}{dt} \equiv \begin{pmatrix} \cos\Omega_\sigma t & \sin\Omega_\sigma t & 0 \\ -\sin\Omega_\sigma t & \cos\Omega_\sigma t & 0 \\ 0 & 0 & 1 \end{pmatrix}. \tag{2.2.27}$$

Notice that the differential operators on the left hand side of equation (2.2.18) altogether describe a time differentiation along the unperturbed orbit (2.2.24) and (2.2.25). We may invert this differentiation by integrating equation (2.2.18) with respect to time along the unperturbed particle trajectory as

$$\delta f_\sigma(\vec{v})\exp[i(\vec{k}\cdot\vec{r}-\omega t)]$$

$$\equiv -\frac{Z_\sigma e}{m_\sigma}\int_{-\infty}^{t} dt'\left[\frac{\partial f_\sigma(\vec{v}')}{\partial \vec{v}'}\right]\cdot\bar{\bar{T}}(\vec{k},\omega;\vec{v}')\cdot\delta\vec{E}\exp[i(\vec{k}\cdot\vec{r}'-\omega t')], \tag{2.2.28}$$

or

$$\delta f_\sigma(\vec{v}) \equiv -\frac{Z_\sigma e}{m_\sigma}\int_{0}^{\infty} d\tau\left[\frac{\partial f_\sigma(\vec{v}')}{\partial \vec{v}'}\right]\cdot\bar{\bar{T}}(\vec{k},\omega;\vec{v}')\cdot\delta\vec{E}\exp[-i\phi(\tau)] \tag{2.2.29}$$

where

$$\phi(\tau) \equiv \vec{k}\cdot(\vec{r}-\vec{r}') - \omega\tau$$

$$\tau \equiv t - t'.$$

The evaluation of the integral in equation (2.2.29) leads to the calculation of the induced current density (2.2.14) and thereby the dielectric tensor via equations (2.1.10) and (2.1.23).

### 2.2.1 The Dielectric Tensor

In order to obtain the dielectric tensor we have to perform the velocity space integral in equation (2.2.14). The integration is performed in cylindrical coordinates in velocity space, with the $z$ axis along the direction of the external magnetic field, Figure (2-1). The unperturbed velocity distribution functions $f_\sigma(\vec{v})$ in equation (2.2.29) may be written as functions of the components $v_\parallel$ and $v_\perp$ of the velocity, parallel and perpendicular to the external magnetic field. Let us set

$$\vec{v} \equiv v_\perp\cos\theta\hat{x} + v_\perp\sin\theta\hat{y} + v_\parallel\hat{z}. \tag{2.2.30}$$

Equation (2.2.24) then becomes

$$v'_x \equiv v_\perp\cos(\Omega_\sigma\tau + \theta)$$

$$v'_y \equiv v_\perp\sin(\Omega_\sigma\tau + \theta)$$

$$v'_z \equiv v_\parallel.$$

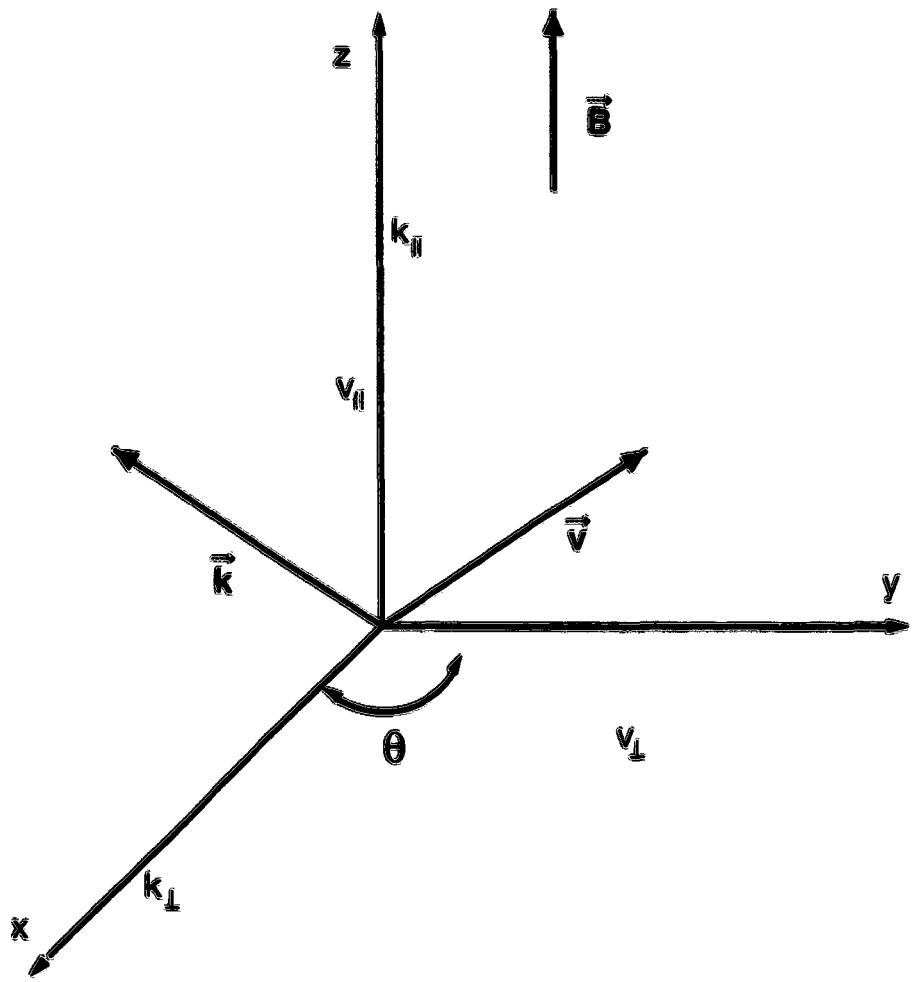


Figure 2-1: Configuration of various vectors

Now we can calculate the induced current density (2.2.14) as

$$\delta\vec{j} = -\sum_{\sigma} \frac{(Z_\sigma e)^2 n_\sigma}{m_\sigma} \int_0^{2\pi} d\theta \int_0^{\infty} v_\perp dv_\perp \int_{-\infty}^{\infty} dv_\parallel$$

$$\int_0^{\infty} d\tau \vec{v} \left[\frac{\partial f_\sigma(\vec{v})}{\partial \vec{v}}\right] \cdot \bar{\bar{T}}(\vec{k},\omega;\vec{v}) \cdot \delta\vec{E} \exp[-i\phi(\tau)] \qquad (2.2.31)$$

and the dielectric tensor

$$\bar{\bar{\epsilon}}(\vec{k},\omega) \equiv \bar{\bar{I}} + \sum_{\sigma} \frac{\omega_{\sigma}^2}{i\omega} \int_0^{2\pi} d\theta \int_0^{\infty} v_{\perp} dv_{\perp} \int_{-\infty}^{\infty} dv_{\parallel}$$

$$\int_0^{\infty} d\tau \, \vec{v} \left[ \frac{\partial f_{\sigma}(\vec{v}')}{\partial \vec{v}'} \right] \cdot \bar{\bar{T}}(\vec{k},\omega;\vec{v}') \cdot \delta\vec{E} \exp[-i\phi(\tau)]. \qquad (2.2.32)$$

To carry out the integrations we specifically choose the wave vector $\vec{k}$ to be in the $x = z$ plane (Figure 2-1), and write

$$\vec{k} \equiv k_{\perp}\hat{x} + k_{\parallel}\hat{z}. \qquad (2.2.33)$$

After a substantial amount of algebra ([Stix, 1992]) we find

$$\bar{\bar{\epsilon}}(\vec{k},\omega) \equiv \left(1 - \frac{\omega_p^2}{\omega^2}\right) \bar{\bar{I}} - \sum_{\sigma} \frac{\omega_{\sigma}^2}{\omega^2} \sum_{n=-\infty}^{\infty} \int d\vec{v} \left( \frac{n\Omega_{\sigma}}{v_{\perp}} \frac{\partial f_{\sigma}}{\partial v_{\perp}} + k_{\parallel} \frac{\partial f_{\sigma}}{\partial v_{\parallel}} \right) \frac{\bar{\bar{\Pi}}_{\sigma}(v_{\perp}, v_{\parallel}; n)}{n\Omega_{\sigma} + k_{\parallel} v_{\parallel} = \omega} \qquad (2.2.34)$$

where

$$\bar{\bar{\Pi}}_\sigma(v_\perp, v_\parallel; n) \equiv \begin{pmatrix} \frac{n^2\Omega_\sigma^2}{k_\perp^2} J_n^2 & iv_\perp \frac{n\Omega_\sigma}{k_\perp} J_n J_n' & v_\parallel \frac{n\Omega_\sigma}{k_\perp} J_n^2 \\ -iv_\perp \frac{n\Omega_\sigma}{k_\perp} J_n J_n' & v^2 (J_n')^2 & -iv_\parallel v_\perp J_n J_n' \\ v_\parallel \frac{n\Omega_\sigma}{k_\perp} J_n^2 & iv_\parallel v_\perp J_n J_n' & v_\parallel^2 J_n^2 \end{pmatrix},$$

$$\int d\bar{v} \equiv 2\pi \int_0^\infty v_\perp dv_\perp \int_{-\infty}^{\infty} dv_\parallel$$

$$J_n \equiv J_n(z), \qquad J_n' \equiv \frac{dJ_n(z)}{dz}, \qquad z \equiv \frac{k_\perp v_\perp}{\Omega_\sigma}$$

$$\omega_p^2 \equiv \sum_\sigma \omega_\sigma^2, \qquad \omega_\sigma \equiv \left( \frac{n_\sigma Z_\sigma^2 e^2}{m_\sigma \epsilon_0} \right)^{\frac{1}{2}}$$

Equation (2.2.34) represents the dielectric tensor for a general hot magnetized plasma.

**The Dielectric Response Function** The dielectric response function of a plasma is defined as

$$\epsilon(\bar{k}, \omega) \equiv \frac{\bar{k} \cdot \bar{\bar{\epsilon}}(\bar{k}, \omega) \cdot \bar{k}}{k^2}, \tag{2.2.35}$$

therefore we can express it using equation (2.2.34) as

$$\epsilon(\bar{k}, \omega) \equiv 1 - \sum_\sigma \frac{\omega_\sigma^2}{k^2} \sum_{n=-\infty}^{\infty} \int d\bar{v} \left( \frac{n\Omega_\sigma}{v_\perp} \frac{\partial f_\sigma}{\partial v_\perp} + k_\parallel \frac{\partial f_\sigma}{\partial v_\parallel} \right) \frac{J_n(z)}{n\Omega_\sigma + k_\parallel v_\parallel - \omega}. \tag{2.2.36}$$

This is the Vlasov dielectric response function and it describes the dielectric properties of the plasma. Equation (2.2.36) can be further simplified by specifying the distribution

functions $f_\sigma(\vec{v})$.

### 2.2.2 Dielectric Response in Maxwellian Plasmas

For simplicity consider a one component plasma with a Maxwellian distribution expressed by

$$f_M(v_\perp, v_\parallel) \equiv \left(\frac{m}{2\pi T}\right)^{3/2} \exp\left[-\frac{m(v_\perp^2 + v_\parallel^2)}{2T}\right]. \tag{2.2.37}$$

After substituting (2.2.37) in equation (2.2.34) we get the expression for the dielectric tensor of the Vlasov plasmas in thermodynamic equilibrium as

$$\bar{\bar{\epsilon}}(\vec{k},\omega) \equiv \bar{\bar{I}} - \left(\frac{\omega_p}{\omega}\right)^2 \left\{ \sum_{n=-\infty}^{\infty} \frac{Z_0}{Z_n} \bar{\bar{\Pi}}(\beta, Z_n; n)[1 - W(Z_n)] - Z_0^2 \hat{z}\hat{z} \right\} \tag{2.2.38}$$

where

$$\bar{\bar{\Pi}}(\beta, Z_n; n) \equiv \begin{pmatrix} \frac{n^2}{\beta}\Lambda_n(\beta) & in\Lambda_n'(\beta) & \frac{k_\parallel}{k_\parallel}\frac{n}{\sqrt{\beta}} Z_n \Lambda_n(\beta) \\ -in\Lambda_n'(\beta) & \frac{n^2}{\beta}\Lambda_n(\beta) - 2\beta\Lambda_n'(\beta) & -i\frac{k_\parallel}{k_\parallel}\sqrt{\beta} Z_n \Lambda_n'(\beta) \\ \frac{k_\parallel}{k_\parallel}\frac{n}{\sqrt{\beta}} Z_n \Lambda_n(\beta) & i\frac{k_\parallel}{k_\parallel}\sqrt{\beta} Z_n \Lambda_n'(\beta) & Z_n^2 \Lambda_n(\beta) \end{pmatrix}$$

$$Z_n \equiv \frac{\omega - n\Omega}{|k_\parallel|\sqrt{T/m}}$$

$$\beta \equiv \frac{k_\perp^2 T}{m\Omega^2}$$

$$\Lambda_n(\beta) \equiv I_n(\beta)\exp(-\beta)$$

The functions $I_n(\beta)$ are the modified Bessel functions of the $n$−th order and the functions $\Lambda_n(\beta)$ appear commonly in a theoretical treatment of Maxwellian plasmas in a magnetic field. For many applications it suffices to evaluate $\Lambda_n(\beta)$ to lowest or perhaps first order in $\beta$.

### 2.2.3 Ion Cyclotron Instability due to Temperature Anisotropy

Temperature anisotropy is one form of deviation, in velocity space, from a thermal distribution. When the energy contained in the cyclotron motion exceeds the energy associated with the parallel motion ($T_{\perp\beta} > T_{\parallel\beta}$), a possibility arises that the energy of the cyclotron motion is fed into the plasma oscillation in the vicinity of the cyclotron frequency ([Kennel and Petschek, 1966]), at $\omega \cong k v_\parallel \pm \Omega_g$. An energy imbalance between the parallel and perpendicular degrees of freedom may be described by assigning two different temperatures, $T_\perp$ and $T_\parallel$, in the velocity distributions:

$$f(v_\perp, v_\parallel) = \left(\frac{m}{2\pi T_\perp}\right)\sqrt{\frac{m}{2\pi T_\parallel}}\exp\left[-\frac{v_\perp^2}{2(T_\perp/m)} - \frac{v_\parallel^2}{2(T_\parallel/m)}\right]. \qquad (2.2.39)$$

Such an anisotropic distribution is more likely to occur in the ions rather than in the electrons, because the relaxation times for the Maxwellization of the electrons are much smaller than the ones for the ions:

$$\tau_{ee} : \tau_{ii} : \tau_{ei} \quad \sim \quad 1 : \sqrt{\frac{m_i}{m_e}} : \frac{m_i}{m_e} \qquad (2.2.40)$$

This makes the use of Maxwellian distributions with unequal ion and electron temperatures reasonable. Also because of this reason, we can assume equation (2.2.39) only for the ions. Using this distribution function in equation (2.2.34) and then using the definition (2.2.35),

we get for the dielectric response function

$$\epsilon(k,\omega) \equiv 1 + \frac{k_e^2}{k^2} W\left(\frac{\omega}{|k_\parallel|\sqrt{T_e/m_e}}\right)$$

$$+ \frac{k_i^2}{k^2}\left\{1 + \sum_n \left(1 + \frac{T_\parallel}{T_\perp}\frac{n\Omega}{\omega - n\Omega}\right)\left[W\left(\frac{\omega - n\Omega}{|k_\parallel|\sqrt{T/m}}\right) - 1\right]\Lambda_n(\beta)\right\} \quad (2.2.41)$$

where ([Ichimaru, 1992])

$$W(z) \equiv 1 - z\exp\left(-\frac{z^2}{2}\right)\int_0^z dy \exp\left(\frac{y^2}{2}\right) + i\sqrt{\frac{\pi}{2}}\, z \exp\left(-\frac{z^2}{2}\right). \quad (2.2.42)$$

Let us assume that the plasma has a mixture of cold electrons, cold protons and hot anisotropic protons. The dispersion relation now has the form

$$D \equiv \frac{k^2c^2}{\omega^2} = \epsilon_{cold} = \epsilon_{hot} \equiv 0. \quad (2.2.43)$$

where $\epsilon_{hot}$ is expressed above in equation (2.2.41) and $\epsilon_{cold} \equiv (\vec{k}\cdot\bar{\bar{\epsilon}}_{cold}\cdot\vec{k})/k^2$ is the dielectric response function for two fluid cold plasma waves, with $\bar{\bar{\epsilon}}_{cold}$ derived earlier, equations (2.1.36), (2.1.42), (2.1.43) and (2.1.44). Equation (2.2.43) determines a complex frequency

$$\omega \equiv \omega_k + i\gamma_k. \quad (2.2.44)$$

For the excitation to be long lived and well defined, the growth rate $\gamma_k(>0)$ has to be much smaller than the real part $\omega_k$ of the frequency ([Ichimaru, 1992]) :

$$\frac{\gamma_k}{\omega_k} \ll 1. \quad (2.2.45)$$

In this case D may have a Taylor expansion near $\omega \equiv \omega_k$, so that

$$D(\omega,\vec{k}) \equiv \left(\frac{\partial Re(D)}{\partial\omega}\right)_{\omega\equiv\omega_k}(\omega - \omega_k + i\gamma_k). \quad (2.2.46)$$

Hence we can find a useful expression for the growth rate near the resonant frequency $\omega_k$:

$$\gamma_k \equiv Im(\omega) \equiv -\frac{Im(D(\omega_k, \vec{k}))}{\left(\frac{\partial Re(D)}{\partial \omega}\right)_{\omega=\omega_k}}. \tag{2.2.47}$$

We find $Im(\omega)$ by noting that the argument of $W$, $(\omega - n\Omega)/(|k_{||}|\sqrt{T/m}) \gg 1$, and consequently using the large argument expansion for $W$ ([Ichimaru, 1992])

$$Im(\omega) \equiv \frac{\sqrt{\pi}\eta\Omega_i[Re(\omega) - \Omega_i]^2}{|k_{||}|\sqrt{T/m}[Re(\omega) - \Omega_i]Re(\omega)}$$

$$\{\Omega_i - (A+1)[Re(\omega) - \Omega_i]\} \exp\left(-\frac{[Re(\omega) - \Omega_i]^2}{k^2(|k_{||}|\sqrt{T/m})^2}\right) \tag{2.2.48}$$

where $i$ denotes the ion species for the hot ions, $\eta$ is the ratio of the number density of hot protons to the plasma number density ($\eta \ll 1$), and

$$A \equiv \frac{T_\perp}{T_{||}} - 1 \tag{2.2.49}$$

is the hot ion anisotropy.

For the R mode (fast or high frequency mode), resonance occurs when $\omega - kv_{||} \equiv -\Omega_i$ and $v_{||} > \omega/k$, indicating that particles moving faster than the phase velocity of the wave are resonant with the wave. The L mode has a resonance at $\omega - kv_{||} \equiv \Omega_i$, and consequently it is limited to frequencies less than $\Omega_i$ in the vicinity of the resonance. The particles must be traveling in the opposite direction to the phase velocity of the wave. The wave grows if

$$A < \frac{-\omega}{\Omega_i + \omega} \tag{2.2.50}$$

for the R mode and

$$A > \frac{\omega}{\Omega_i - \omega} \tag{2.2.51}$$

for the L mode. The R mode is unstable if the hot ions have $T_{\perp} > T_{\parallel}$, whereas the L mode is unstable if $T_{\parallel} > T_{\perp}$. We will see later in this chapter that these conditions do not hold exactly in this form, and there is a more significant form for the temperature anisotropy that yields instability for the mode that we are interested in, the L mode.

## 2.3 Influence of the Solar Wind Dynamic Pressure on the Production of Electromagnetic Ion Cyclotron Waves

One of the many possible ways to deviate from anisotropy in a plasma is to have different temperatures for the parallel and perpendicular (to the magnetic field) degrees of freedom, in other words to have a temperature anisotropy ($T_{\perp} \neq T_{\parallel}$). This will allow the growth of the so-called temperature anisotropy instabilities ([Gary, 1993]). The temperature anisotropy more often observed in space plasmas is the one with $T_{\perp} > T_{\parallel}$. The reason for this is not that perpendicular heating is more likely to occur in space plasmas, but because parallel heated particles leave the region of energization along the ambient magnetic field more quickly. This is not true for the solar corona, where there is recent evidence of preferential perpendicular heating. There are several instabilities that may arise in a plasma with $T_{\perp} \neq T_{\parallel}$ ([Gary et al., 1976]), but the most important ones are the mirror and proton cyclotron instabilities. In an electron-proton plasma under the conditions $T_e \cong T_p$ and $\beta_p \leq 6$, the fastest growing mode is the proton cyclotron anisotropy instability ([Kennel and Petschek, 1966]). This will have a maximum growth along the background magnetic field ($\vec{k} \times \vec{B}_0 \equiv 0$), circular left hand polarization in that direction of propagation, and evolves out of the Alfven proton cyclotron wave if the anisotropy is gradually increased.

The solar wind dynamic pressure is one of the macroscopic forces that can drive the

plasma towards increasing temperature anisotropy. This process can be easily understood if one considers the Chew-Goldberger-Low equations for decoupled parallel and perpendicular degrees of freedom ([Chew et al., 1956]).

### 2.3.1 The CGL Equations

Since the CGL equations play an important role in explaining the production of cyclotron waves, we will sketch their derivation in this subsection ([Hollweg, 1986]). To find the CGL equations we first find a general moment equation for a function of the seven-dimensional space consisting of time, configuration space and velocity space, and then take two particular cases for this function, the parallel and perpendicular (to the magnetic field) kinetic energies of a particle. Let us start from the Boltzmann equation for any plasma species:

$$\frac{\partial f}{\partial t} + \vec{v} \cdot \nabla f + \vec{a} \cdot \frac{\partial f}{\partial \vec{v}} \equiv \frac{\delta f}{\delta t} \tag{2.3.1}$$

where $\vec{a}$ is the acceleration due to the long range forces acting on the plasma (electric, magnetic and gravitational), and the right hand side is the collision term representing the short range forces (Coulomb collisions, wave-particle interactions and other effects not included in $\vec{a}$). The distribution function $f$ is also a function of time, space and velocity ($f \equiv f(\vec{r}, \vec{v}, t)$). The density is defined as

$$n \equiv \int f d^3\vec{v} \tag{2.3.2}$$

where the integral is over the three velocity coordinates. All integrals from here on are defined over the entire velocity space unless otherwise specified. For an arbitrary function $\Psi(\vec{r}, \vec{v}, t)$ we define the average over the velocity space as

$$\langle \Psi \rangle \equiv \frac{1}{n} \int \Psi f d^3\vec{v} \tag{2.3.3}$$

Next we will find a general moment equation satisfied by such a function of time, space and velocity. To do this we multiply the Boltzmann equation (2.3.1) with $\Psi$ and integrate over the velocity space. There are three terms in equation (2.3.1); we will calculate each term separately:

Term I:

$$\int \Psi \frac{\partial f}{\partial t} d^3\vec{v} = \frac{\partial}{\partial t}\int \Psi f d^3\vec{v} = \int f \frac{\partial \Psi}{\partial t} d^3\vec{v} = \frac{\partial n\langle\Psi\rangle}{\partial t} = \left\langle \dot{\Psi} \right\rangle \tag{2.3.4}$$

Term II:

$$\int \Psi \vec{v}\cdot\nabla f d^3\vec{v} = \int \vec{v}\cdot\nabla(\Psi f) d^3\vec{v} = \int f\vec{v}\cdot\nabla\Psi d^3\vec{v}$$

$$= \int \left[\nabla\cdot(\Psi f\vec{v}) - \Psi f\nabla\cdot\vec{v}\right] d^3\vec{v} = n\langle\vec{v}\cdot\nabla\Psi\rangle$$

$$= \nabla\cdot n\langle\Psi\vec{v}\rangle = n\langle\vec{v}\cdot\nabla\Psi\rangle \tag{2.3.5}$$

where we used the fact that $\nabla\cdot\vec{v} = 0$, since $\vec{r}$ and $\vec{v}$ are independent variables.

Term III:

$$\int \vec{a}\cdot\frac{\partial f}{\partial \vec{v}}\Psi d^3\vec{v} = \int \left[\vec{g} + \frac{q}{m}\left(\vec{E} + \vec{v}\times\vec{B}\right)\right]\cdot\left[\frac{\partial(f\Psi)}{\partial\vec{v}} - f\frac{\partial\Psi}{\partial\vec{v}}\right] d^3\vec{v}$$

$$= -n\left(\vec{g} + \frac{q}{m}\vec{E}\right)\cdot\left\langle\frac{\partial\Psi}{\partial\vec{v}}\right\rangle - n\frac{q}{m}\left\langle(\vec{v}\times\vec{B})\cdot\frac{\partial\Psi}{\partial\vec{v}}\right\rangle \tag{2.3.6}$$

Here the term $\int \frac{\partial(f\Psi)}{\partial v} d^3\vec{v}$ has vanished because $(f\Psi) \to 0$ when $v \to \infty$, in other words the behavior of the $f\Psi$ product is dominated by $f$ at large $v$, and $f \to 0$ very rapidly as $v \to \infty$.

We can now write down the general moment equation for an arbitrary function $\Psi(\vec{r}, \vec{v}, t)$:

$$\frac{\partial}{\partial t} n \langle \Psi \rangle = \left\langle \dot{\Psi} \right\rangle + \nabla \cdot n \langle \Psi \vec{v} \rangle - n \langle \vec{v} \cdot \nabla \Psi \rangle - n \left( \vec{g} + \frac{q}{m} \vec{E} \right) \cdot \left\langle \frac{\partial \Psi}{\partial \vec{v}} \right\rangle$$

$$= n \frac{q}{m} \left\langle (\vec{v} \times \vec{B}) \cdot \frac{\partial \Psi}{\partial \vec{v}} \right\rangle \equiv \int \Psi \frac{\delta f}{\delta t} d^3 \vec{v} \qquad (2.3.7)$$

Equation (2.3.7) is an important general equation for the kinetic theory. One can obtain the mass conservation equation by replacing $\Psi \equiv m$, or the momentum equation by replacing $\Psi \equiv m\vec{v}$. We are going to proceed in finding the CGL equations by first letting

$$\Psi \equiv \frac{1}{2} m w_{\parallel}^2 \qquad (2.3.8)$$

The details of this calculation are given in Appendix B. After a significant amount of algebra the moment equation for the parallel particle energy becomes:

$$\frac{d}{dt} \ln \left( \frac{p_{\parallel} B^2}{\rho^3} \right) \equiv \frac{-2}{p_{\parallel}} \nabla \cdot \vec{q}_{\parallel} + \frac{2\rho}{p_{\parallel}} \left\langle w_{\parallel} \vec{w} \cdot (\vec{w} \cdot \nabla \hat{b}) \right\rangle$$

$$+ 2 \frac{\hat{b} \cdot \vec{D}}{B} + \frac{m}{p_{\parallel}} \int \frac{\delta f}{\delta t} \left( w_{\parallel}^2 - \frac{3 p_{\parallel}}{\rho} \right) d^3 \vec{v} \qquad (2.3.9)$$

We will show that in the case of protons all the terms on the right hand side of equation (2.3.9) are small enough so that they can be neglected, in which case we obtain the first of the two CGL equations:

$$\frac{d}{dt} \ln \left( \frac{p_{\parallel} B^2}{\rho^3} \right) \equiv 0, \qquad (2.3.10)$$

or

$$\frac{p_{\parallel} B^2}{\rho^3} \equiv constant \qquad (2.3.11)$$

moving with the flow.

Here are some arguments for neglecting the terms on the right hand side of equation (2.3.9). The first two terms on the right hand side have the dimension of parallel heat flux. Inside the magnetosphere on closed field lines particles mirror between the two hemispheres, therefore the distributions are symmetric with respect to the direction along the field line (around some parallel bulk velocity which doesn't have to be zero). This implies that for every particle moving in one direction along the magnetic field there is a particle moving in the opposite direction with the same velocity in the frame of the bulk motion, therefore the parallel heat flux in the frame of the bulk motion is zero. In the third term of the right hand side the quantity $\vec{\vec{D}}$ is significant only when there is diffusion of the magnetic field, which is not the case for our situation where the field is frozen-in. The plasma that we are interested in is collisionless most of the time, so the last term which represents the collisions can also be neglected for now. We will see later that when there are wave-particle interactions this term will couple the parallel and perpendicular degrees of freedom and this collision term can no longer be neglected.

Let us go back now to equation (2.3.7), and let

$$\Psi \equiv \frac{1}{2} m v_{\perp}^2. \tag{2.3.12}$$

In this case we get an equation that involves the perpendicular pressure (see Appendix B):

$$\frac{d}{dt} \ln\left(\frac{p_{\perp}}{\rho B}\right) = -\frac{\hat{b} \cdot \vec{\vec{D}}}{B} - \frac{1}{p_{\perp}} \left( \nabla \cdot \vec{q}_{\perp} + \rho \left\langle w_{\parallel} \vec{w} \cdot (\vec{w} \cdot \nabla \hat{b}) \right\rangle \right)$$

$$+ \frac{m}{p_{\perp}} \int \left( \frac{w_{\perp}^2}{2} - \frac{p_{\perp}}{\rho} \right) \frac{\delta f}{\delta t} d^3 \vec{v} \tag{2.3.13}$$

For protons we can neglect all the terms on the right hand side of equation (2.3.13) for the

same reasons for which we neglected all the terms on the right hand side of equation (2.3.9). We can now write down the second of the two CGL equations as

$$\frac{d}{dt}\ln\left(\frac{p_\perp}{\rho B}\right) = 0, \tag{2.3.14}$$

or

$$\frac{p_\perp}{\rho B} \equiv constant \tag{2.3.15}$$

moving with the flow.

Equations (2.3.11) and (2.3.15) are the CGL equations ([Chew et al., 1956]) and they represent the one- and two-dimensional gas equivalents of the well known three-dimensional adiabatic equation

$$\frac{p}{\rho^\gamma} \equiv constant \tag{2.3.16}$$

with the adiabatic coefficient $\gamma \equiv (n+2)/n \equiv 5/3$ and number of degrees of freedom $n \equiv 3$. We can rewrite the CGL equation in terms of the parallel and perpendicular temperatures $T_\parallel$ and $T_\perp$, by recalling that $p \sim \rho T$:

$$\frac{d}{dt}\left(\frac{p_\parallel B^2}{\rho^3}\right) \equiv \frac{d}{dt}\left(\frac{T_\parallel B^2}{\rho^2}\right) \equiv 0 \tag{2.3.17}$$

$$\frac{d}{dt}\left(\frac{p_\perp}{\rho B}\right) \equiv \frac{d}{dt}\left(\frac{T_\perp}{B}\right) \equiv 0 \tag{2.3.18}$$

These equations have a simple interpretation. Let us consider a cylindrical flux tube of length $L$ and area $A$ with a constant number of particles $N$. For a "frozen-in" flux tube the product $B \cdot A \equiv constant$, therefore $B \sim A^{-1}$. Because the number of particles $N$ is

fixed we also have $\rho \equiv N(LA)^{-1}$, so now we can rewrite equations (2.3.17) and (2.3.18) by replacing $B$ and $\rho$, as

$$\frac{d}{dt}\left(\frac{T_{\parallel}}{(N/L)^2}\right) \equiv 0 \tag{2.3.19}$$

$$\frac{d}{dt}\left(\frac{T_{\perp}}{(N/A)}\right) \equiv 0 \tag{2.3.20}$$

Let $\rho_1 \equiv N/L$ and $\rho_2 \equiv N/A$ be the one-dimensional density per unit length along the field line and the two-dimensional density per unit area perpendicular to the field line, respectively. With these definitions equations (2.3.17) and (2.3.18) become

$$\frac{d}{dt}\left(\frac{T_{\parallel}}{\rho_1^2}\right) \equiv 0 \tag{2.3.21}$$

$$\frac{d}{dt}\left(\frac{T_{\perp}}{\rho_2}\right) \equiv 0 \tag{2.3.22}$$

which are the appropriate adiabatic equations ($T/\rho^{\gamma-1} \equiv constant$) for a one- and two-dimensional gas. Thus equations (2.3.17) and (2.3.18) represent adiabatic equations of state for the decoupled parallel and perpendicular dimensions, and they are often called the double-adiabatic equations of state.

### 2.3.2 Increase of the Temperature Anisotropy

In this subsection we are going to use the CGL equations (2.3.17 and 2.3.18) to show how the temperature anisotropy of the hot proton populations will increase when the magnetosphere is compressed. Let us consider a flux tube inside the magnetosphere that contains a distribution of hot protons with the initial parallel and perpendicular temperatures $T_{\parallel i}$

and $T_{\perp 1}$ respectively. The initial length of the flux tube is $L_1$, the cross section area is $A_1$ and the total number of particles is assumed to be constant $N$. After the compression the tube will be squeezed ($A_2 < A_1$), like in Figure (2-2). The tube could also be elongated ($L_2 > L_1$), but this is not necessary for the increase of temperature anisotropy, as we will see next.

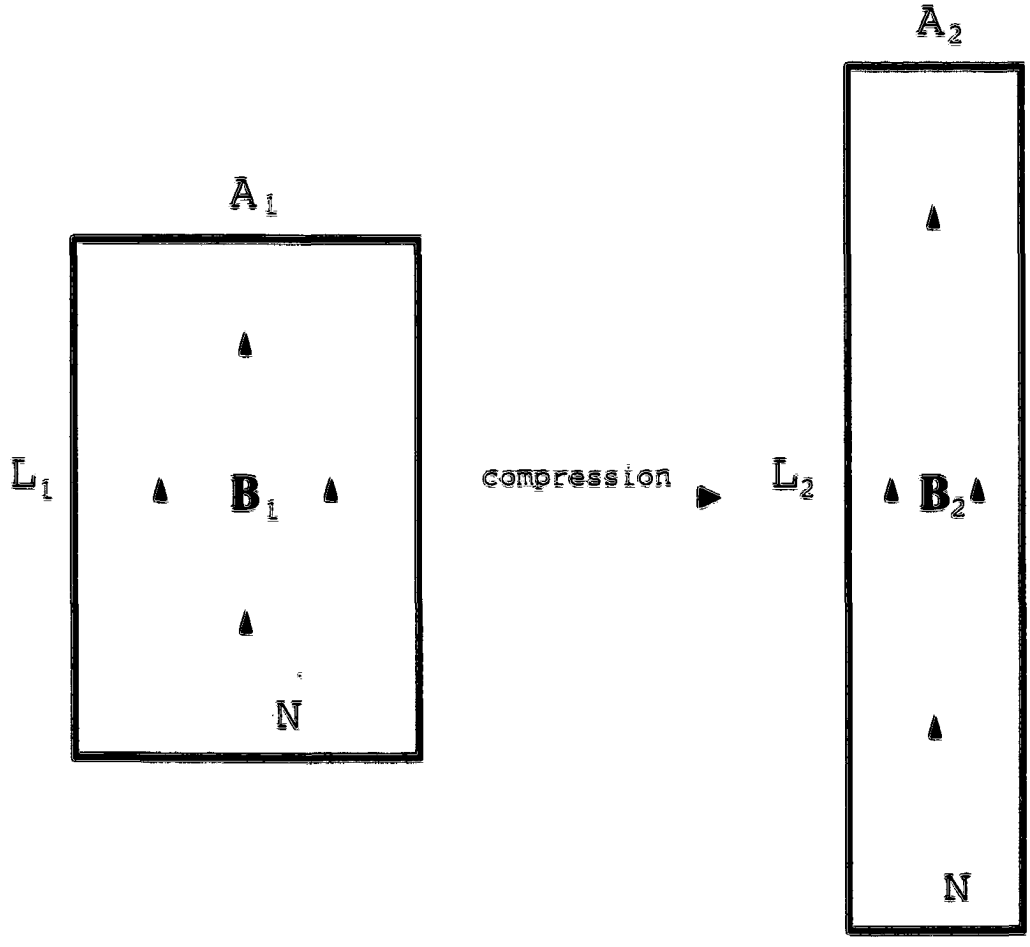


Figure 2-2: The result of a magnetospheric compression on a flux tube inside the magnetosphere: the tube is squeezed ($A_2 < A_1$) and elongated ($L_2 > L_1$).

$T_\perp$. If the field is "frozen-in" then $B \cdot A \equiv constant$, hence $B \sim A^{-1}$, but from (2.3.17) we have $T_\perp \sim B$, therefore

$$T_\perp \sim B \sim A^{-1} \tag{2.3.23}$$

and since $A_2 < A_1$ we get that

$$T_{\perp 2} > T_{\perp 1} \tag{2.3.24}$$

so the compression of the flux tube increases the perpendicular temperature of the hot proton distribution.

$T_\parallel$. We assumed that the total number of particles inside the flux tube remains constant during the compression. This implies that the number density of the particles inside the flux tube varies inversely proportional with the volume of the tube $\rho \sim (L \cdot A)^{-1} \sim L^{-1}B$ (after using $B \cdot A \equiv constant$). Now use equation (2.3.17) to get

$$T_\parallel \sim \rho^2 B^{-2} \sim L^{-2} \tag{2.3.25}$$

and since $L_2 > L_1$ we get that

$$T_{\parallel 2} < T_{\parallel 1} \tag{2.3.26}$$

The consequence of the elongation of the flux tube is the decrease of the parallel temperature of the protons inside the tube. We conclude that a compression of the magnetosphere will result into an increase of the inner-magnetospheric hot proton distributions temperature anisotropy:

$$A_2 \equiv \frac{T_{\perp 2}}{T_{\parallel 2}} - 1 > A_1 \equiv \frac{T_{\perp 1}}{T_{\parallel 1}} - 1. \tag{2.3.27}$$

### 2.3.3 Production Mechanism of Proton Cyclotron Waves. Current Understanding

We have seen so far that the compression of the magnetosphere due to some external cause (like the solar wind dynamic pressure) will result in increased temperature anisotropy of the magnetospheric hot proton populations. These proton populations are of solar wind origin and they drift from the plasma sheet to the outer magnetosphere on open drift paths. The next question to answer is how long this process can go on, or how much the temperature anisotropy can be increased. In section (2.2.3) we have shown that the proton cyclotron mode becomes unstable for hot proton populations with positive temperature anisotropy, $A_p \equiv T_\perp/T_\parallel - 1 > 0$. Hence we expect that at some threshold anisotropy, $A_p \equiv A_{pt}$, the production of cyclotron waves will start and further increase of the temperature anisotropy will be limited by the pitch angle scattering of the protons by the cyclotron waves. The physical meaning of this phenomenon is illustrated in Figure (2-3). This type of diagram was first introduced by [Dusenbery and Hollweg, 1981]. The orange ellipses represent contour plots of proton phase space densities in $v_\parallel - v_\perp$ space. Consider a proton cyclotron wave traveling in the positive $v_\parallel$ direction with the phase velocity $v_{ph} \equiv \omega/k$. In the frame of the wave protons can move along lines of equal energy represented by the green circles centered at $(v_\parallel \equiv \omega/k,\ v_\perp \equiv 0)$. Let us consider two points on a line of equal kinetic energy in the wave frame, points $A$ and $B$. Point $A$ is situated on a contour of higher density than point $B$, therefore there are more particles at point $A$ in phase space than there are at point $B$. This density gradient between $A$ and $B$ will be the driver for the diffusion of particles in the direction from $A$ to $B$, indicated by the arrow. This phenomenon is called pitch angle

diffusion or pitch angle scattering (the pitch angle of particles, $\arctan(v_\perp/v_\parallel)$, decreases when moving from $A$ to $B$). Note that in the process of pitch angle diffusion, the protons, even though they move on circles of constant energy in the frame of the wave, they move closer to the origin in phase space, therefore they lose energy. This energy is picked up by the wave. In this interpretation the wave will grow as long as there are more particles with higher pitch angle on circles of equal energy in the frame of the wave. The temperature anisotropy provides the free energy for the proton cyclotron instability, and the pitch angle scattering will act towards reducing the anisotropy.

In general plasma instabilities will grow in the presence of a strong plasma anisotropy; the resulting enhanced fluctuations will scatter the particles so as to reduce that anisotropy. If a macroscopic driving force continually pushes the plasma toward increased anisotropy, the microscopic action to reduce this anisotropy can lead to a relatively steady state balance which corresponds to the instability threshold ([Manheimer & Boris, 1977]). For relatively homogeneous space plasmas this threshold represents a limited closure relation for the truncation of the fluid equations. This closure relation is limited in the sense that it is not valid under all conditions, but it only represents a bound for the parameter of concern (the temperature anisotropy).

This kind of relationship was first observed in the highly compressed terrestrial magnetosheath. [Anderson et al., 1994] have shown that the proton temperature anisotropy well satisfies an inverse correlation with the proton parallel $\beta$ of the form

$$\frac{T_{\perp p}}{T_{\parallel p}} - 1 \equiv \frac{0.85}{\beta_{\parallel p}^{0.48}} \tag{2.3.28}$$

where $\beta_{\parallel p} \equiv 8\pi n_p T_{\parallel p}/B^2$. Linear Vlasov theory has been used to show that such a re-

lationship corresponds to the threshold condition of the electromagnetic proton cyclotron anisotropy instability ([Gary and Lee, 1994]). Later [Gary et al., 1994] have shown from data analysis and computer simulations that a similar relationship

$$\frac{T_{\perp p}}{T_{\parallel p}} - 1 = \frac{0.4}{\beta_{\parallel p}^{0.15}} \tag{2.3.29}$$

holds for the plasma in the outer magnetosphere. Equation (2.3.29) corresponds to a threshold of the proton cyclotron instability and it represents the upper bound on the proton temperature anisotropy. A relationship of this form should not only be observed in the magnetosheath or in the outer magnetosphere, but also in any collisionless, sufficiently homogeneous plasma in which the proton cyclotron instability is excited.

This relation can be used to predict whether a plasma is unstable with respect to the proton cyclotron instability, if one possessed the measured particle distribution function. Such an instability analysis was done by [Anderson et al., 1996b] using magnetic field, particle, and plasma wave data from the Active Magnetosphere Particle Tracer Explorers / Charge Composition Explorer (AMPTE/CCE). They have analyzed proton distribution functions during periods of cyclotron wave observations (active periods), and during periods with no waves (quiet periods). The temperature anisotropies of the proton distributions during active periods were lying along the (2.3.29) curve whereas those during quiet events were lying below this curve (Figure 2-4). Curve A effectively separates the active and quiet events.

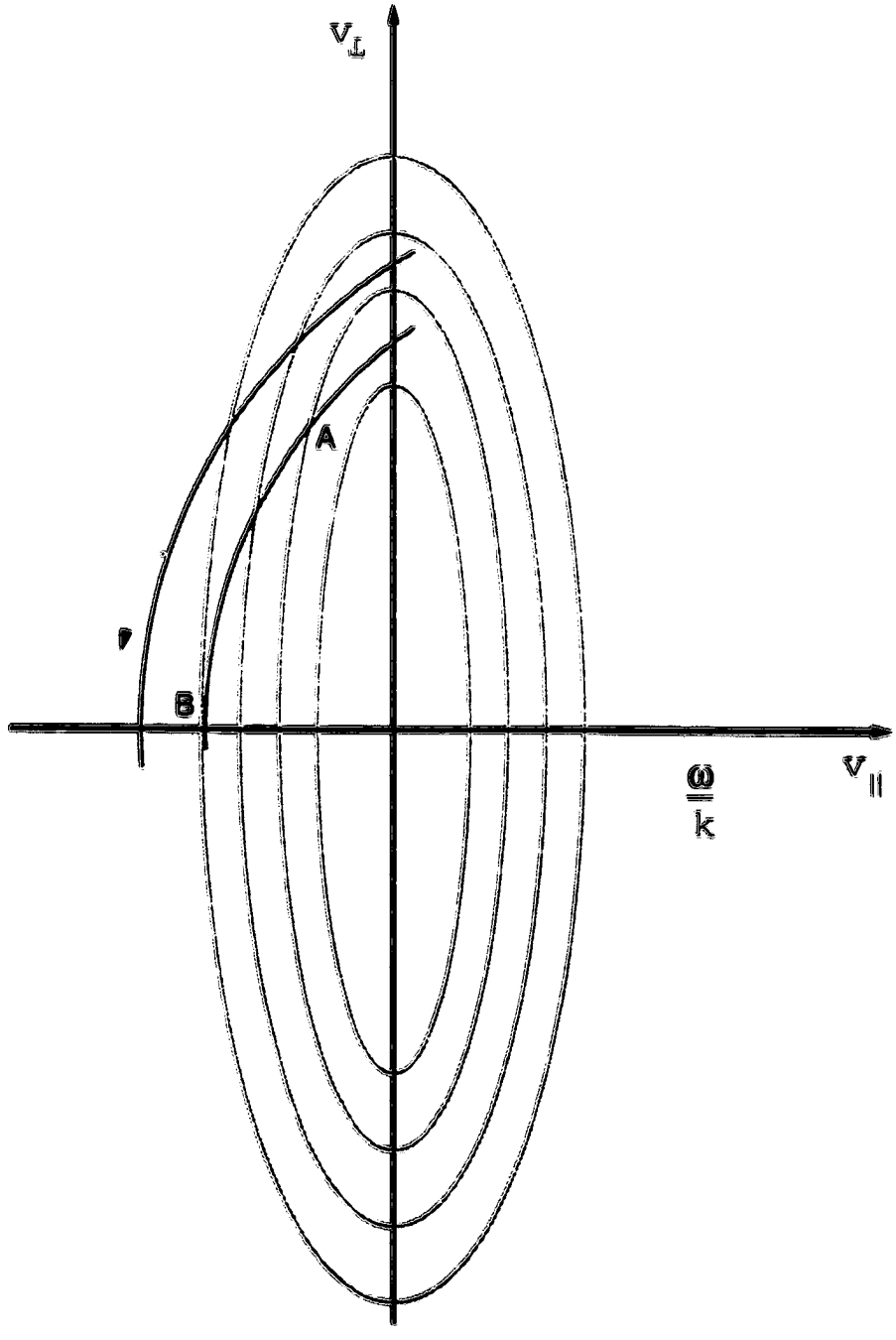


**Figure 2-3: Pitch angle scattering in velocity space.**

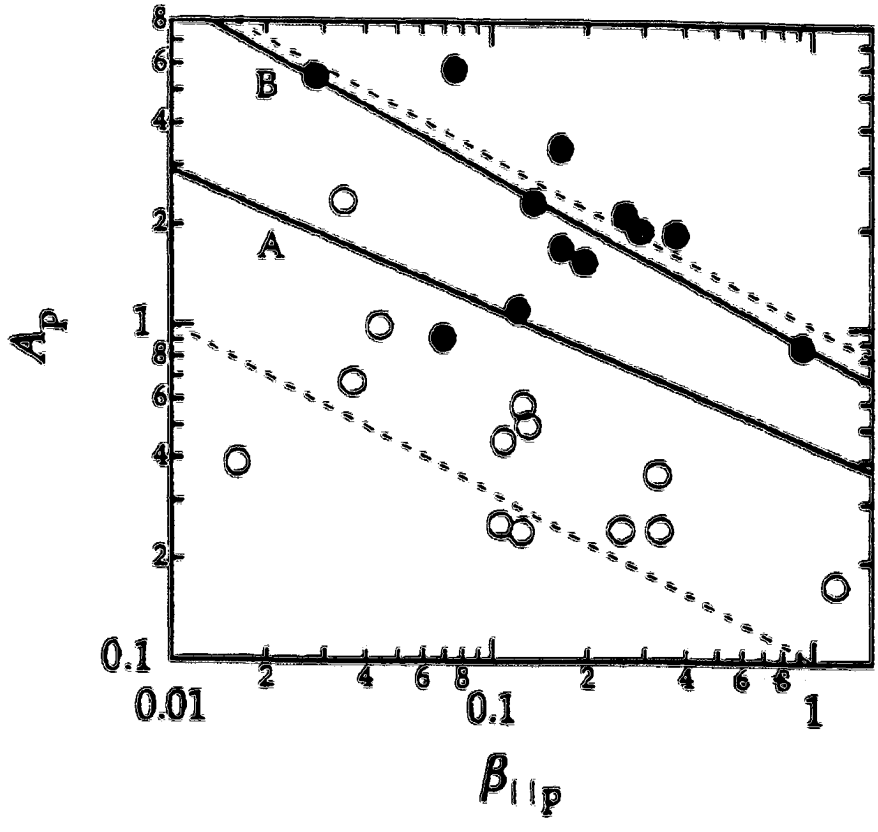


Figure 2-4: Plot of $A_p$ versus $\beta_{\|p}$ [Anderson et al., 1996b]

# Chapter 3

# Data Analysis Techniques

## 3.1 Ground Station Location and Micropulsation Data Analysis

We have used ground magnetic field data from three of our micropulsation stations located ideally for our study. The first station is situated in Iqaluit, the capital of the Nunavut region of the Canadian Northwest Territories. The other two stations are situated in Antarctica. One of them is at the geographic South Pole, at an auroral geomagnetic latitude, while the other antarctic station, BAS A81, is located at a slightly lower geomagnetic latitude. The geomagetic latitudes of these stations locate them at the footprint of terrestrial magnetic field lines that belong to the equatorial outer magnetosphere during magnetic daytime (6 a.m. to 6 p.m. local magnetic time), therefore the locations of these stations are ideal for studying phenomena that occur in the outer magnetosphere earthward of the low latitude boundary layer, where Pc1 waves are produced. The geographic and corrected geomagnetic coordinates of these three stations together with the magnetic local time at noon Universal Time are summarized in Table (3.1).

The entire process of data collection is described in Appendix A. To achieve the purpose of our study we have to analyze dynamic spectra of these data. The code that produces the spectra was written in the IDL programming language, a high level language very well suited for data analysis and visualization and very popular among the space physics community. The raw data from the magnetometers is a discrete ordered time series of voltage values of

Table 3.1: The global positioning of the search coil magnetometers used in our study.

| Station | Geographic Latitude | Geographic Longitude | Geomagnetic Latitude | Geomagnetic Longitude | UT of 12:00 MLT |
|---|---|---|---|---|---|
| Iqaluit | 63.8 | 291.4 | 73.3 | 14.3 | 16:07 |
| South Pole | -90.0 | 0.0 | -74.0 | 18.4 | 15:30 |
| BAS A81 | -81.5 | 3.0 | -68.5 | 36.1 | 14:18 |

$\partial \vec{B}/\partial t$, equally spaced in time with a period of 0.1 seconds between consecutive samples (10 Hz sampling rate) for the Iqaluit and South Pole data sets, and 0.5 seconds (2 Hz) for the BAS A81 data set. For this particular study we needed to analyze dynamic spectra in the wave frequency range of up to 1.0 Hz. We describe here all the steps involved in obtaining a dynamic spectrogram.

**Step 1** The frequency for the data series necessary to give a 1 Hz Nyquist frequency is equal to 2 samples per second. The first step in obtaining the spectrum is bringing the raw data frequency to this value of 2 Hz by averaging together every five consecutive samples (for Iqaluit and South Pole only: the BAS A81 data doesn't need any averaging since it is already recorded at 2 Hz). This process of averaging the raw data is equivalent to high pass filtering it.

**Step 2** Next we need to group the data points into windows of a certain number of points. The algorithm used for the Fast Fourier Transform (FFT from here on) requires that the number of points in every window is a power of two. We picked the width of our windows to be 128 data points for the following reason: the resulting Fourier transform array will have the same number of elements (128), which correspond to 128 frequency values between -1

Hz and 1 Hz, or 64 frequency values between 0 and 1 Hz if we look at the positive frequencies only (the spectrum is symmetric about the 0 Hz frequency). These 64 frequency values offer a good enough resolution for the 0 to 1 Hz interval, and they will appear in the spectrogram as one vertical array. The first window contains the first 128 data points of the averaged data array corresponding to the time period to be analyzed (fig. 3-1). To pick the second window of 128 data points we slide by 60 points into the data array, so the second window will contain data points from number 60 to number 187 in the data array. This sliding period of 60 points is also recommended by the FFT algorithm (it should be roughly one half of the size of the window). We continue this process of grouping the data points into windows until the whole data array to be analyzed is "covered" by these windows.

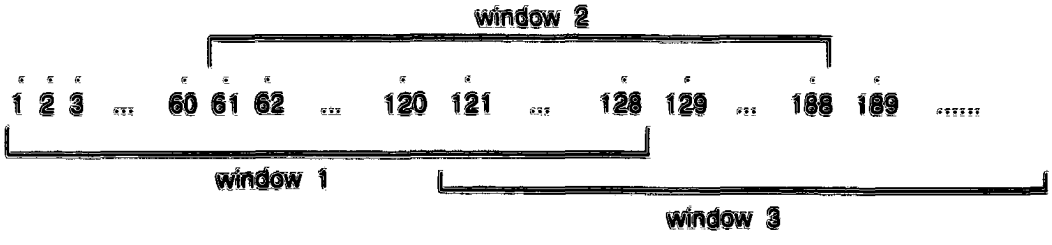


Figure 3-1: Grouping the data points in windows

In steps 3 and 4 we perform several operations on each of the data windows, resulting in the transformed arrays that are ready to be plotted.

**Step 3** Before performing the FFT on every data window we need to multiply it with a window function (fig. 3-2, b) that changes gradually from zero to a maximum and then back to zero. This particular type of window is called a Hann window. Note that grouping the data points the way we described earlier is equivalent to multiplying the whole data

array with a step function which is equal to 1 for the 128 points picked for the window and is 0 for the rest of the data points. By multiplying the data window with the Hann window we smooth out the edges, the resulting product decreasing slowly to 0 towards both ends of the array, therefore avoiding leakage from one frequency to another, as described in [Press et al., 1992], chapter "Data Windowing". This procedure is illustrated in fig. 3-2.

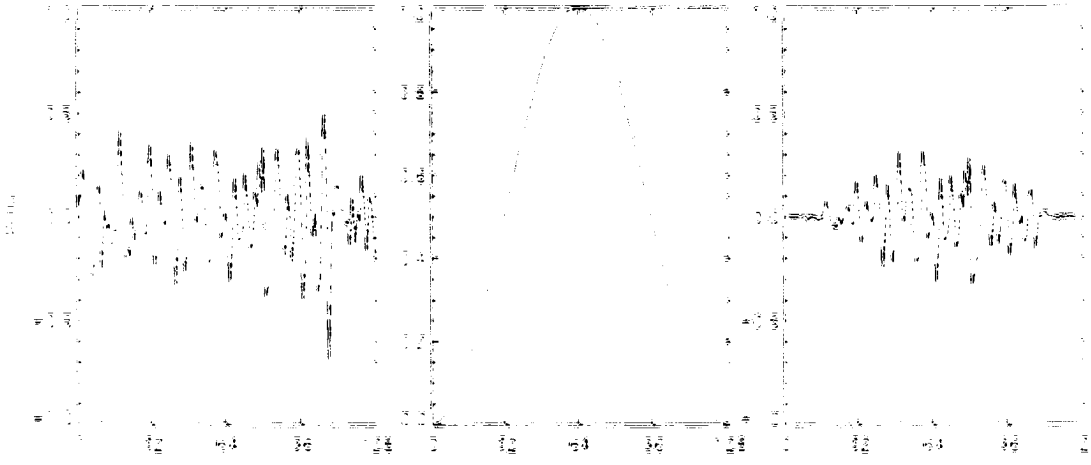

(a) raw data (b) Hann window (c) product

Figure 3-2: Illustrating the effect of hanning

**Step 4** At this stage we are ready to perform the FFT as described in the IDL manuals [IDL Reference Guide, 1995]. For each of the data windows we get a 128 element complex array. In order to obtain the power spectrum from this complex array we take its magnitude (absolute value) and then square it, after which we retain the positive frequencies only, that is half of the resulting array (due to symmetry about the 0 Hz frequency). Optionally we could (and we do) operate on these arrays with the log function, to bring the numbers into a more convenient range.

**Step 5** We are now ready to build an image for the dynamic spectrogram. What we have so far is a number of arrays of 64 elements each, equal to the number of windows. Each of these arrays is indexed by the 64 frequency values between 0 and 1 Hz and will contain the wave power at all these frequencies, for the corresponding data window. The time spacing of these arrays is determined by multiplying the sliding period (60) with the sampling interval of the data (.5 s), so the resulting time resolution is 30 seconds. When we chose the number of elements of a window for the FFT as described earlier, we took into account the balance between the frequency resolution (1/64 Hz, "vertical resolution") and the time resolution (30 s, "horizontal resolution"). The result of increasing one of these quantities is decreasing the other one. For example if we had picked the next higher power of 2 for the number of points of a window, i.e. 256, the frequency resolution would have increased to 1/128 Hz whereas the time resolution would have decreased to 60 seconds. The spectrogram's axes labels will be time in seconds for the abscissa (x-axis) and frequency in Hertz for the ordinate (y-axis). The Fourier Transformed arrays are imaged as consecutive vertical bars, with a color assigned for every element of every array. The color ranges are described by a scaled color bar that accompanies the spectrogram (fig. 3-4, top panel).

## 3.2 WIND Satellite Orbit and Data Analysis

The WIND satellite was launched successfully on November 1, 1994, from Cape Canaveral, Florida, on a Delta II launch vehicle. Together with Geotail, Polar and SOHO projects, they constitute a cooperative satellite project designated the International Solar Terrestrial Physics (ISTP) program which aims at gaining improved understanding of the physics of solar terrestrial relations. Designed to be a solar wind monitor, WIND has provided mea-

surements of the solar-wind plasma before it reaches the Earth. Figure 3-3 is a projection of the satellite's orbit on the $(X-Y)_{GSE}$ plane for the period of interest in our study. The GSE (Geocentric Solar Ecliptic) coordinate system is centered at the center of the Earth, the x-axis points towards the sun, the z-axis is perpendicular on the ecliptic plane and points towards North, and the y-axis completes a right handed Cartesian coordinate system. The satellite did not go very far away from the ecliptic plane, maintaining its $Z_{GSE}$ position between =20 and 20 Earth Radii. There are numerous experiments on board. Following is a list of all the experiments on WIND:

- Hot Plasma and Charged Particles (3DP)
- Transient Gamma Ray and EUV Spectrometer (TGRS)
- Magnetic Field Instrument (MFI)
- Plasma and Radio Waves (WAVES)
- Solar Wind Experiment (SWE)
- Energetic Particle Acceleration, Composition and Transport (EPACT)
- Solar Wind and Suprathermal Ion Composition Studies (SWICS/STICS)
- Gamma Ray Burst Detector (KONUS)

In our study we use data from the Solar Wind Experiment ([Ogilvie et al., 1995]) and the Magnetic Field Instrument ([Lepping et al., 1995]). The data is available in the Common Data Format, a self-describing data abstraction developed by NSSDC (National Space Science Data Center) for the storage and manipulation of multidimensional data in a discipline-independent fashion. We extract and use the following solar wind key parameters:

- density ($cm^{-3}$)
- velocity components ($km/s$), GSE coordinates
- interplanetary magnetic field (IMF) components ($nT$), GSE coordinates
- spacecraft location (Earth Radii), GSE coordinates

Using these parameters we calculate the magnitude of the wind velocity ($v_{sw} \equiv v_x^2 + v_y^2 + v_z^2$), the solar wind dynamic pressure ($p_{dyn} \equiv n_{sw} m_p v_{sw}^2$, where $m_p$ is the mass of a proton), the magnitude of the IMF ($B \equiv B_x^2 + B_y^2 + B_z^2$) and the IMF cone angle or spiral angle ($ConeAngle \equiv cos^{-1}(B_x/B)$). In our study we will use the solar wind dynamic pressure as a measure of the force exerted by the solar wind on the magnetosphere, and we will neglect the plasma pressure and the magnetic pressure because they are much smaller than the dynamic pressure. Figure 3-4 is an example of the format that we chose for plotting the wind parameters:

- panel 2 ⇒ the solar wind dynamic pressure
- panel 3 ⇒ the solar wind velocity
- panel 4 ⇒ the magnitude of the IMF
- panel 5 ⇒ the IMF cone angle
- panel 6 ⇒ the IMF $B_z$

The first panel contains the dynamic spectrogram of the magnetometer data, as we specified earlier. The black trace represents the total wave power between 0.1 Hz and 1.0 Hz. This frequency range overlaps over the boundary of two types of Pc pulsations, the Pc1 range (0.2

Hz to 5.0 Hz) and the Pc2 range (0.1 Hz to 0.2 Hz). [Saito, 1969, Fukunishi et al., 1981], and includes the Pc1/2 frequency range (0.1 Hz to 0.4 Hz). [Popecki, 1991]. The spectrogram is time-shifted with respect to the Universal Time at the bottom of the plot (and therefore with the wind parameters), by the time it takes an interplanetary discontinuity to reach the ground from WIND. We calculated this time by considering radial advection of the discontinuity at the plasma bulk speed from the satellite to the magnetopause ($D_{sat-mpause}/v_{sw}$), to which we added an extra two minutes to account for the propagation of a disturbance through the magnetosphere to a flux tube and down the flux tube to the ground observatory. Recent interest in space weather with an emphasis on geomagnetic forecasting using L1 solar wind monitors have made determining these time-shifts the subject of many studies [Farrugia et al., 1989, Paularena et al., 1998, Richardson et al., 1998]. In the [Paularena et al., 1998] study of the correlations between spacecraft, a histogram of the maximum correlation as a function of extra lag is performed (Figure 6). The histogram strongly peaks near zero on a scale from =50 to 50 minutes, implying that the advection shift is a good approximation of the propagation time for the structures being correlated.

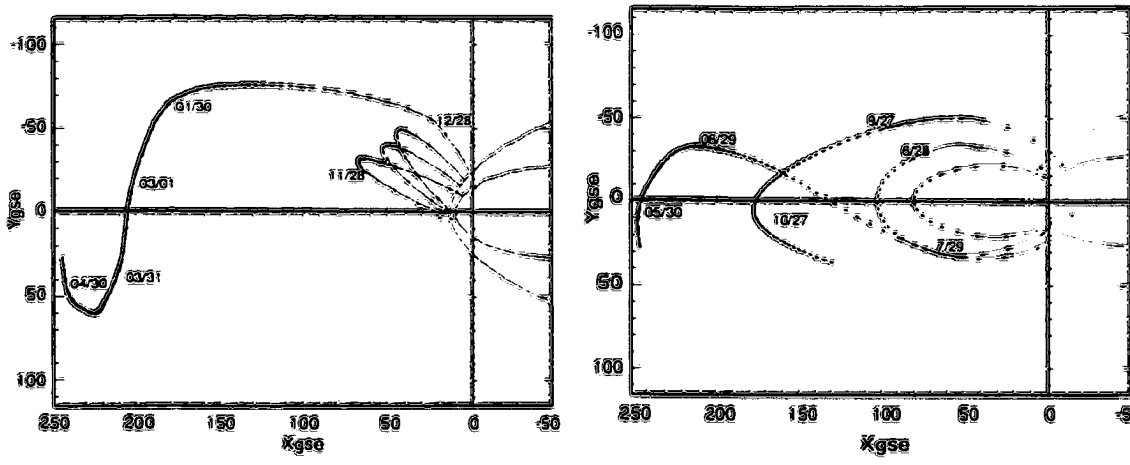


(a) WIND orbit 11/94 - 05/95

(b) WIND orbit 05/95 - 11/95

(c) WIND orbit 11/95 - 05/96

(d) WIND orbit 05/96 - 11/96

**Figure 3-3: WIND orbits for four 6 month periods**

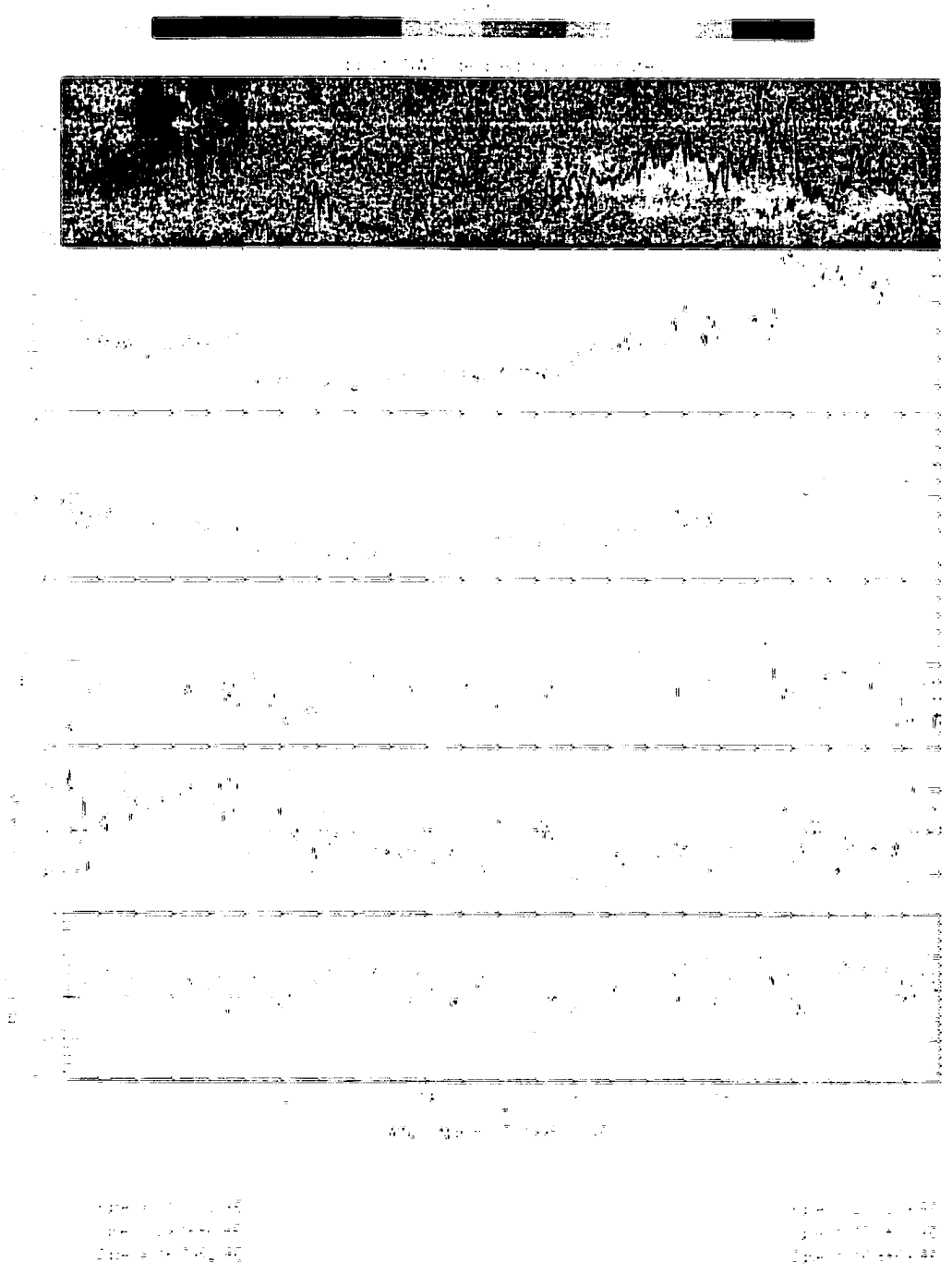

Figure 3-4: Example of wind parameters plot

# Chapter 4

# Results and Conclusions

We have described in the previous chapter the methods that we used to process the experimental data for this study. In this chapter we first analyze a few individual events, then present the statistics from the two different approaches used in the study, the ground ⇒ wind approach (look at the ground data first and then look for a cause in the solar wind data) and wind ⇒ ground (look for solar wind pressure events first and then look at the ground response). Finally we discuss and conclude the results of this work.

## 4.1 Case Studies

The idea for our study came from simultaneous observations of the solar wind dynamic pressure (as measured by the WIND satellite) and power spectra of Pc1 waves on the ground. Figure (4-1) is an example of such an observation. The first thing to note in this figure is the way the dynamic pressure behaves (second panel from the top): it is relatively constant (around 1 nPa) until 13:35 UT when it suddenly jumps about 0.5 nPa, then it continues to gradually increase up to about 6 nPa at 16:27 UT when it suddenly drops back to 1 nPa. In the top panel the variation of the total wave power matches fairly well the variation of the dynamic pressure. Note the jump at 13:35 UT, the gradual increase, and then the drop at 16:27 UT. Also note the little dip in the power at 14:30 UT caused probably by the simultaneous pressure dip. This variation is also illustrated very well in the spectrogram: the wave train commences at the pressure jump, the color changes towards higher power,

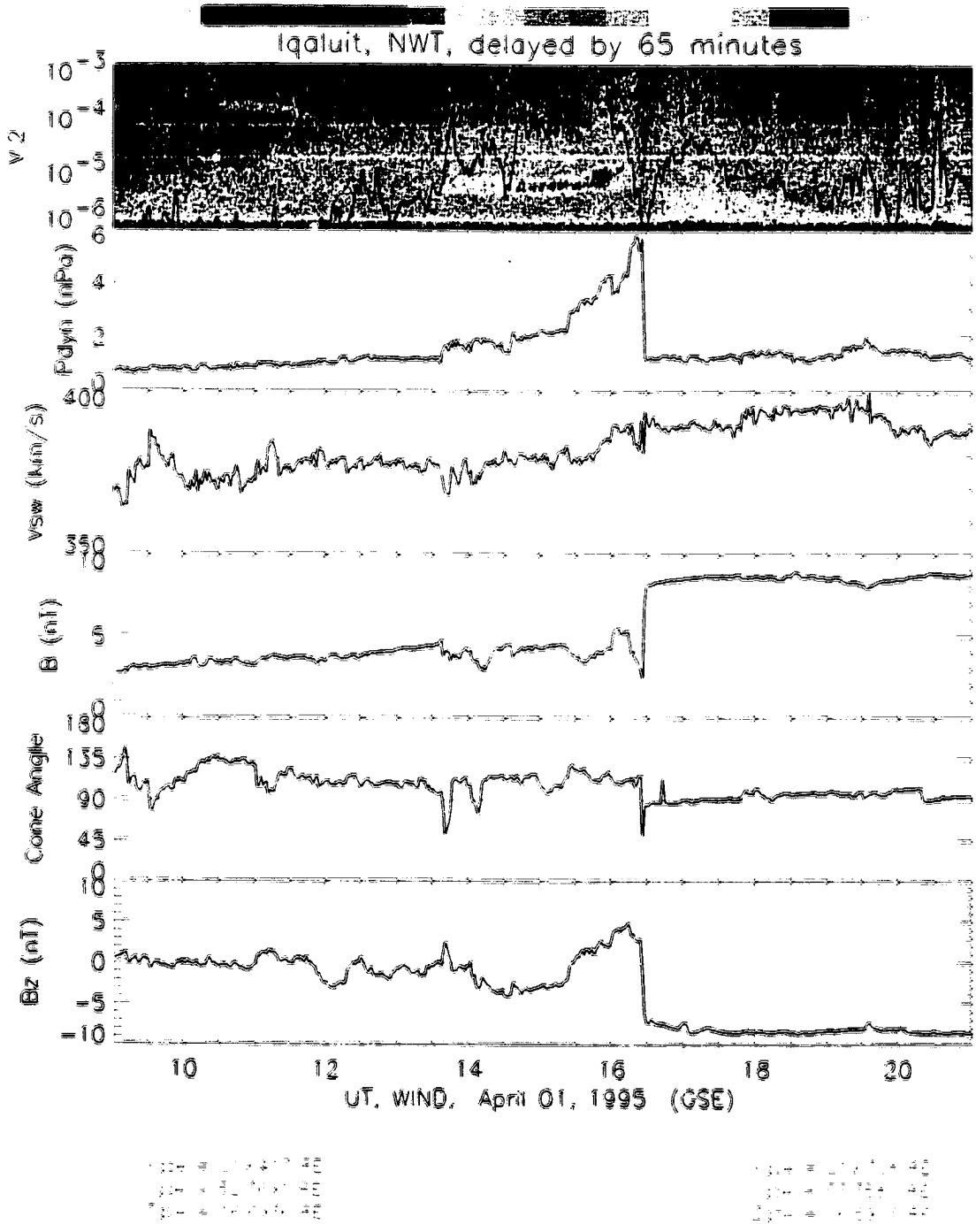


**Figure 4-1: Wind parameters and Iqaluit micropulsation spectrum, April 01, 1995**

and then the wave activity suddenly stops at the pressure drop. An interesting thing to note here is the increase in the wave frequency that accompanies the pressure increase; this is due to the increase of the magnetic field at the wave source during the compression. After 16:30 UT the wave power picks up again despite the pressure remaining constant, but the nature of the waves changes. The waves after 16:30 UT are Pi1 waves; they are the result of the sudden southward turning of the IMF Bz (bottom panel) which induces erosion at the nose of the magnetopause accompanied by day-side particle precipitation in the ionosphere. The last thing to note here is the position of the satellite, very far upstream ($X_{GSE} \equiv 219$ RE) and very far off the Sun-Earth line ($Y_{GSE} \equiv 53$ RE). We mentioned this because we will see later in this chapter what the influence of the position of the satellite is on the similarity of the variation of the pressure and the wave power.

A similar example, this time from the Antarctic station BAS-A81, is presented in Figure (4-2). There is a jump in the dynamic pressure at 12:15 UT, accompanied by a jump in the total power and the start of a Pc1 wave train. For the next half hour the pressure keeps rising, and so do the power and the frequency of the wave. At 12:40 UT the pressure reaches a plateau at 5 nPa, and then it stays constant for the next two hours, when it suddenly drops back to $\sim$ 1.5 nPa. The wave production is maintained during the plateau and it ends simultaneous with the pressure drop at 14:40 UT. After this time the IMF Bz turns southward and particle precipitation begins, accompanied by the production of Pi1 waves. The satellite is still fairly far upstream ($X_{GSE} \equiv 150$ RE) but is a lot closer to the Sun-Earth line ($Y_{GSE} \equiv -10$ RE).

Another interesting example, a little different from the previous ones, is given in Figure (4-3). The pressure increases abruptly from 0.5 nPa to 2.2 nPa at 13:00 UT. This jump is

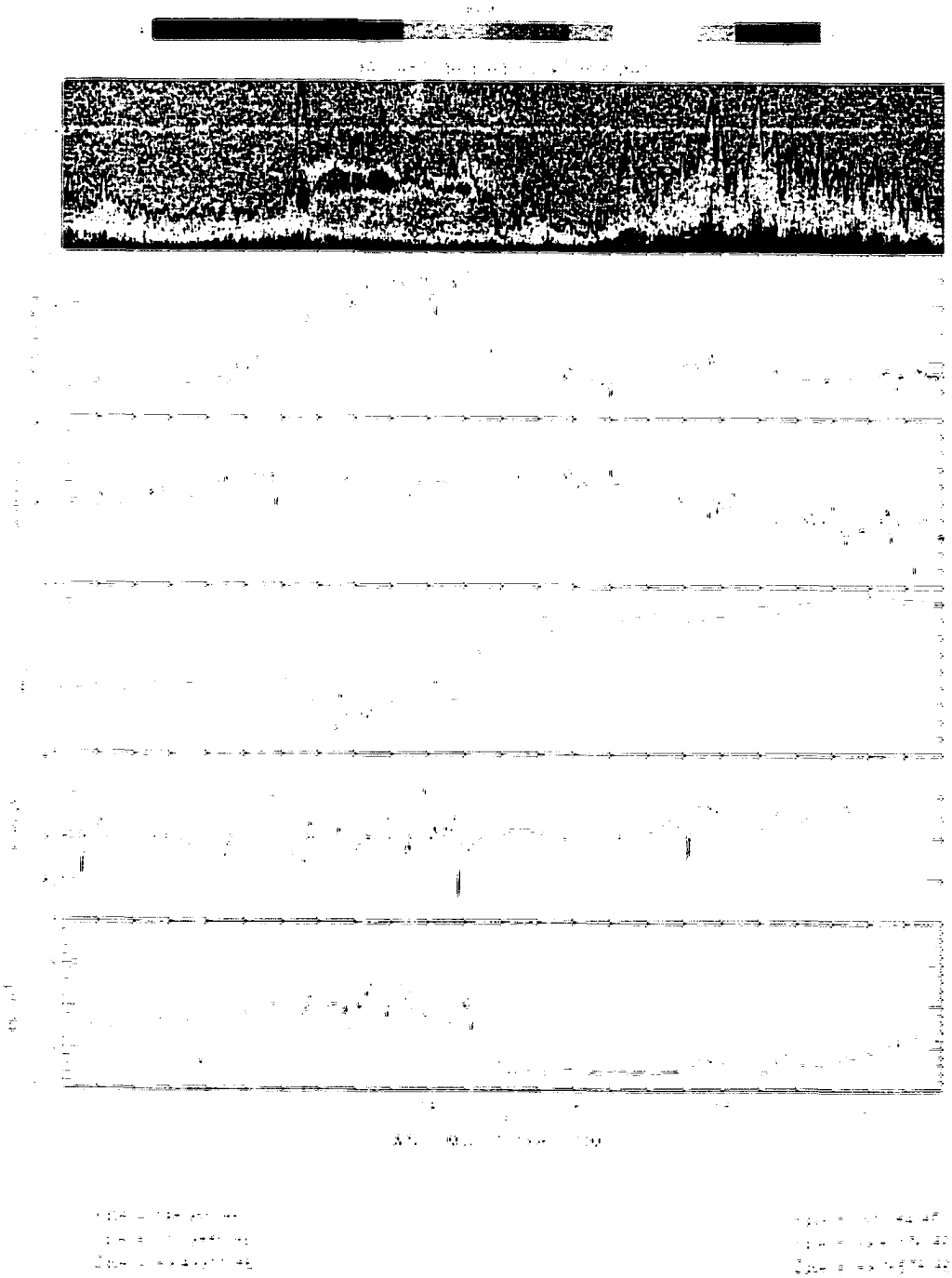

Figure 4-2: Wind parameters and BAS-A81 micropulsation spectrum, May 27, 1996

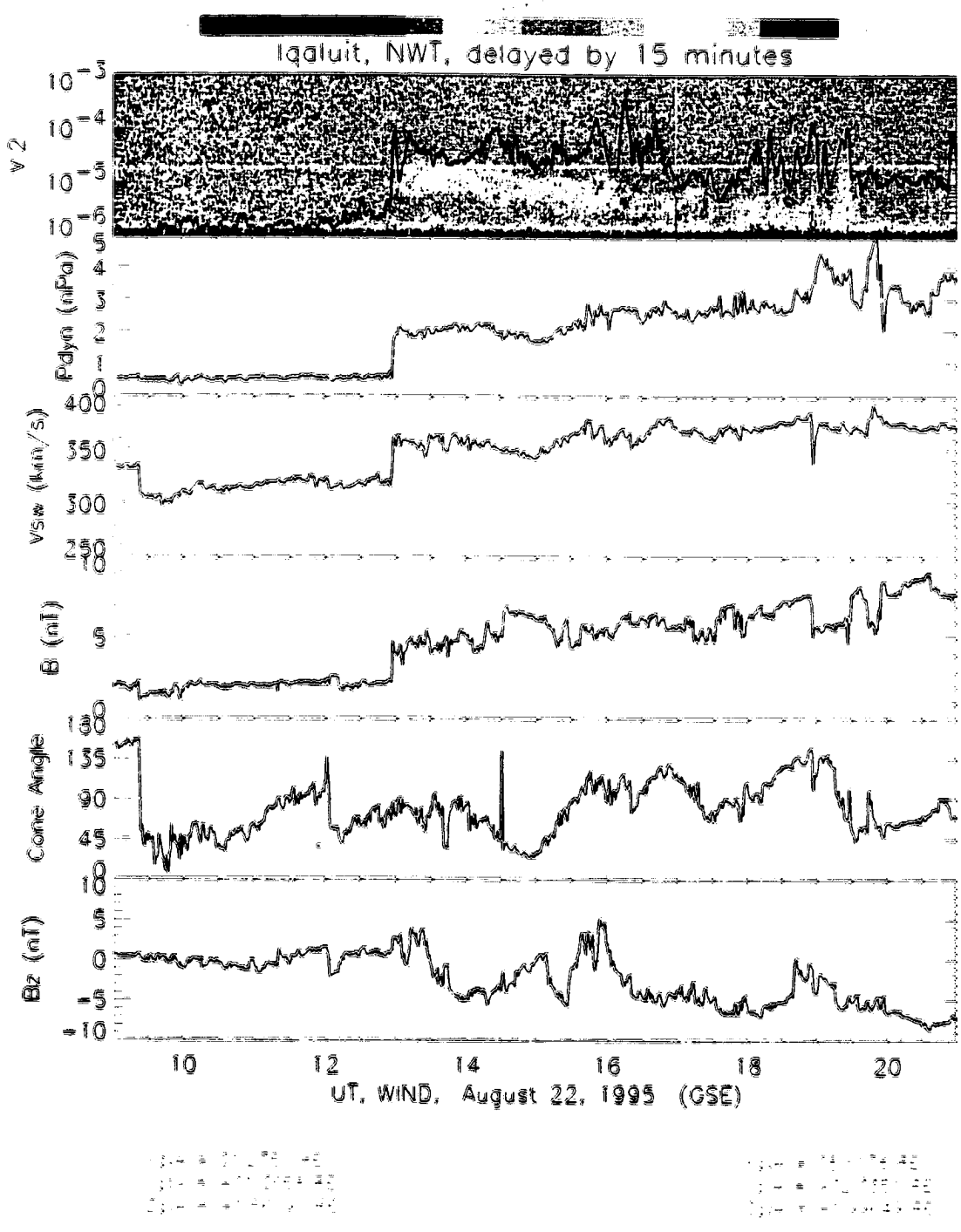


**Figure 4-3: Wind parameters and Iqaluit micropulsation spectrum, August 22, 1995**

accompanied by a jump in the total wave power and a commencement of a wave train in the spectrogram. After the jump the pressure increases very slowly (about 0.43 nPa/hour) towards dusk, up to 5 nPa at 20:00 UT. The wave power does not "feel" the slow pressure increase, so it stays approximately constant for a long time (4 hours), until the Pc1 train stops. The slow pressure gradient cannot move the source into a stronger magnetic field region, so the wave frequency does not increase either. On the contrary, the source moves into the afternoon, so the magnetic field at the source decreases, resulting in a decrease of the wave frequency. The sustained relatively high pressure maintains the wave production up to late afternoon (17:00 UT) when the compression on the dusk flank is not strong enough anymore to push the proton population source to marginal cyclotron wave instability, and the wave production stops.

One final example of a pressure-driven Pc1 wave train is shown in Figure (4-4). Besides the features that we have seen in the earlier examples (pressure jumps and drops accompanied by wave power jumps and drops, or sustained high pressure accompanied by continuous wave production), here we see a gradual pressure decrease from 4.5 nPa at 15:00 UT to about 2 nPa at 16:30 UT. Accordingly, the wave power gradually drops and the wave spectrum gradually fades away until the wave productions stops. A summary of the different solar wind pressure features and their effect as seen on the ground is presented in Table (4.1).

Before going on to the statistical analysis we want to show an example of an event where a relatively large increase in the dynamic pressure had no influence on the Pc1 wave production as measured with the magnetometers, Figure (4-5). Later on this event will be called a non-matching event. Note the gradual pressure increases from 11 : 30 UT to 14 : 00 UT and from 18 : 00 UT to 18 : 45 UT with no equivalent Pc1 wave power increases.

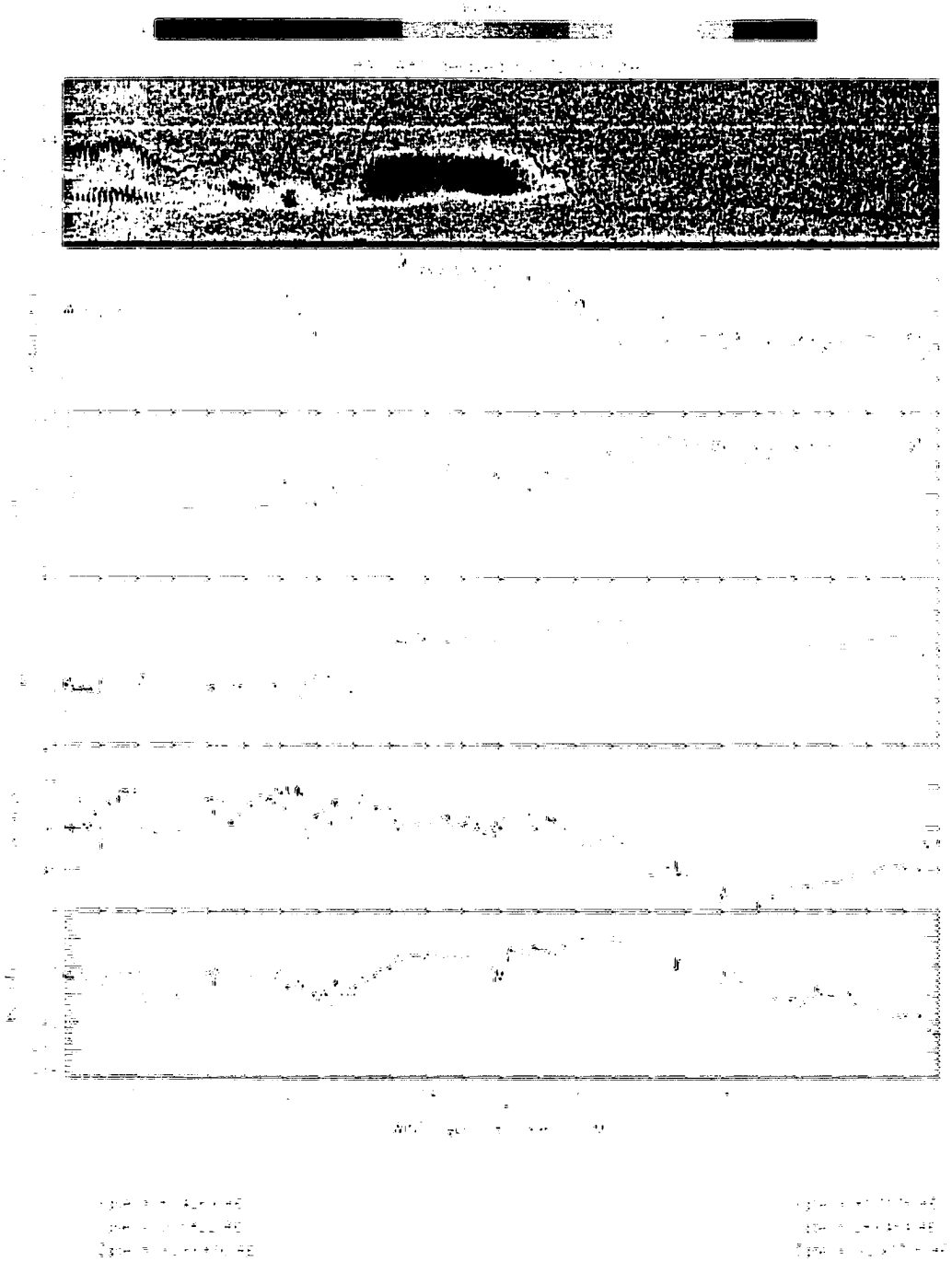

**Figure 4-4: Wind parameters and BAS-A81 micropulsation spectrum, April 08, 1996**

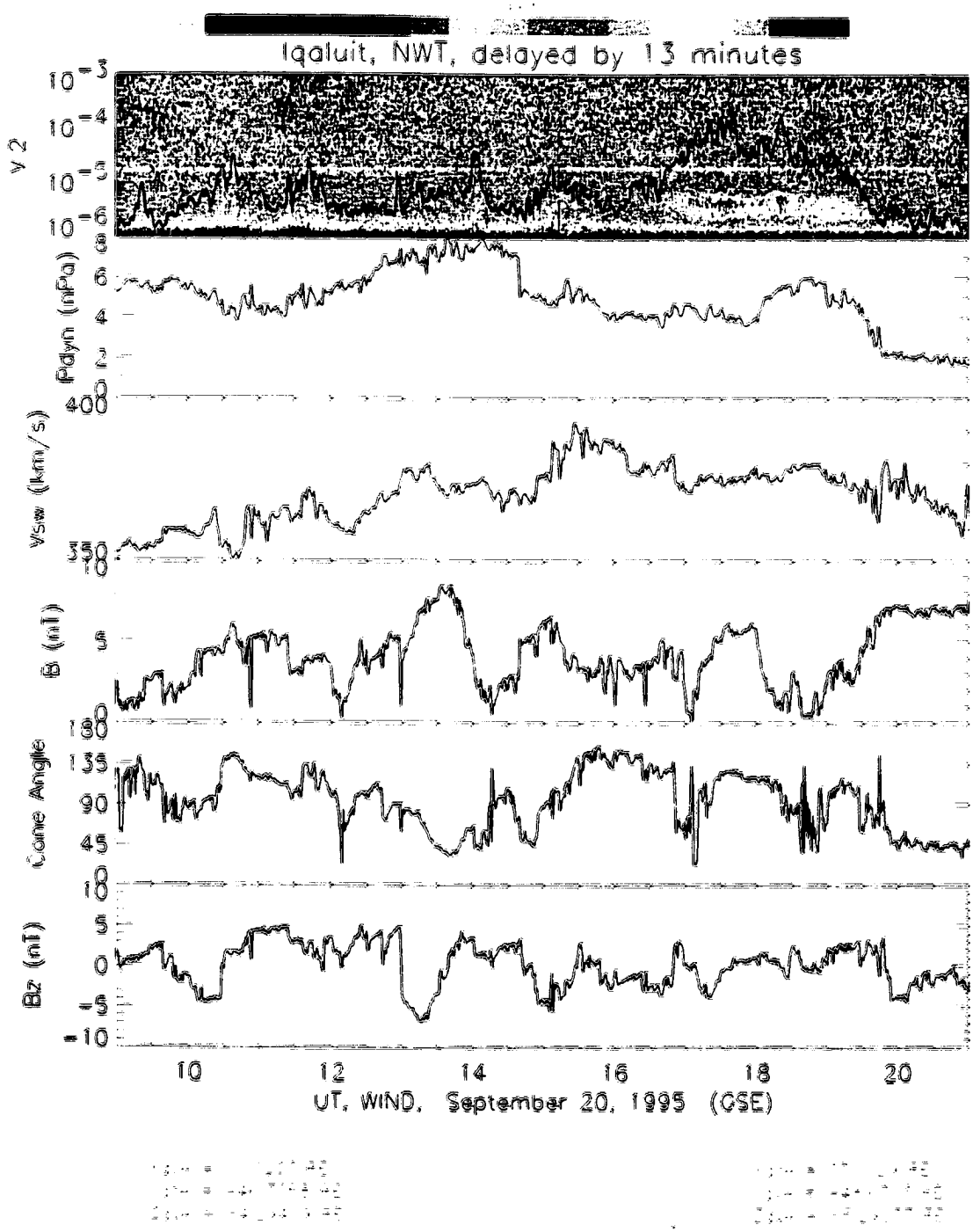


**Figure 4-5: Wind parameters and Iqaluit micropulsation spectrum, September 20, 1995**

Table 4.1: Summary of the pressure features and their effect on the ground.

| Feature | Effect on the ground |
|---|---|
| pressure jump | sudden wave commencement or amplification |
| gradual pressure increase | gradual wave power and wave frequency increase |
| gradual pressure decrease | gradual wave power decrease |
| sudden pressure drop | sudden wave power drop and end of wave train |

## 4.2 Statistical Study

After observing events like the ones presented in the previous section we decided to study the influence of the solar wind dynamic pressure on the production of proton cyclotron waves from a statistical point of view. The time interval of data collection for this study spans a two year period (1995 and 1996) near the solar minimum. We have chosen the three stations Iqaluit, South Pole and BAS-A81, for several reasons. Two of the reasons were the data quality and data coverage; we have a very good micropulsation station ideally located in Sondre Stromfjord, Greenland, but the data coverage for the time interval that we picked for our study was poor. The data were also fairly noisy, so we decided against using this station for our study. Iqaluit station functioned properly during the first half of our study time, so we chose Iqaluit as our northern hemisphere station. The South Pole station is magnetically conjugate with Iqaluit, so together they make a good set of stations for conjugacy studies. BAS-A81 functioned remarkably well during the second half of our study (it was not installed for the first half of our study time). BAS-A81 is located at a lower geomagnetic latitude than South Pole; this set of stations can be used for latitude dependency studies. South Pole was the station that provided data for the whole study

Table 4.2: Data coverage for the time interval of our study.

| Year | Iqaluit | South Pole | BAS-A81 |
|---|---|---|---|
| 1995 | 266 | 263 | 0 |
| 1996 | 0 | 279 | 347 |

interval, even though the data were not as clean as the data from Iqaluit and BAS-A81. Our stations are built such that comparison with one another is possible (they have the same parameters, such as sensitivity and frequency response), but there are local factors (such as proximity to other instruments or power sources, wind, power interruptions) that make the quality of the data quite different from one station to another. The micropulsation data coverage, in days, for all the three stations is summarized in Table (4.2).

### 4.2.1 Approach 1: Ground → Wind

With all these data available we began our work by plotting all the data in the style of Figures (4-1) to (4-4). Our intent was to look at the spectrograms first (top panel) and to isolate wave events, then look at the dynamic pressure and judge whether it had an influence on the production of the waves. We had to have a definition for what we meant by a wave event for our study. We call a wave event a wave train that is clearly seen in the spectrogram, is Pc1 type (band-limited frequency) and is at least 0.5 hours long. The relationship between isolated sudden ($< 5$ min) impulses (magnetic field increases of at least 10 nT due to modest magnetospheric compressions) and enhancements or onset of Pc1 at high latitude ground stations is well established ([Olson and Lee, 1983], [Anderson and Hamilton, 1993]). In this

Table 4.3: Statistics for Approach 1, ground → wind.

| Year | Wave events | Station | Matching events | Non-matching events | No data |
|---|---|---|---|---|---|
| 1995 | 121 | Iqaluit | 24 (20%) | 97 (80%) | 0 |
| | | South Pole | 20 (17%) | 97 (83%) | 4 |
| 1996 | 184 | BAS-A81 | 33 (18%) | 151 (82%) | 0 |
| | | South Pole | 21 (12%) | 151 (88%) | 12 |

study we deal with relatively long duration wave trains, from 0.5 hours up to 12 hours (the whole day-side!), and stronger compressions (see section 4.2.2). A careful review of the examples given in the previous section shows that not only the total power matches fairly well the variation of the dynamic pressure. If we define an upper cutoff frequency for the waves, which would be a value of the frequency at the upper frequency part of the band (basically a line that goes through points of the same color at the top of the band), we can see that also this upper cutoff frequency follows the pressure variations fairly well. This is true as long as the pressure gradient is large enough (we will see what large enough means in section 4.2.2), but is no longer valid for events like the one in Figure (4-3). We decided for our study to compare the total wave power with the solar wind dynamic pressure. We called a matching event an event for which the total wave power variation matches the variation of the solar wind dynamic pressure. The statistics for this approach are summarized in Table (4.3). The first column contains the total number of events observed in each of the two years at the first station from the second column, corresponding to the respective year. The

third column contains the number of matching events for the respective station together with the percentage of the total number of wave events in brackets. For year 1995 we looked at the Iqaluit data first, hence the 0 in the 'No data' column. We have isolated 121 wave events; for all but 4 of these events data were also available from the South Pole station. We found that only in 24 of the 121 events observed at Iqaluit the total wave power matched the variations of the solar wind dynamic pressure. This represents only 20% of the total number of wave events. The statistics at South Pole were even lower due to those few data dropouts. For year 1996 we looked at BAS-A81 data and we isolated 184 events, about 50% more than in the previous year at Iqaluit; this is not surprising since the data coverage at BAS-A81 is about 30% better than at Iqaluit, as can be seen from Table (4.2). Only 33 of these events were matching events, which is only 18% of the total number of wave events. The relative number of matching events from the two years is about the same, showing that the statistics are good enough. This approach shows that only approximately one out of five wave events has the solar wind dynamic pressure as the obvious cause. For the rest of the events the dynamic pressure was relatively low (2 nPa) and constant.

These results were not exactly what we were expecting to see. We noticed one thing however: the solar wind dynamic pressure during the matching events was on average about 2 nPa higher than the pressure during the non-matching events. This fact determined us to reconsider the approach of the study and to start over by looking at the WIND data first, sort it according to some criteria and then look at its effects on the ground.

### 4.2.2 Approach 2: Wind ⇒ Ground

Looking at the wind dynamic pressure first we needed a definition for a pressure event and then some criteria to separate pressure events. We chose the most obvious criteria: the amount of pressure change and the rate of its change. After carefully analyzing all the data we decided on the following definition for a pressure event: a pressure event is any pressure increase or decrease that has an absolute pressure variation between the final and initial pressures of at least 0.6 nPa, has an absolute rate of pressure change of at least 0.55 nPa/hour, and is at least 1/2 hour long if it is pulse type (up and down). The 1/2 hour length separates our events from the sudden impulse type of events which have a maximum duration of 10 minutes. Note that with this definition of a pressure event we could have several pressure events in one day, e.g. the pressure rise and drop in Figure (4-1), which were counted as two matching events. Also note that we could miss events for which the dynamic pressure is high enough (to create wave-generating compression) to start with; this situation is however very unlikely to occur since sustained high pressure almost never lasts for 12 hours continuously, so we could at least catch the decompression in our plots (which we did in several cases). A wave event is defined the same way as in the previous section. One last thing to note here is that in the process of counting we did not count as non-matching events the pressure drops that occurred while waves were not present on the ground. We left out these types of events because we could not specify their effect on the waves, since there were no waves. The statistics for this second approach are summarized in Table (4.4). In the Iqaluit-WIND data we have counted 120 pressure events. We recall here that we had 266 days of data coverage at Iqaluit (4.2) and quality WIND data was

Table 4.4: Statistics for Approach 2, wind → ground.

| Year | Pressure events | Station | Matching events | Non-matching events | No data | Noisy (useless data) |
|---|---|---|---|---|---|---|
| 1995 | 120 | Iqaluit | 95 (80%) | 24 (20%) | 0 | 1 |
| | | South Pole | 64 (70%) | 27 (30%) | 13 | 12 |
| 1996 | 107 | BAS-A81 | 71 (84%) | 14 (16%) | 0 | 22 |
| | | South Pole | 58 (74%) | 20 (26%) | 27 | 2 |

available for all but 13 of these days. For those 13 days either the satellite was inside the magnetosphere or there simply were data gaps. Out of these 120 pressure events one was too noisy to determine anything. 95 (80%) of them were matching events and 24 (20%) were non-matching events. In the calculation of the percentages we excluded the noisy event. The South Pole station had lower quality data reflected by the 13 missing data events and 12 noisy data events. The wave power in the South Pole data was much weaker than the power at Iqaluit resulting in the increase of the number of non-matching events. In 1996 there were a few more WIND data drop-outs (21 days) than in 1995. We have isolated 107 pressure events. BAS-A81 data had long periods of very noisy signal so we couldn't study 22 of the pressure events. 71 of the remaining events (84%) were matching events and 14 (16%) were non-matching. We again omitted the noisy events in the calculation of these percentages. The South Pole station data had some gaps again (for 27 of the events) and the wave signatures were much weaker than those at BAS-A81.

## 4.3 Discussion and Conclusions

We have studied the influence of the solar wind dynamic pressure on the integrated wave power of geomagnetic pulsations with the frequencies in the 0.1-1.0 Hz band from a statistical point of view. Roughly 80% of the pressure events (as defined in the previous section) had a clear influence on the production or enhancement of the waves observed on the ground. The physical interpretation of this phenomenon is believed to be the following. Enhanced solar wind dynamic pressure impinging on the subsolar magnetopause compresses the magnetospheric flux tubes in the outer magnetosphere. As a result of this compression the temperature anisotropy of the hot proton populations present on those flux tubes increases, driving the proton distributions towards cyclotron instability and Pc1 wave production. If the pressure keeps continually pushing the plasma towards increased anisotropy, the microscopic action to reduce this anisotropy (pitch angle scattering) can lead to a steady state balance corresponding to the instability threshold, and wave production can be maintained for long time intervals.

In our first approach from the previous section we found that there are many more wave events that are not related to solar wind dynamic pressure variations ( 80%). As other authors have suggested [Fairfield et al., 1990, Lin et al., 1996a, Lin et al., 1996b, Sibeck and Korotova, 1996] pressure pulses downstream of the Earth's bowshock can be generated by other causes than the dynamic pressure, e.g. sudden changes in the interplanetary magnetic field (IMF) orientation, or the interaction of low cone angle IMF with the bowshock. However, these pressure pulses could mostly be the cause of Pc1 bursts and they cannot explain the long duration wave trains observed.

We suggest a mechanism similar to the solar wind pressure driven one, only this time the compression is spatial, in the sense that the compression is produced by the drift of the proton populations from the flank of the magnetosphere into the more compressed dayside magnetosphere. Hot anisotropic proton populations with the velocity distribution anisotropy close to the threshold value drift from the dusk flank of the magnetosphere towards noon (Figure 4-6). As they drift into the stronger magnetic field of the compressed

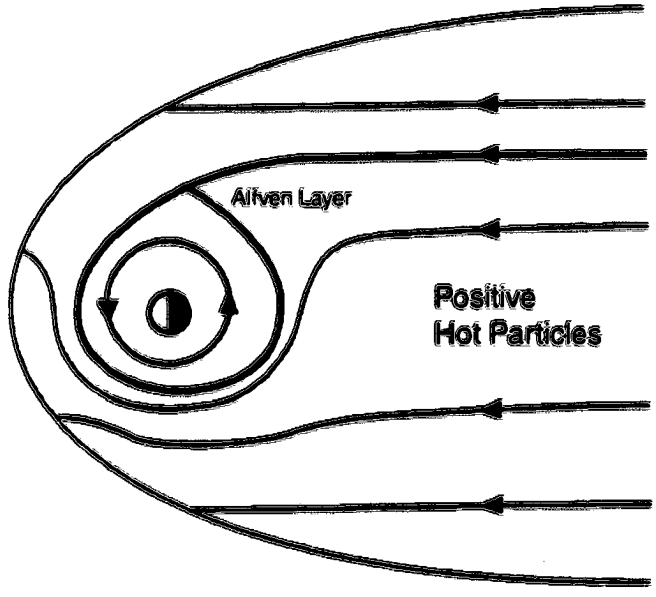


Figure 4-6: Drift direction of hot anisotropic protons [Kivelson and Russell, 1995]

subsolar magnetosphere their equatorial pitch angle increases, driving the distributions towards instability threshold. This hypothesis is in agreement with our observations of universal time distributions of wave events (Figure 4-7) at our Antarctic ground station BAS-A81. In Figure (4-7) we plotted the number of hours of wave events as a function of

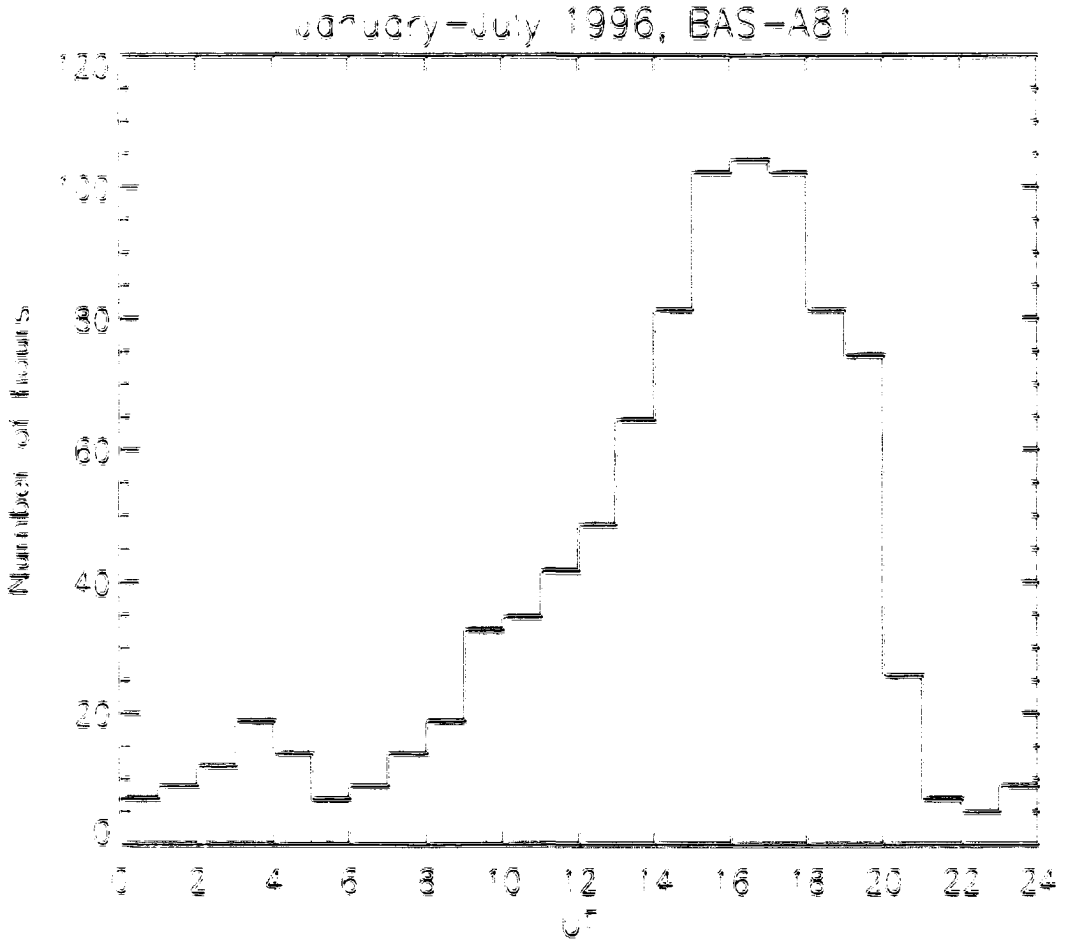


**Figure 4-7: UT distribution of wave events**

Table 4.5: Ap index as derived from the Kp index.

| Kp = | 0 | 0+ | 1- | 1 | 1+ | 2- | 2 | 2+ | 3- | 3 | 3+ | 4- | 4 | 4+ |
|---|---|---|---|---|---|---|---|---|---|---|---|---|---|---|
| Ap = | 0 | 2 | 3 | 4 | 5 | 6 | 7 | 9 | 12 | 15 | 18 | 22 | 27 | 32 |
| Kp = | 5- | 5 | 5+ | 6- | 6 | 6+ | 7- | 7 | 7+ | 8- | 8 | 8+ | 9- | 9 |
| Ap = | 39 | 48 | 56 | 67 | 80 | 94 | 111 | 132 | 154 | 179 | 207 | 236 | 300 | 400 |

the time of occurrence, for the time period January-July 1996. The local magnetic noon for BAS-A81 is at 14 : 18 UT. The distribution peaks strongly in the afternoon where the hot proton distributions drift from the dusk flank; most of these protons exit the magnetosphere around noon.

Since this proposed mechanism requires injection of particles on open drift orbits (Figure 4-6), we tried to see if there is any connection between the presence of waves and the level of disturbance in the Earth's magnetic field due to substorms. We chose to look at the Ap index, which is the linear equivalent of the Kp index. The Kp index is a planetary three hour range index computed from 13 geomagnetic observatories between 44 degrees and 60 degrees northern or southern geomagnetic latitudes. It is a quasi-logarithmic index of the 3-hourly range in magnetic activity relative to an assumed quiet-day curve. The scale is 0 to 9 expressed in thirds of a unit, e.g. 5- is 4 2/3, 5 is 5 and 5+ is 5 1/3. The Ap index is derived from the Kp index as illustrated in Table 4.5. We plotted a histogram of the Ap index during all the wave events observed between January and July 1996 (Figure 4-8, blue line) and compared it to a histogram of all the Ap index values for the same period of

time (red line, normalized to the blue distribution). As it can be seen from these figures, there is no obvious difference between the two distributions of Ap values. We conclude that we could not see any relationship between the level of geomagnetic disturbance and the presence of Pc1 waves. One reason for failing to see this connection could be because

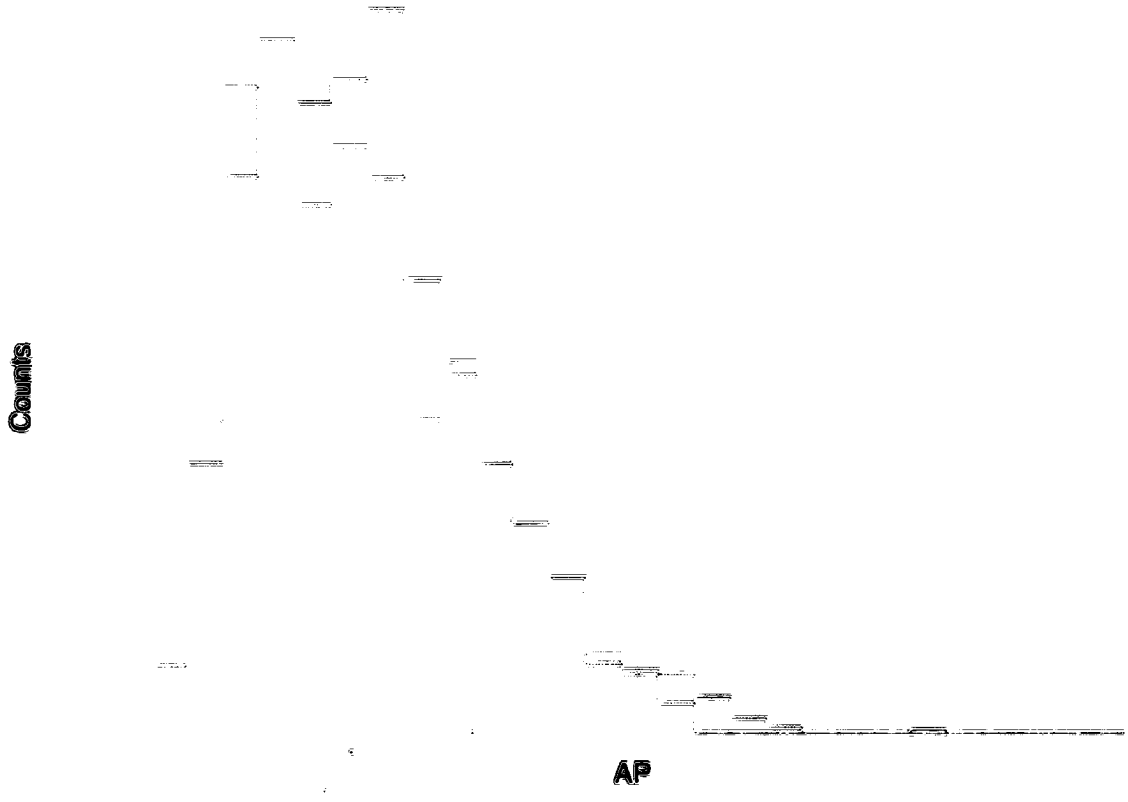


Figure 4-8: Distribution of Ap index for the entire January-July 1996 period (blue), and during wave events only (red)

the Kp index (and therefore also Ap) is calculated from mid-latitude stations. A better index that we could have used in our study is the auroral electrojet index (AE), which is a measure of the electron precipitation at high latitudes. Unfortunately these AE data were not available for the years covered in our study.

**Is WIND a good solar wind monitor?** One question that has arisen during the study was how good of a solar wind monitor the WIND satellite is, since its orbit often places it at fairly large distances from the Earth or from the Sun-Earth line, and the possibility arises that some of the solar wind features measured at the satellite's position would never reach the Earth. We tried to answer this question at least for the purpose of our study. In an earlier study of the relationship between interplanetary conditions and the ground-based Dst index, [Burton et al., 1975] have found a good correlation between increases in the solar wind dynamic pressure and increases in the Dst index. The Dst index is a measure of the worldwide deviation of the H component of the Earth's magnetic field at mid-latitude ground stations from their quiet day values. Dst is a widely used parameter in the study of geomagnetic storms, but in our case we will use it as a measure of the magnetospheric compression. We have plotted the solar wind dynamic pressure from WIND and the Dst index for the two years of our study. The Dst index data was detrended in order to remove the influence of the magnetospheric ring current. An example plot is shown in Figure 4-9 where the green line represents the pressure on a scale of 0 to 10 nPa and the red line represents the Dst index on a scale of −150 to 50 nT. In order to find a criterion for choosing the pressure increases, we have taken the average values of the pressure, first for the entire two years and then separately for the matching events of our study. We have found that the average solar wind pressure during the whole study interval was 2.2 nPa whereas the average pressure during the matching events was 4.1 nPa. Hence we chose to study the influence on the Dst of any pressure increase above 4 nPa (the dotted line in Figure 4-9). We found that 180 of the total of 226 pressure increases above 4 nPa have produced a positive Dst excursion of 30 nT or more, representing a percentage of 80%. This means

that for the purpose of our study WIND was a good solar wind pressure monitor. Another indicator of the appropriateness of the use of WIND pressure data for our study is a plot of the projection of the satellite's position on the ecliptic plane (Figure 4-10) during our matching events. It can be clearly seen that the matching events are not confined within a certain distance to the Earth or within a certain distance from the Sun-Earth line, but they occur everywhere along the satellite's sunward side orbit. The possibility still exists that some solar wind features that hit the Earth might not have been observed by the satellite, and these could also account for some of the wave events seen on the ground that have no connection with the satellite data. [Paularena et al., 1998], in their study of correlations between WIND, IMP-8 and Interball-1 satellites, found no dependence of the correlation on spacecraft separation in either $X_{gse}$ or $Y_{gse}$. The fact that we observe matching events when the satellite is far from the Sun-Earth line (50 RE) or very far upstream (200 RE) is in agreement with the [Paularena et al., 1998] study.

We have noticed in several occasions that production or enhancement of waves was caused by pressure jumps that were smaller than the chosen lower limit of 0.6 nPa for a pressure event (e.g. the jump at 13:35 UT on April 1, 1995, Figure 4-1). The opposite case when wave production or enhancement was not induced by a larger than 0.6 nPa pressure jump or increase was also observed (covered in the non-matching events statistics). This means that choosing the same lower limit for all the events is somewhat inappropriate; depending on the specific conditions for each event (e.g. how close to instability a particle population's distribution anisotropy is, or the mere presence of a hot anisotropic proton population in the outer magnetosphere at that time), the same pressure jump could or could not induce wave production or enhancement. What our study concludes is that in most of

the cases a pressure variation of at least 0.6 nPa will affect the production or enhancement of proton cyclotron waves. The same discussion also holds for the chosen pressure gradient of 0.55 nPa/hour. These lower limits for the pressure variation and the pressure gradient could be parameterized if one knew the distribution function of the hot outer-magnetospheric proton populations. Here is a scenario of the calculations that can be made in order to predict whether a pressure variation can induce proton cyclotron instability: the solar wind dynamic pressure and the z-component of the interplanetary magnetic field can be used to accurately predict the position of the magnetopause [Shue et al., 1998], which in turn can be used to calculate the magnetospheric magnetic field at the location of the wave source [Tsyganenko, 1995]. Hence we can calculate the parallel plasma beta $\beta_{\parallel p}$, and then using equation (2.3.29) of Chapter 2, with the calculated temperature anisotropy, we could determine whether the plasma is unstable to proton cyclotron waves.

**Summary**

- By looking at the ground data first we found that for only 19% of the wave events the the total wave power variation was similar to the variation of the solar wind dynamic pressure .
- In the second approach we looked at the solar wind pressure data first and we found that 82% of the pressure variations of at least 0.6 nPa and at least 0.55 nPa/hour were the cause of similar wave power variations on the ground.
- We found that for the purpose of our study the WIND satellite was a good solar wind monitor. 80% of the solar wind dynamic pressure increases above 4 nPa were the

cause of a positive Dst excursion of at least 30 nT. In a scatter plot of the satellite's $X = Y_{gse}$ position we found matching pressure-wave power events as far as 60 RE off the Sun-Earth line and as far as 200 RE upstream of the Earth.

- The cause of the 81% remaining wave events could be the increase in the proton populations' temperature anisotropy due to drifting into the stronger magnetic field of the subsolar magnetosphere.

- Since Pc1 waves are created by wave-particle interactions with magnetospheric hot anisotropic proton populations, we expected to find a correlation between some magnetic disturbance index (that would reflect the presence of the hot protons) and periods with waves. We found no such correlation in the Ap index; the better indicator would have been the AE index but we had no AE index data available.

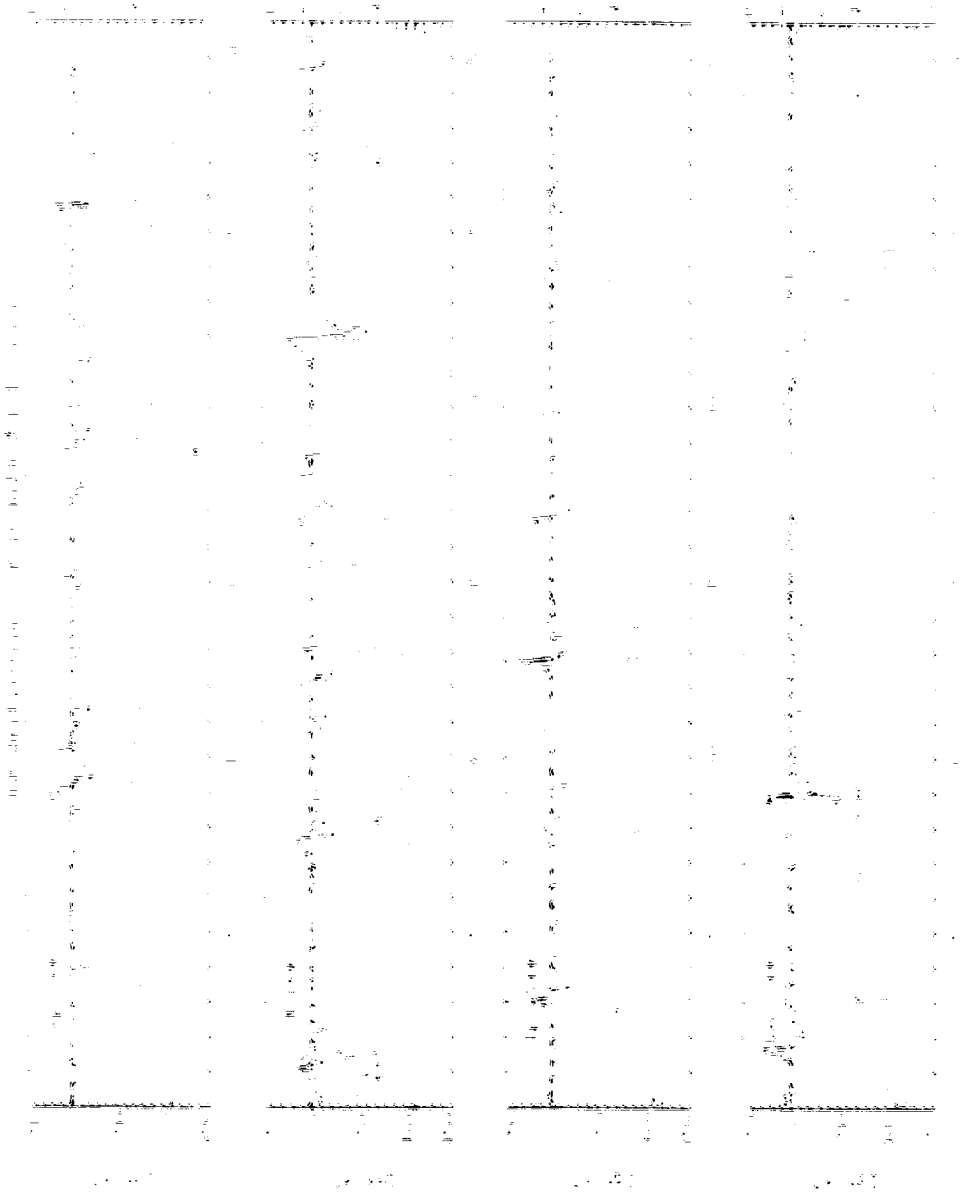

**Figure 4-9: Solar wind pressure from WIND and the ground-based Dst index**

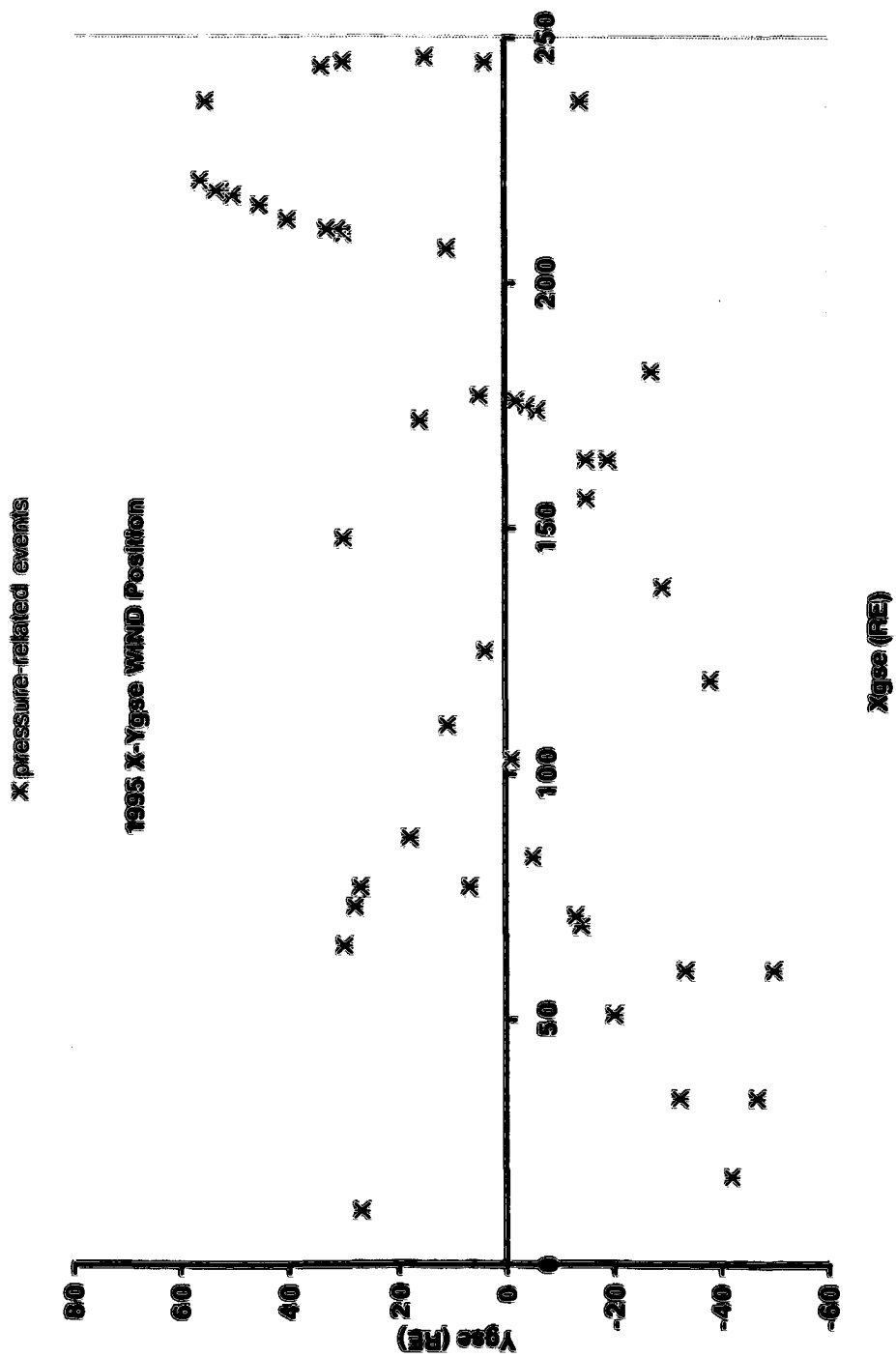


Figure 4-10: WIND position during matching events

# Bibliography


[Anderson et al., 1990] Anderson, B. J., K. Takahashi, R. E. Erlandson, and L. J. Zanetti, Pc 1 pulsations observed by AMPTE/CCE in the Earth's outer magnetosphere, *Geophys.Res.Lett., 17*, 1853, 1990.

[Anderson et al., 1992a] Anderson, B. J., R. E. Erlandson, and L. J. Zanetti, A statistical study of Pc 1-2 Pulsations in the equatorial magnetosphere 1. equatorial occurence *J.Geophys.Res, 97*, 3075, 1992.

[Anderson et al., 1992b] Anderson, B. J., R. E. Erlandson, and L. J. Zanetti, A statistical study of Pc 1-2 Pulsations in the equatorial magnetosphere 2. wave properties, *J.Geophys.Res, 97*, 3089, 1992.

[Anderson and Hamilton, 1993] Anderson, B. J., and D. C. Hamilton, Electromagnetic ion cyclotron waves stimulated by modest magnetospheric compressions *J.Geophys.Res, 98*, 11369, 1993.

[Anderson et al., 1994] Anderson, S. A. Fuselier, S. P. Gary, and R. E. Denton, Magnetic spectral signatures in the Earth's magnetosheath and plasma depletion layer, *J.Geophys.Res, 99*, 5877, 1994.

[Anderson et al., 1996a] Anderson, B. J., R. L. Arnoldy, R. E. Erlandson, M. J. Engebretson, J. Alford, Source region of 0.2 to 1.0 Hz geomagnetic pulsation bursts, *Geophys.Res.Lett., 7*, 769, 1996.

[Anderson et al., 1996b] Anderson, B. J., R. E. Denton, G. Ho, D. C. Hamilton, S. A. Fuselier, and R. J. Strangeway Observational test of local proton cyclotron instability in the Earth's magnetosphere, *J.Geophys.Res, 101*, 21527, 1996.

[Arnoldy et al., 1996a] Arnoldy, R. L., L. J. Cahill, Jr., M. J. Engebretson, L. J. Lanzerotti, A. Wolfe, Review of hydromagnetic wave studies in the antarctic, *Rev.Geophys, 26*, 1, 181-207, 1988.

[Arnoldy et al., 1996b] Arnoldy, R. L., M. J. Engebretson, J. L. Alford, R. E. Erlandson and B. J. Anderson, Magnetic impulse events and associated Pc 1 bursts at dayside high latitudes, *Geophys.Res.Lett., 23*, 769, 1996.

[Baumjohann and Treumann, 1996] Baumjohann, W. and R. A. Treumann, *Basic Space Plasma Physics*, Imperial College Press, 1996.

[Bolshakova et al., 1980] Bolshakova, O. B., V. A. Troitskaya, and K. G. Ivanov, High latitude Pc 1-2 geomagnetic pulsations and their connection with location of the dayside polar cusp, *Planet.Space Sci., 28*, 1, 1980.

[Burton et al., 1975] Burton, R. K., R. L. McPherron, and C. T. Russell, An empirical relationship between interplanetary conditions and Dst, *J.Geophys.Res. 80*, 4204, 1975.

[Chew et al., 1956] Chew, G. F., M. L. Goldberger, F. E. Low, The Boltzmann equation and the one-fluid hydromagnetic equations in the absence of particle collisions, *Proc.R.Soc.London, Ser.A, 236*, 112, 1956.

[Cornwall, 1965] Cyclotron instabilities and electromagnetic emission in the ultra low frequency and very low frequency ranges, *J.Geophys.Res., 70*, 61, 1965.

[Dusenbery and Hollweg, 1981] , Dusenbery, P. B., and J. V. Hollweg, Ion-cyclotron heating and acceleration of solar wind minor ions, *J.Geophys.Res., 86*,, 153, 1981.

[Dyrud et al., 1997] Dyrud, L. P., M. J. Engebretson, J. L. Posch, W. J. Hughes, H. Fukunishi, R. L. Arnoldy, P. T. Newell, R. B. Horne, Ground observations and possible source regions of two types of Pc 1-2 micropulsations at very high latitudes, *J.Geophys.Res., 102*, 27011, 1997.

[Fairfield et al., 1990] Fairfield, D. H., W. Baumjohann, G. Paschmann, H. Luhr, and D. G. Sibeck, Upstream pressure variations associated with the bow shock and their effects on the magnetosphere, *J.Geophys.Res., 95*, 3773, 1990.

[Farrugia et al., 1989] Farrugia, C. J., M. P. Freeman, S. W. H. Cowley, and D. J. Southwood, Pressure-driven magnetopause motions and attendant response on the ground, *Planet.Space Sci., 37*, 589, 1989.

[Fraser, 1975] Fraser, B. J., Ionospheric duct propagation and Pc1 pulsation sources, *J.Geophys.Res., 80*, 2790, 1975.

[Fukunishi et al., 1981] Fukunishi, H., T. Toya, K. Koike, M. Kuwashima and M. Kawamura, Classification of hydromagnetic emissions based on frequency-time spectra, *J.Geophys.Res., 86*, 9029, 1981.

[Gary et al., 1976] Gary, S. P., M. D. Montgomery, W. C. Feldman and D. W. Forslund, Proton temperature anisotropy instabilities in the solar wind, *J.Geophys.Res., 81*, 1241, 1976.

[Gary, 1993] Gary, S. P., *Theory of Space Plasma Microinstabilities*, Cambridge University Press, 1993.

[Gary and Lee, 1994] Gary, S. P., and M. A. Lee, The ion cyclotron anisotropy instability and the inverse correlation between proton anisotropy and proton beta, *J.Geophys.Res., 99*, 11297, 1994.

[Gary et al., 1994] Gary, S. P., M. B. Moldwin, M. F. Thomsen, D. Winske, and D. J. McComas, Hot proton anisotropies and cool proton temperatures in the outer magnetosphere, *J.Geophys.Res., 99*, 23603, 1994.

[Hayashi et al., 1981] Hayashi, K., S. Kokubun, T. Oguti, T. Tsuruda, S. Machida, T. Kitamura, O. Saka, T. Watanabe, The extent of Pc1 source region in high latitudes, *Can.J.Phys., 59*, 1097, 1981.

[Hollweg, 1986] Hollweg, J. V., Viscosity and the Chew-Goldberger-Low equations in the solar corona, *Ap.J., 306*, 730, 1986.

[Ichimaru, 1992] Ichimaru, S. *Statistical Plasma Physics, Volume 1*, Second edition, Addison-Wesley, 1992.

[IDL Reference Guide, 1995] Research Systems Incorporated, *IDL Reference Guide*, Vol 1, 1995.

[Jacobs and Watanabe, 1967] Jacobs, J. A., and T. Watanabe, Theoretical notes on whistlers and periodic emissions in the hydromagnetic regime, *Planet.Space Sci., 15*, 799, 1967.

[Kato and Tonegawa, 1995] Kato, Y., and Y. Tonegawa, Pc 1 pulsations observed at Cambridge Bay in the cusp region and Forth Smith in the auroral region, *Mem.Nat.Inst.Pol.Res. 42*, 52, 1995.

[Kaufman, 1997] Kaufman, R. L., *Plasma Physics*, UNH, 1997.

[Kennel and Petschek, 1966] Kennel, C. F., H. E. Petschek, Limit on stably trapped particle fluxes, *J.Geophys.Res., 71*, 1, 1966.

[Kivelson and Russell, 1995] Kivelson, M. G., and C. T. Russell, *Introduction to Space Physics*, Cambridge University Press, 1995.

[Kozyra et al., 1984] Kozyra, J. U., T. E. Cravens, A. F. Nagy, and E. G. Fontheim, Effects of energetic heavy ions on electromagnetic ion cyclotron wave generation in the plasmapause region, *J.Geophys.Res., 89*, 2217, 1984.

[Lepping et al., 1995] Lepping, R. P., M. H. Acuna, L. F. Burlaga, W. M. Farrell, J. A. Slavin, K. H. Schatten, F. Mariani, N. F. Ness, F. M. Neubauer, Y. C. Whang, J. B. Byrnes, R. S. Kennon, P. V. Panetta, J. Scheifele, and E. M. Worley, The WIND magnetic field investigation, *Space Sci.Rev., 71*, 207, 1995.

[Lichnohn, 1967] Lichnohn, H. B., Cyclotron-resonance amplification of VLF and ULF whistlers, *J.Geophys.Res., 72*, 39, 1967.

[Lin et al., 1996a] Lin, Y., L. C. Lee, and M. Yan, Generation of dynamic pressure pulses downstream of the bowshock by variations in the interplanetary magnetic field orientation, *J.Geophys.Res., 101*, 479, 1996.

[Lin et al., 1996b] Lin, Y., D. W. Swift, and L. C. Lee, Simulation of pressure pulses in the bowshock and magnetosheath driven by variations in the interplanetary magnetic field direction, *J.Geophys.Res., 101*, 27251, 1996.

[Manheimer & Boris, 1977] Manheimer, W., and J. P. Boris, Marginal stability analysis - A simpler approach to anomalous transport in plasmas, *Comments Plasma Phys. Controlled Fusion, 3*, 15, 1977.

[Menk et al., 1992] Menk, F. W., B. J. Fraser, H. J. Hansen, P. T. Newell, C.-I. Meng, and R. J. Morris, Identification of the magnetospheric cusp and cleft using Pc 1-2 ULF pulsations, *J.Atmos.Terr.Phys., 54*, 1021, 1992.

[Morris and Cole, 1991] Morris, R. J., and K. D. Cole, High latitude Pc 1-2 continuous magnetic pulsations: A ground signature of the polar cusp and cleft projection, *Planet.Space Sci., 39*, 1473, 1991.

[Obayashi, 1965] Obayashi, T. Hydromagnetic whistlers, *J.Geophys.Res., 70*, 1069, 1965.

[Ogilvie et al., 1995] Ogilvie, K. W., D. J. Chornay, R. J. Fritzenreiter, F. Hunsaker, J. Keller, J. Lobell, G. Miller, J. D. Scudder, E. C. Sittler, Jr., R. B. Torbert, D. Bodet, G. Needell, A. J. Lazarus, J. T. Steinberg, J. H. Tappan, A. Mavretic, and E. Gergin, SWE, a comprehensive plasma instrument for the WIND spacecraft, *Space Sci.Rev., 71*, 55, 1995.

[Olson and Lee, 1983] Olson, J. V., and L. C. Lee, Pc 1 wave generation by sudden impulses, *Planet.Space Sci., 31*, 295, 1983.

[Parady, 1974] *Measurement of low frequency magnetic fluctuations in the magnetosphere*, Dissertation, University of Minnesota, 1974.

[Paschmann et al., 1979] Paschmann, G., N. Sckopke, S. J. Bame, J. R. Asbridge, J. T. Gosling, C. T. Russell, and E. W. Greenstadt, Association of low-frequency waves with suprathermal ions in the upstream solar wind, *Geophys.Res.Lett. 6*, 209, 1979.

[Paularena et al., 1998] Paularena, K. I., G. N. Zastenker, A. J. Lazarus, and P. A. Dalin, Solar wind plasma correlations between IMP 8, Interball-1, and Wind, *J.Geophys.Res., 103*, 14601, 1998.

[Perraut et al., 1978] Perraut, S., R. Gendrin, P. Robert, A. Roux, C. De Villedary, and D. Jones, ULF waves observed with magnetic and electric sensors on GEOS-1, *Space Sci.Rev., 22*, 347, 1978.

[Popecki, 1991] *A statistical study of narrow bandwidth, high latitude geomagnetic pulsations*, Dissertation, University of New Hampshire, December, 1991.

[Popecki et al., 1993] Popecki, M. A., R. L. Arnoldy, M. J. Engebretson, L. J. Cahill, Jr., High latitude ground observations of Pc 1/2 micropulsations, *J.Geophys.Res., 98*, 21481, 1993.

[Press et al., 1992] Press, H. W., S. A. Teukolsky, W. T. Vetterling, B. P. Flannery, *Numerical Recipes in C, The Art of Scientific Computing*, Cambridge University Press, Second Edition, 1992.

[Richardson et al., 1998] Richardson, J. D., F. Dashevskiy, and K. I. Paularena, Solar wind plasma correlations between L1 and Earth, *J.Geophys.Res., 103*, 14619, 1998.

[Roux et al., 1982] Roux, A., S. Perraut, J. L. Rauch, C. de Villedary, G. Kremser, A. Korth, and D. T. Young, Wave-particle interactions near $\Omega_{He^+}$ observed on board GEOS 1 and 2 2. Generation of ion cyclotron waves and heating of $He^+$ ions, *J.Geophys.Res., 87*, 8174, 1982.

[Saito, 1969] Saito, T., Geomagnetic Pulsations, *Space Sci. Rev., 10* 318, 1969.

[Samson, 1991] Samson, J. C., Geomagnetic Pulsations and Plasma Waves in the Earth's Magnetosphere, *Geomagnetism, Vol. 4*, Academic Press Limited, 1991.

[Shue et al., 1998] Shue, J.-H., P. Song, C. T. Russell, J. T. Steinberg, J. K. Chao, G. Zastenker, O. L. Vaisberg, S. Kokubun, H. J. Singer, T. R. Detman, and H. Kawano, Magnetopause location under extreme solar wind conditions, *J.Geophys.Res., 103*, 17691, 1998.

[Sibeck and Korotova, 1996] Sibeck, D. J., G. I. Korotova, Occurence patterns for transient magnetic field signatures at high latitudes, *J.Geophys.Res., 101*, 13413, 1996.

[Stix, 1992] Stix, T. H., *Waves in Plasmas*, American Institute of Physics, 1992.

[Tsyganenko, 1995] Tsyganenko, N. A., Modeling the Earth's magnetospheric magnetic field confined within a realistic magnetopause, *J.Geophys.Res., 100*, 5599, 1995.

[Young et al., 1981] D. T. Young, S. Perraut, A. Roux, C. de Villedary, R Gendrin, A. Korth, G. Kremser, and D. Jones, Wave-particle interactions near $\Omega_{He^+}$ observed on board GEOS 1 and 2 1. Propagation of ion cyclotron waves in a $He^+$ rich plasma, *J.Geophys.Res., 86*, 6755, 1981.

# Appendices

# Appendix A

# Micropulsation data collection.

## A.1 The Antennas

At every station there are three induction antennas, each measuring one of the Cartesian components of the Earth's magnetic field variation ($\partial B_x/\partial t$, $\partial B_y/\partial t$, $\partial B_z/\partial t$). The voltage induced in an antenna is directly proportional to the variation of the magnetic flux through the antenna:

$$V \propto -\frac{\partial \Phi}{\partial t}$$

where

$$\Phi \equiv \iint_A \vec{B} \cdot d\vec{a},$$

is the magnetic flux through the antenna.

The antennas were designed so that their sensitivity is maximized while maintaining a reasonable physical size (a cylinder 90 cm long and 6.35 cm in diameter). This is much smaller than the old coils (1.83 m long and 15.2 cm in diameter) designed by Bodo Parady at the University of Minnesota ([Parady, 1974]). The final design included 16 small coils wound with 10,000 turns of gauge 28 coated magnet wire per coil (Figure A-1), connected in series and placed around a 76.2 cm long $\mu$-metal rod (high magnetic permeability). The resulting sensitivities were approximately 150 $\mu V\, nT^{-1} Hz^{-1}$ . The sensitivity is defined as the amplitude of the antenna output signal in Volts, when the magnetic field oscillates

with an amplitude of 1 nT and a frequency of 1 Hz. Figure A-2 shows the schematics of a complete station. The signal from each antenna is inputed into a preamplifier (Figure A-3) with a nominal gain of 121. From the output of the preamplifier the signal goes through a short (1 m) cable into the junction box. All of the components described so far are buried into the ground at the location of the magnetic field measurement. From the junction box the signal is transported through a long (150 - 300 m) cable to the location where the measurements are recorded, an enclosed area. Here the signals are inputed into three identical amplifiers (Figure A-4) with a gain of 244. The gains for the preamplifiers and the amplifiers where chosen so that the final output signals are at full range ±10 Volts for a variation of the magnetic field with an amplitude of 2.4 nT and a frequency of 1 Hz (this is called a "$2.4nT\ Hz$ full scale". ). This can be illustrated by calculating the output voltage for a magnetic field variation of 2.4 nT at 1 Hz, by multiplying this value with the sensitivity and the gains of the preamplifiers and amplifiers:

$$V_{full\ scale} = 2.4\,(nT\,Hz) * 150\,(\mu V/nT/Hz) * 121 * 244 \cong 10\,V.$$

We chose the $2.4nT\ Hz$ full scale in order to be able to compare quantitatively our measurements with the Parady design coil measurements. One of the fundamental differences between the current design of the antennas and the old design is the mechanical enclosure of the coils. Note that in our design (Figure A-1) the enclosure is a plexiglass tube, while the old antennas ([Parady, 1974]) were enclosed in a 9.5 mm thick aluminum tube.

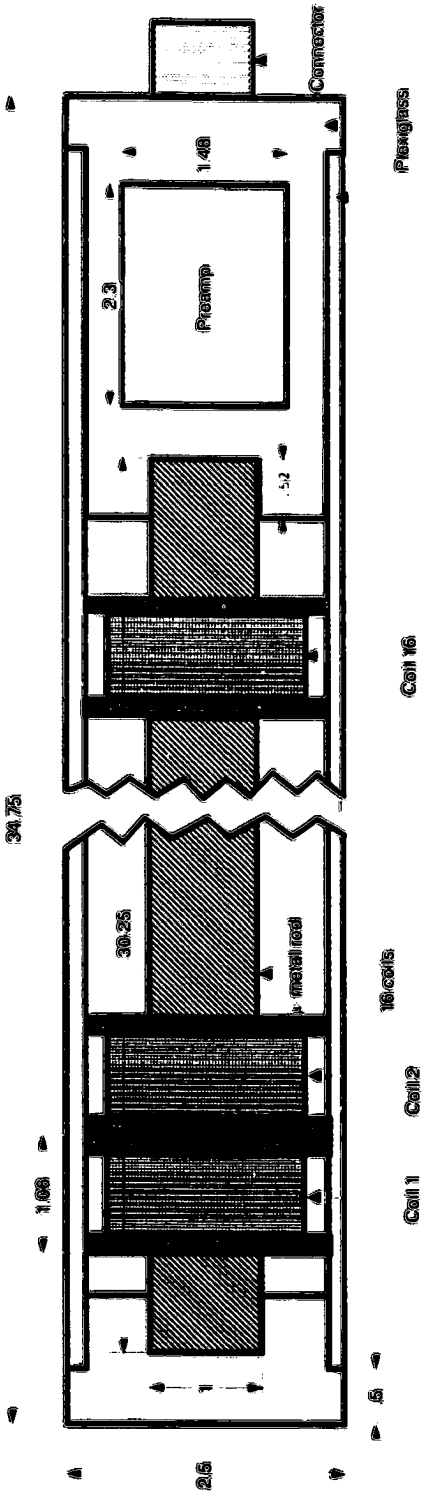


Figure A-1: Schematics of a search coil antenna.

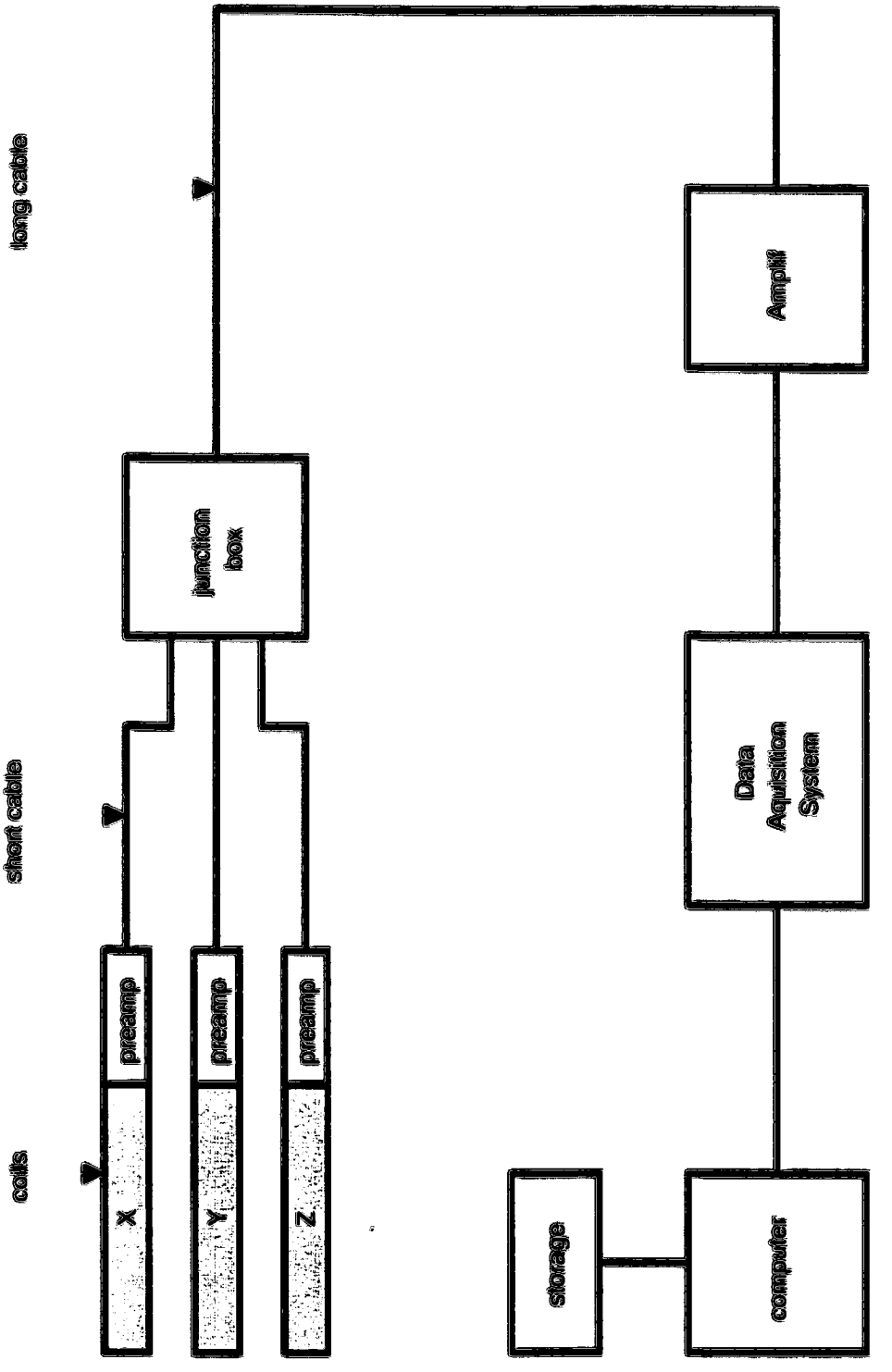


Figure A-2: Schematics of a micropulsation station.

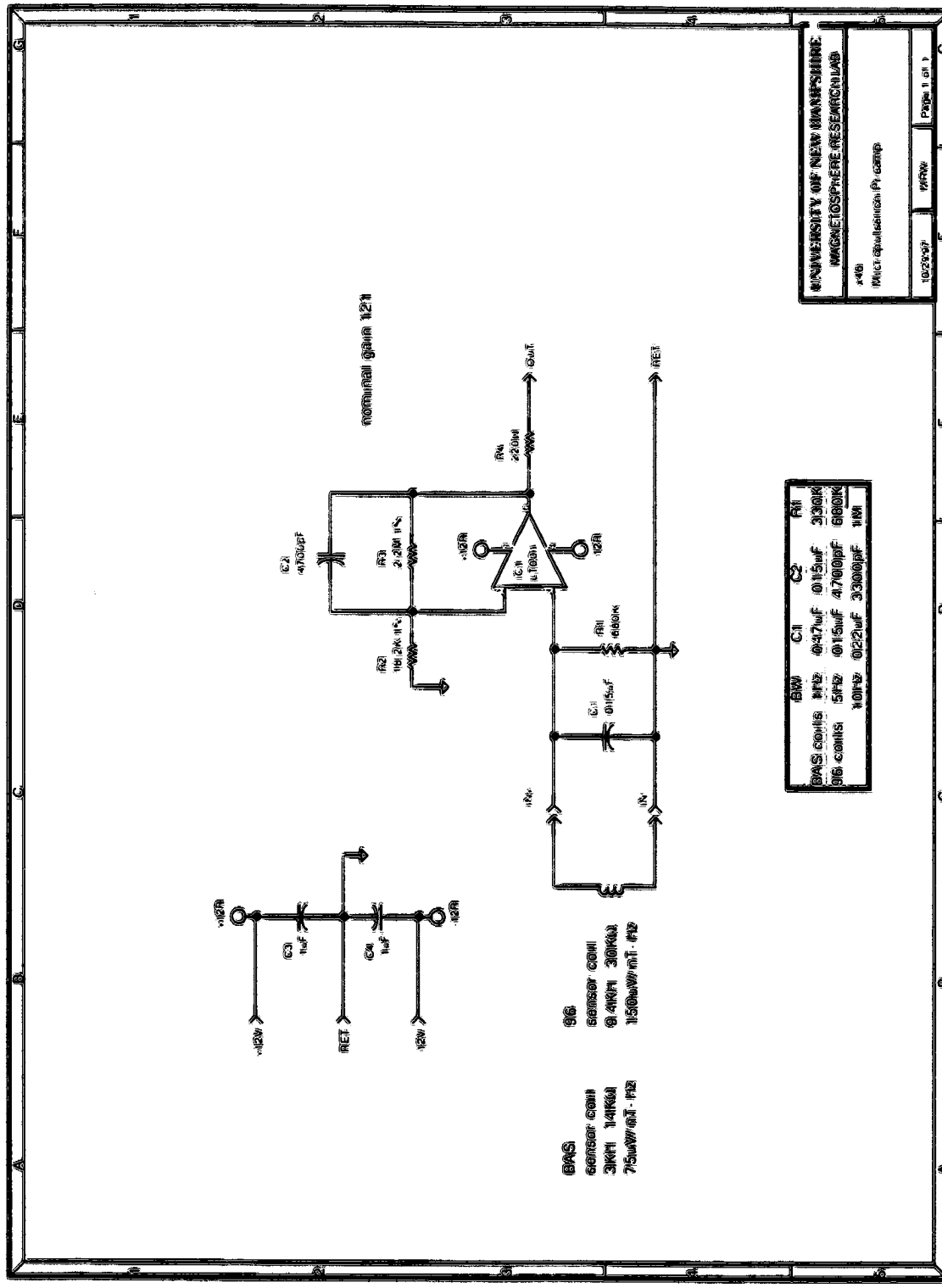


Figure A-3: Micropulsation Preamplifier.

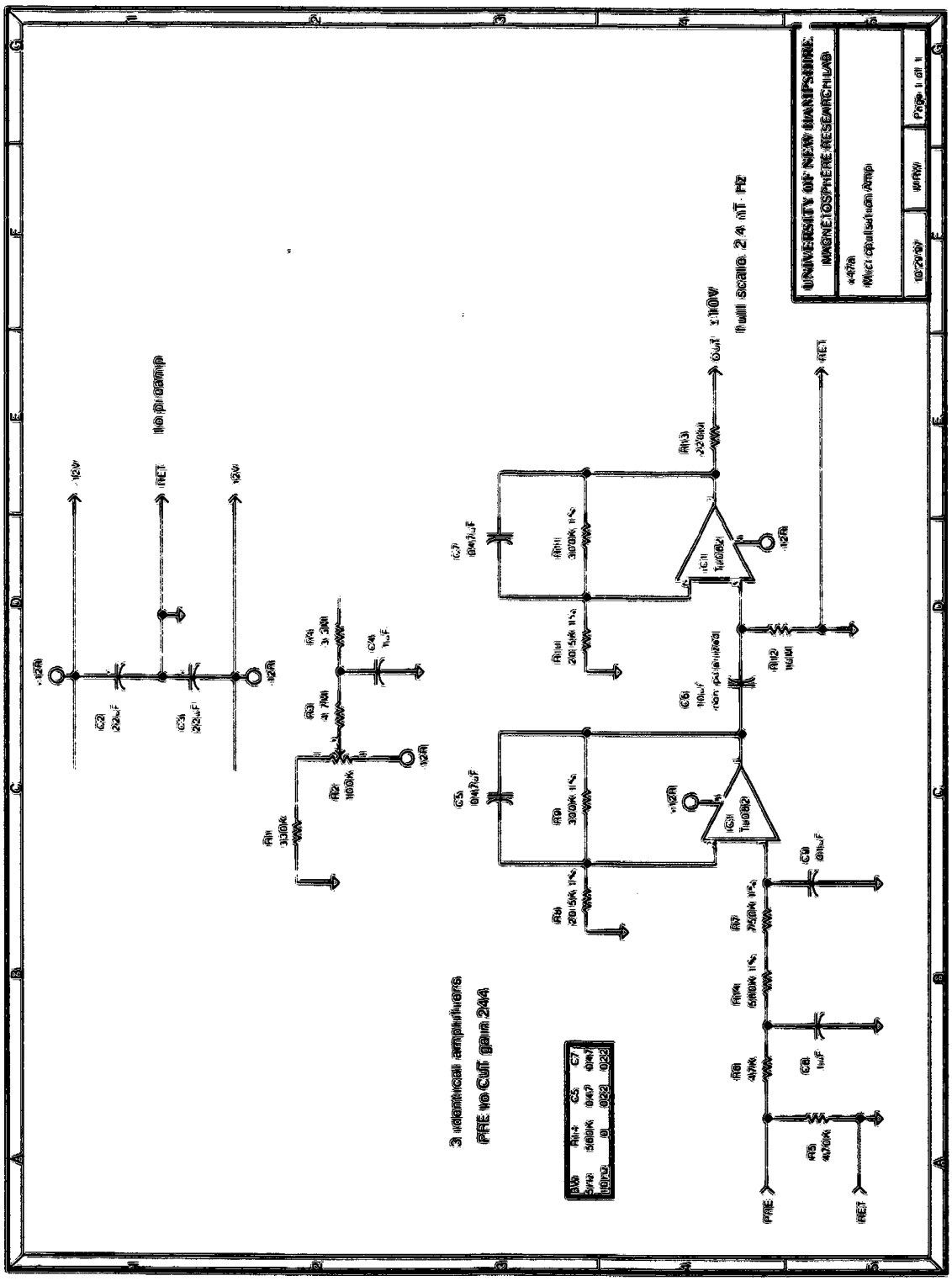


**Figure A-4: Micropulsation Amplifier.**

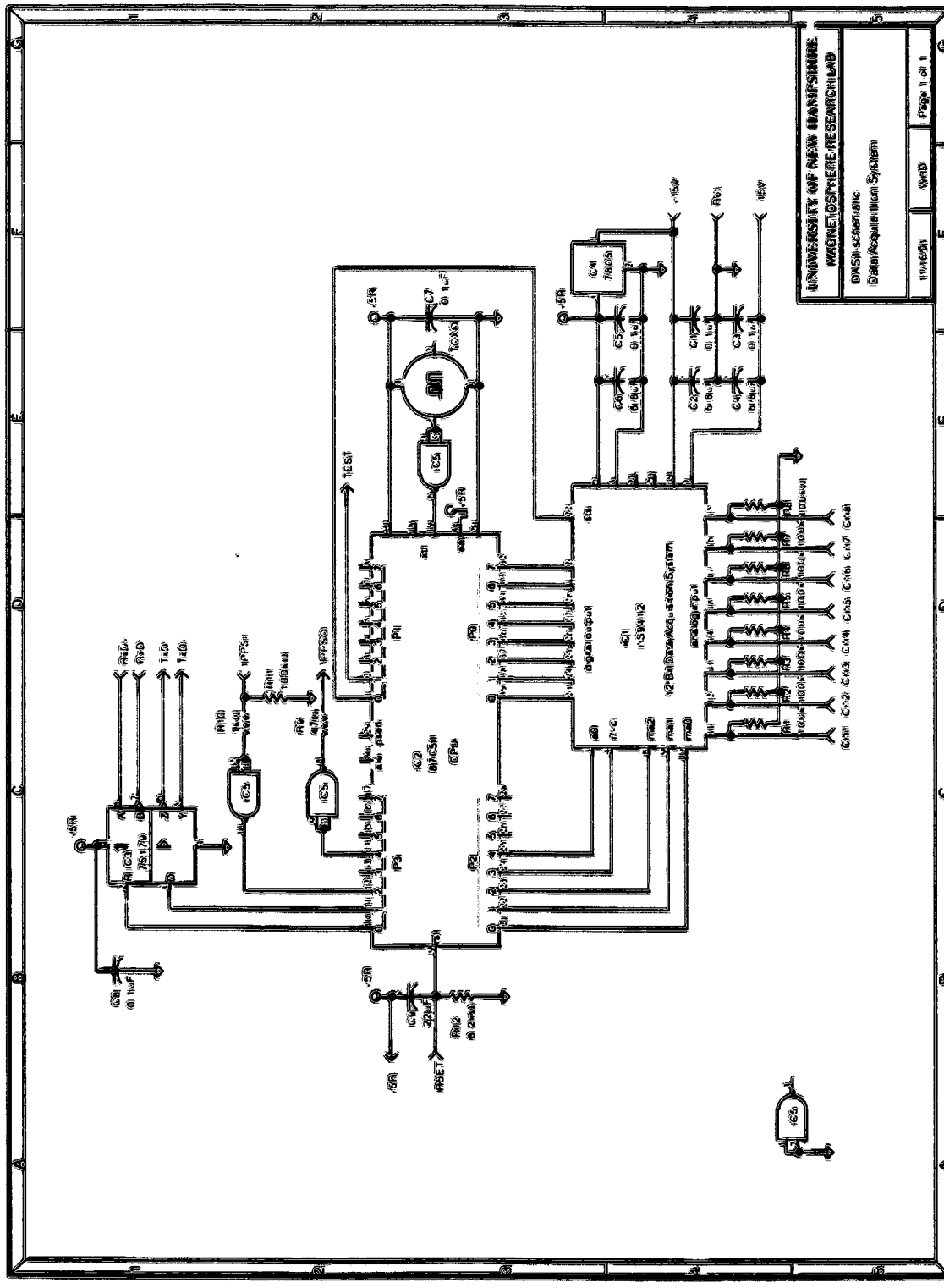


Figure A-5: Schematics of the Data Aquisition System.

## A.2 Data Aquisition System

After being amplified, the signal goes into the Data Acquisition System (DAS). The DAS consists of a Central Processing Unit (CPU) and a 10 Volt - 12 bit Analog to Digital (A to D) Converter (Figure A-5). The A to D converter takes the ±10 Volt signal and encodes it linearly into $2^{12}$ possible digital values between 0 and 4096 integer or between 0000 and 0FFF hexadecimal. This is usually written as:

$$[-10, +10]\,V \Rightarrow [0000, 0001, ..., 0FFE, 0FFF]_{HEX}$$

Note that the first figure of the encoded signal is always $0_{HEX}$ or $0000_{digital}$, so the first four bits of the 16 bit (2 byte) word are never used. Every encoded value is represented by 12 bits only, resulting in the name "12-bit" for the A to D converter. The resolution of the encoded signal is therefore limited by this 12-bit encoding to 20/4096 Volts. The CPU commands the A to D converter, more specifically it "tells" it when to sample. The sampling frequency in our case is 10 Hz, resulting in a Nyquist frequency of 5 Hz. The Nyquist frequency represents the maximum frequency that can be resolved by the fast Fourier transform, and it is equal to half of the sampling frequency ($f_{Nyquist} = 5Hz$ in our case). The CPU also sends the encoded signal to the computer's serial port. The data is recorded on the storage unit (usually an IOMEGA zip disk of 100 MB capacity) in a file that will contain consecutive two-byte words.

At the beginning of every recording the software that runs the DAS will automatically open a data file for every axis and will create a resource fork with housekeeping information. The resource fork is a hidden MacIntosh file that stays attached to the data file. The information contained in the housekeeping resource fork is:

- station name
- axis
- start time
- sampling frequency
- scaling

The Magnetosphere Research Laboratory engineers (Mark Widholm and Hank Dolben) have written a simple programming language called DOTSpad (Discrete Ordered Time Series), which is specifically designed to display these data. DOTSpad automatically reads the housekeeping information.

## A.3 Calibration

Every set of coils has been calibrated in the laboratory before being shipped into the field for measurements. In order to understand the response of the coils to different frequency fluctuations we need to obtain the frequency response of the coils. To do that we place the coil in a pure sinusoidal magnetic field for which we know and can vary the amplitude and frequency. The amplitude of the coil output is recorded for frequencies in the range of interest (0 to 5 Hz) and then plotted as a function of frequency. Figure (A-6) is an example of frequency response for one of the coils.

The calibration is also needed to make sure that the coil sensitivities are close to the projected ones. An example of the data collected during the calibration of one set of coils is presented in Table (A.1). In this case we placed the coils at a distance of 112 inches away

Table A.1: Sample calibration for a set of micropulsation coils.

| coil | freq | dist | out | sens |
|---|---|---|---|---|
| X | 0.5 | 112 | 1.83 | 162 |
| Y | 0.5 | 112 | 1.86 | 165 |
| Z | 0.5 | 112 | 1.91 | 169 |
| X | 1.0 | 112 | 3.82 | 169 |
| Y | 1.0 | 112 | 3.74 | 165 |
| Z | 1.0 | 112 | 3.78 | 167 |
| X | 2.0 | 112 | 6.25 | 139 |
| Y | 2.0 | 112 | 6.27 | 139 |
| Z | 2.0 | 112 | 6.45 | 143 |
| X | 5.0 | 112 | 8.23 | 73 |
| Y | 5.0 | 112 | 7.66 | 70 |
| Z | 5.0 | 112 | 8.20 | 73 |

from the antenna that was the source of the known magnetic field. We recorded the output and calculated the sensitivity of the coils for four different frequencies (0.5, 1, 2 and 5 Hz). Note how the sensitivity decreases with the increase of the frequency.

The aluminum tube of the old coil design [Parady, 1974] was replaced by plexiglass tubes in the new coil design. The difference between the frequency response of the coils in the two designs is illustrated in Figure A-6. The top plot is a plot of the frequency response of a coil with similar characteristics to the ones used in the field. When the coil was placed inside the aluminum tube (bottom curves) the response had much smaller amplitude. Two different capacitors were used to illustrate the effect of bringing the resonant L-C peak within the frequency range of the plot. The solid lines are the results of a theoretical model and the symbols are actual experimental data points. The bottom plot is a theoretical model of

the frequency response of the Bodo coils ([Parady, 1974]) inside and outside the aluminum tube. This plot illustrates the fact that the signal from coils inside the aluminum tube is strongly damped for most of the frequency range that they were designed for. This was the reason for which the new coils design feature a plexiglass tube instead of the old aluminum tube.

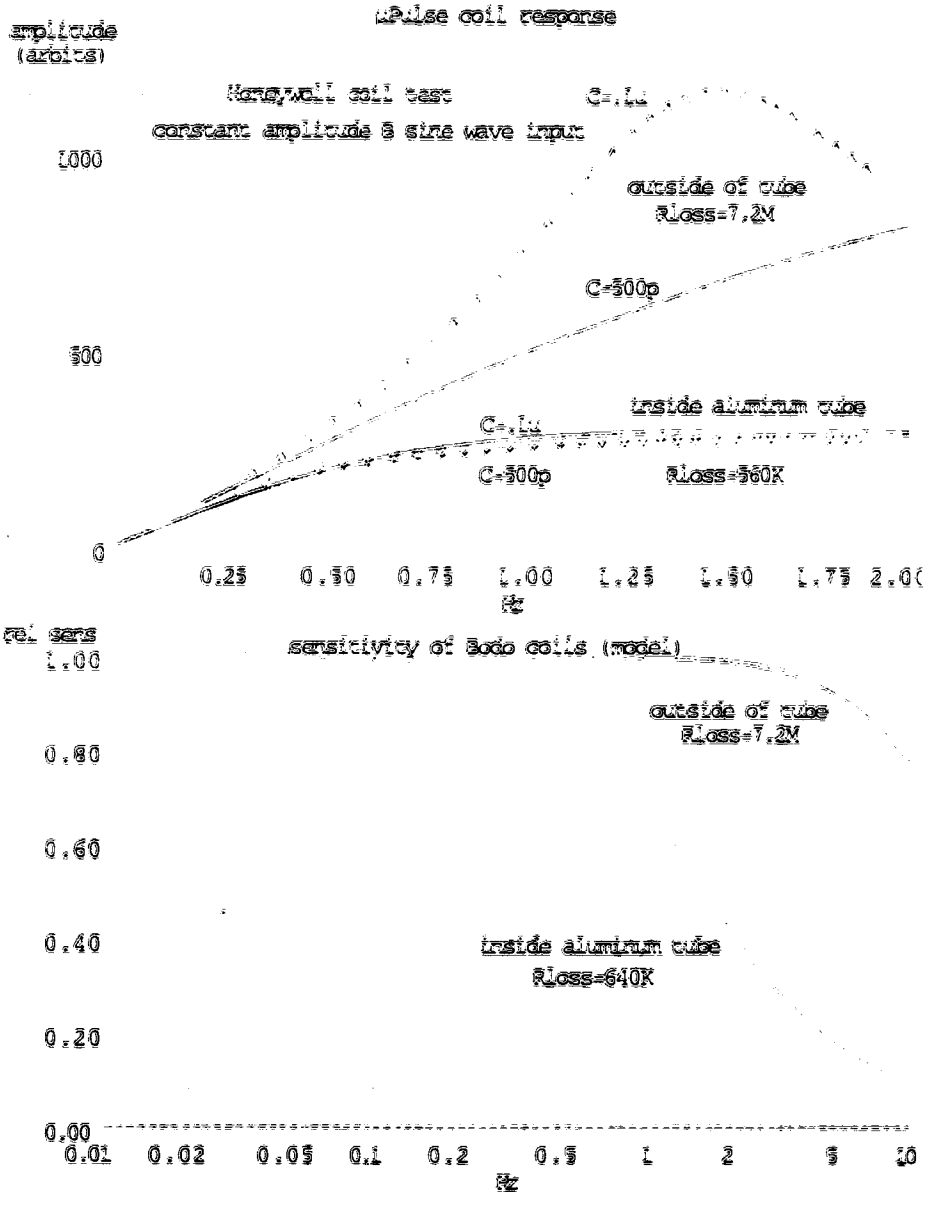


**Figure A-6: Comparison of the frequency response for two different coil designs.**

# Appendix B

# Derivation of the CGL equations.

## B.1 The moment equation for the parallel kinetic energy

In chapter 2 we found the general moment equation for an arbitrary function $\Psi(\vec{r},\vec{v},t)$, equation (2.3.7). To find the first of the CGL equations we take

$$\Psi \equiv \frac{1}{2}mv_{\parallel}^2 \tag{B.1.1}$$

where

$$v_{\parallel}^2 \equiv \vec{v}\cdot\hat{b} \qquad and \qquad \hat{b} \equiv \frac{\vec{B}}{|\vec{B}|}. \tag{B.1.2}$$

$\Psi$ is dependent on the coordinate $\vec{r}$ through $\hat{b}$. Let us calculate the different derivatives involved in the equation:

$$\frac{\partial\Psi}{\partial t} \equiv \frac{\partial}{\partial t}\left(\frac{1}{2}mv_{\parallel}^2\right) \equiv mv_{\parallel}\vec{v}\cdot\frac{\partial\hat{b}}{\partial t} \tag{B.1.3}$$

$$\frac{\partial\Psi}{\partial\vec{v}} \equiv \frac{\partial}{\partial\vec{v}}\left(\frac{1}{2}mv_{\parallel}^2\right) \equiv mv_{\parallel}\hat{b} \tag{B.1.4}$$

$$\begin{aligned}\nabla\Psi &\equiv \nabla\left(\frac{1}{2}mv_{\parallel}^2\right) \equiv mv_{\parallel}\nabla(\vec{v}\cdot\hat{b})\\ &\equiv mv_{\parallel}\left(\vec{v}\times\nabla\times\hat{b}+\hat{b}\times\nabla\times\vec{v}+\vec{v}\cdot\nabla\hat{b}+\hat{b}\cdot\nabla\vec{v}\right)\\ &\equiv mv_{\parallel}(\vec{v}\cdot\nabla\hat{b}+\vec{v}\times\nabla\times\hat{b})\end{aligned} \tag{B.1.5}$$

It is convenient to separate the bulk motion of the distribution and define

$$\vec{w} \equiv \vec{v} - \vec{V} \tag{B.1.6}$$

where $\vec{V} \equiv \langle \vec{v} \rangle$. Note that according to the definition of $\vec{V}$ we have $\langle \vec{w} \rangle \equiv 0$, so $\vec{w}$ is the speed of the thermal motion. We can define the parallel pressure as

$$p_{\parallel} \equiv \rho \left\langle w_{\parallel}^2 \right\rangle \tag{B.1.7}$$

and the parallel heat flux:

$$\vec{q}_{\parallel} \equiv \rho \left\langle w_{\parallel}^2 \vec{w} \right\rangle \tag{B.1.8}$$

Let us calculate each average in equation (2.3.7) separately:

$$\langle \Psi \rangle \equiv \left\langle \frac{1}{2} m v_{\parallel}^2 \right\rangle \equiv \frac{1}{2} m \left( V_{\parallel}^2 + \left\langle w_{\parallel}^2 \right\rangle + 2 V_{\parallel} \langle w_{\parallel} \rangle \right)$$

$$\equiv \frac{1}{2} m \left( V_{\parallel}^2 + \frac{p_{\parallel}}{\rho} \right) \tag{B.1.9}$$

$$\left\langle \dot{\Psi} \right\rangle \equiv m \langle v_{\parallel} \vec{v} \rangle \cdot \frac{\partial \vec{b}}{\partial t} \equiv m \left( V_{\parallel} \vec{V} + \langle w_{\parallel} \vec{w} \rangle \right) \cdot \frac{\partial \vec{b}}{\partial t} \tag{B.1.10}$$

$$\langle \Psi \vec{v} \rangle \equiv \frac{1}{2} m \left\langle v_{\parallel}^2 \vec{v} \right\rangle$$

$$\equiv \frac{1}{2} m \left[ V_{\parallel}^2 \vec{V} + 2 V_{\parallel} \langle w_{\parallel} \vec{w} \rangle + \vec{V} \left\langle w_{\parallel}^2 \right\rangle + \left\langle w_{\parallel}^2 \vec{w} \right\rangle \right]$$

$$\equiv \frac{1}{2} m \left[ V_{\parallel}^2 \vec{V} + 2 V_{\parallel} \langle w_{\parallel} \vec{w} \rangle + \frac{p_{\parallel}}{\rho} \vec{V} + 2 \frac{\vec{q}_{\parallel}}{\rho} \right] \tag{B.1.11}$$

$$\langle \vec{v}\cdot\nabla\Psi\rangle \equiv m\left\langle v_{\|}\vec{v}\cdot(\vec{v}\cdot\nabla\hat{b})\right\rangle$$

$$\equiv m\left[V_{\|}\left\langle \vec{w}\cdot(\vec{w}\cdot\nabla\hat{b})\right\rangle + \left\langle (w_{\|}\vec{w}+w_{\|}\vec{V})\cdot(\vec{w}\cdot\nabla\hat{b})\right\rangle\right]$$

$$+ m\left(V_{\|}\vec{V}+\langle w_{\|}\vec{w}\rangle\right)\cdot\left(\vec{V}\cdot\nabla\hat{b}\right) \qquad \text{(B.1.12)}$$

$$\left\langle\frac{\partial\Psi}{\partial\vec{v}}\right\rangle \equiv mV_{\|}\hat{b} \qquad \text{(B.1.13)}$$

$$\left\langle(\vec{v}\times\vec{B})\cdot\frac{\partial\Psi}{\partial\vec{v}}\right\rangle \equiv m\left\langle v_{\|}(\vec{v}\times\vec{B})\cdot\hat{b}\right\rangle \equiv 0 \qquad \text{(B.1.14)}$$

At this point we insert equations (B.1.9) - (B.1.14) into equation (2.3.7). Using the mass conservation equation

$$\frac{\partial\rho}{\partial t}+\nabla\cdot\rho\vec{V} \equiv \int m\frac{\delta f}{\delta t}d^3\vec{v} \qquad \text{(B.1.15)}$$

and the scalar product between $V_{\|}\hat{b}$ and the momentum equation

$$\frac{\rho}{2}\frac{dV_{\|}^2}{dt}-\rho V_{\|}\vec{V}\cdot\frac{d\hat{b}}{dt}+V_{\|}(\nabla\cdot\bar{\bar{p}})\cdot\hat{b} \equiv \rho V_{\|}\left(\frac{q}{m}\vec{E}+\vec{g}\right)+mV_{\|}\int w_{\|}\frac{\delta f}{\delta t}d^3\vec{v} \qquad \text{(B.1.16)}$$

we get

$$\frac{1}{2}\frac{\partial p_{\|}}{\partial t}-\rho\langle w_{\|}\vec{w}\rangle\cdot\frac{d\hat{b}}{dt}+\nabla\cdot\left(\frac{1}{2}p_{\|}\vec{V}+\vec{q}_{\|}+\rho V_{\|}\langle w_{\|}\vec{w}\rangle\right)$$

$$-\rho\left\langle(w_{\|}\vec{w}+w_{\|}\vec{V})\cdot(\vec{w}\cdot\nabla\hat{b})\right\rangle - V_{\|}\nabla\cdot(\bar{\bar{p}}\cdot\hat{b}) \equiv \int\frac{1}{2}mw_{\|}^2\frac{\delta f}{\delta t}d^3\vec{v}. \qquad \text{(B.1.17)}$$

If the only anisotropy in the pressure tensor comes from the existence of the magnetic field $\vec{B}$, then the pressure tensor can be expressed in terms of only $p_{\parallel}$ and $p_{\perp}$:

$$p_{ij} \equiv p_{\perp}\delta_{ij} + (p_{\perp} - p_{\parallel})b_i b_j. \tag{B.1.18}$$

This realization of the pressure tensor is called the gyrotropic pressure tensor. We can further simplify equation B.1.17. For example we can write

$$\langle w_{\parallel}\vec{w}\rangle \equiv \langle w_{\parallel}b_i\, w_j c_j\rangle \equiv \frac{p_{ij}}{\rho}b_i c_j \equiv c_j\left[p_{\perp}\delta_{ij}b_i + (p_{\parallel} - p_{\perp})\, b_i b_j b_i\right] \equiv p_{\parallel}\dot{b} \tag{B.1.19}$$

Noting that $\dot{b}\cdot(d\dot{b}/dt) \equiv 0$ (because $\dot{b}$ is a vector of constant magnitude) and using (B.1.19) we can rewrite equation (B.1.17) as

$$\frac{1}{2}\frac{\partial p_{\parallel}}{\partial t} + \frac{1}{2}p_{\parallel}\nabla\cdot\vec{V} + \nabla\cdot\vec{q}_{\parallel} + p_{\parallel}\dot{b}\cdot(\dot{b}\cdot\nabla)\vec{V} = \rho\left\langle(w_{\parallel}\vec{w}\cdot(\vec{w}\cdot\nabla)\dot{b}\right\rangle \equiv \int\frac{1}{2}mw^2\frac{\delta f}{\delta t}d^3\vec{v}. \tag{B.1.20}$$

The behavior of the magnetic field $\vec{B}$ is governed by the induction equation:

$$\frac{\partial\vec{B}}{\partial t} \equiv \nabla\times\left(\vec{V}_i\times\vec{B}\right) + \vec{D}. \tag{B.1.21}$$

where $\vec{D}$ is the magnetic diffusion (it expresses the diffusion of the magnetic field lines):

$$\vec{D} \equiv \frac{c^2}{4\pi\sigma}\nabla^2\vec{B}. \tag{B.1.22}$$

Here we could run into trouble since equation (B.1.21) is written in terms of the center of mass velocity $\vec{V}_i$ while equation (B.1.20) is an equation for each species. Assuming that $\vec{V} \cong \vec{V}_i$ we can use the induction equation to further simplify equation (B.1.20):

$$\frac{d\vec{B}}{dt} \equiv \vec{B}\cdot\nabla V - \vec{B}\nabla\cdot\vec{V} + \vec{D} \tag{B.1.23}$$

Use the mass conservation equation (B.1.15) for the term $\nabla \cdot \vec{V}$:

$$\frac{1}{\rho}\frac{d\vec{B}}{dt} - \frac{\vec{B}}{\rho^2}\frac{d\rho}{dt} = \frac{1}{\rho}\left(\vec{B}\cdot\nabla V + \vec{D}\right) - \frac{\vec{B}}{\rho}\int \frac{m}{\rho}\frac{\delta f}{\delta t}d^3\vec{v} \qquad \text{(B.1.24)}$$

Taking the scalar product of $\hat{b}$ and equation (B.1.24) yields

$$\frac{d}{dt}\left(\ln\frac{B}{\rho}\right) = \hat{b}\cdot\left(\hat{b}\cdot\nabla\vec{V} + \frac{\vec{D}}{B}\right) - \frac{m}{\rho}\int\frac{\delta f}{\delta t}d^3\vec{v}. \qquad \text{(B.1.25)}$$

Inserting this into equation (B.1.20) and again using the mass conservation equation (B.1.15), we obtain

$$\begin{aligned}\frac{d}{dt}\ln\left(\frac{p_{\parallel}B^2}{\rho^3}\right) &= \frac{-2}{p_{\parallel}}\nabla\cdot\vec{q}_{\parallel} + \frac{2\rho}{p_{\parallel}}\left\langle w_{\parallel}\vec{w}\cdot(\vec{w}\cdot\nabla\hat{b})\right\rangle \\ &+ 2\frac{\hat{b}\cdot\vec{D}}{B} + \frac{m}{p_{\parallel}}\int\frac{\delta f}{\delta t}\left(w^2 - \frac{3p_{\parallel}}{\rho}\right)d^3\vec{v}\end{aligned} \qquad \text{(B.1.26)}$$

which is exactly equation (2.3.9) from chapther 2.

## B.2 The moment equation for the perpendicular kinetic energy

This equation is easier to find because we are going to use the equation that we have just found above, equation (2.3.9). We are also going to use the equation for the total thermal energy, obtained by inserting $\Psi = \frac{1}{2}mv^2$ into equation (2.3.7):

$$\frac{d}{dt}\frac{1}{2}Tr\,\vec{\vec{p}} + \frac{1}{2}Tr\,\vec{\vec{p}}\,\nabla\cdot\vec{v} + p_{ij}\frac{\partial V_j}{\partial x_i} = -\nabla\cdot\vec{q} + \frac{1}{2}\int w^2\frac{\delta f}{\delta t}d^3\vec{v}, \qquad \text{(B.2.1)}$$

where $Tr\,\vec{\vec{p}}$ is the trace of the pressure tensor and $\vec{q}$ is the total heat flux

$$\vec{q} \equiv \frac{1}{2}\rho\left\langle w^2\vec{w}\right\rangle. \qquad \text{(B.2.2)}$$

Using the gyrotropic pressure tensor (equation B.1.18), we can express the terms from the left hand side of equation (B.2.1) in terms of $p_{\|}$ and $p_{\perp}$:

$$Tr\,\vec{\vec{p}} \equiv p_{\|} + 2p_{\perp} \tag{B.2.3}$$

$$p_{ij}\frac{\partial V_j}{\partial x_i} \equiv p_{\perp}\delta ij\frac{\partial V_j}{\partial x_i} + (p_{\|} - p_{\perp})\,b_i b_j\frac{\partial V_j}{\partial x_i}$$

$$\equiv p_{\perp}\nabla\cdot\vec{V} + (p_{\|} - p_{\perp})\,\hat{b}\cdot\hat{b}\cdot\nabla\vec{V}. \tag{B.2.4}$$

Now eliminate $p_{\|}$ between equations (B.2.1) and (B.1.26) to obtain

$$\frac{d}{dt}\ln\left(\frac{p_{\perp}}{\rho B}\right) \equiv -\frac{\hat{b}\cdot\vec{\vec{D}}}{B} - \frac{1}{p_{\perp}}\left(\nabla\cdot\vec{q}_{\perp} + \rho\left\langle w_{\|}\vec{w}\cdot(\vec{w}\cdot\nabla\hat{b})\right\rangle\right)$$

$$+ \frac{m}{p_{\perp}}\int\left(\frac{w_{\perp}^2}{2} - \frac{p_{\perp}}{\rho}\right)\frac{\delta f}{\delta t}d^3\vec{v} \tag{B.2.5}$$

which is equation (2.3.13) from Chapter 2.